The Dissertation Committee for Margaret Elise Byers Certifies that this is the approved version of the following dissertation:

Neutron Activation Analysis Method for the Quantification of Biofouling Mitigation for the Recovery of Uranium from Seawater

Committee:

Sheldon Landsberger, Supervisor

Gary Gill, Co-Supervisor

Steve Biegalski

Jiyeon Park

Derek Haas

Neutron Activation Analysis Method for the Quantification of Biofouling Mitigation for the Recovery of Uranium from Seawater

by

Margaret Elise Byers

Dissertation

Presented to the Faculty of the Graduate School of

The University of Texas at Austin

in Partial Fulfillment

of the Requirements

for the Degree of

DOCTOR OF PHILOSOPHY

The University of Texas at Austin

August 2017

Dedication

To my fairytale husband who lets me live in a world of butterflies, rainbows, and uranium from seawater.

Acknowledgements

I would like to first thank my previous adviser, Dr. Erich Schneider. Without all of his guidance, patience, and sheer intellect I would not be where I am today. I would like to thank my current adviser, Dr. Sheldon Landsberger for coming to the rescue of myself, my fellow researchers, and the NRE program as a whole, on multiple occasions. I would also like to thank Dr. Gary Gill, for his willingness to serve as my co-adviser and for the abundant support, and seawater, he has continually offered through-out my time with the seawater project. I would like to thank Dr. Jiyeon Park for introducing me to the world of microbiology and all of the time she spent: teaching me laboratory protocols at Sequim, responding to my constant emails, and preparing liquid media, agar plates, bacteria cultures, and various other supplies for my use. I would like to thank Dr. Steve Biegalski for introducing me to the world of guns, Laplace Transforms, and ANOVA, as well as all of his guidance and support throughout my graduate school experience. I would like to thank Dr. Derek Haas for his flexibility, helpful feedback, and support of the ANS student chapter.

I would also like to thank all of the students and staff at the Nuclear Engineering Teaching Laboratory for the opportunity to conduct all of the necessary experiments in a, usually, safe manner. Given my ETC roots I would also like to thank all of my 7th floor office mates for their encouragement, feedback, ideas, entertainment, and friendship.

Lastly I'd like to thank my family for their continued support throughout all of my endeavors.

Neutron Activation Analysis Method for the Quantification of Biofouling Mitigation for the Recovery of Uranium from Seawater

Margaret Elise Byers, Ph.D.

The University of Texas at Austin, 2017

Supervisor: Sheldon Landsberger

Co-Supervisor: Gary Gill

The ocean naturally contains uranium at a concentration of 3.3ng/g, thus offering thousands of years' worth of nuclear fuel. Although ample uranium currently exists from terrestrial sources, the ability to recover seawater uranium would provide supply security for nuclear power generation, putting it on equal footing with renewable energy technologies. Furthermore, this acts as a hedge against the possibility that conventionally sourced uranium experiences a cost increase. Lastly, extracting uranium from seawater circumvents the environmental impact associated with the retrieval of any land-based resource.

This work supports research being conducted by a consortium of national laboratory and university partners focused on the development of advanced materials with the ability to passively adsorb uranium out of seawater. In experiments by PNNL, the adsorption capacity of these fibers decreased by 30% due to accumulation of marine microorganism. Since the uranium capacity of adsorbents has been identified as a major cost driver of final uranium production cost there is significant impetus to mitigate the effects of biofouling to maximize uranium uptake.

Therefore the aims of this research are to develop and demonstrate a method for mitigating marine biofouling in adsorbents similar to those synthesized by ORNL and to quantify the efficacy and uncertainty of the mitigation technique using neutron activation analysis. Existing marine antifouling strategies were considered for coupling with the recovery of uranium from seawater via the passive scheme but none of these strategies could be directly applied due to their prevention mechanisms or implementation cost. Growing research in the field of silver nanoparticles however offered a possible adsorbent modification. This research aims to take advantage of the proven antibacterial capabilities of silver nanoparticles and extend them to a novel application, the recovery of uranium from seawater.

The doping of surrogate adsorbents with silver nanoparticles was successful in observing a decrease in bioaccumulation and subsequent partial restoration of capacity. The degree to which the capacity was restored was not sufficient however to outweigh the implementation cost of this adsorbent modification. Therefore a break-even analysis was conducted to determine the combinations of adsorbent formulation and resulting performance that would result in a cost savings.

Table of Contents

List of Tables

List of Figures

Chapter 1: Introduction

The world's oceans naturally contain uranium in a concentration of 3.3 ng/g [1], thus offering thousands of years' worth of nuclear fuel. Although ample uranium currently exists from terrestrial sources, the ability to recover uranium in this capacity would provide fuel supply security for nuclear power generation, putting it on nearly equal footing with renewable energy technologies. Additionally the ability to recover this uranium at large scale would provide investors and policy makers with economic security by placing a cost ceiling on the cost of uranium. Furthermore, this acts as a hedge against the possibility that terrestrially sourced uranium experiences a significant cost increase for any reason. Lastly, uranium extraction from seawater circumvents the environmental impact associated with the removal of any land-based resource.

Research currently being carried out by a consortium of national laboratory and university partners, led by Oak Ridge and Pacific Northwest National Laboratories (ORNL and PNNL) is leading to the development of advanced adsorbent materials suitable for large-scale deployment in the ocean. These adsorbent fibers rely upon ocean currents and natural advection of seawater to promote inexpensive, passive recovery of naturally occurring seawater uranium [2]. The backbone of the adsorbent is made of simple High Density Polyethylene (HDPE) fibers, melt-spun from polymer resins. The fibers then undergo radiation induced graft polymerization to attach functional groups in order to achieve the desired properties. The amidoxime ligand provides uranium affinity while a non-polar co-monomer provides hydrophilicity, allowing water to diffuse into the adsorbent. In the referenced scheme adsorbents are then constructed in 60 meter long braids so they may be moored to the bottom of the ocean floor. After a soaking campaign on the order of several days to weeks the braids are winched up to the surface by

workboats. Once the uranium is eluted off the braids they are returned to the ocean so the deployment and elution process can be repeated as many times as is economically favorable. The number of times the adsorbent can be reused is a function of, primarily, the cost of each deployment event as well as the uranium uptake achieved on the given deployment cycle, which degrades overtime due to seawater exposure.

Multiple experiments have proven that when uranium adsorbing fibers are placed in a bioactive marine environment, the mass of uranium recovered relative to those exposed to filtered, biologically inert seawater decreases due to the presence of micro-organisms. These experiments have shown that a biofilm forms on the adsorbent, and this biofilm is suspected to act to physically block the uranium binding sites from making contacting with the water, and the uranyl ions it contains [3]. Since the uranium capacity of the adsorbent has been classified as a major cost driver of final uranium production cost [4], there is a significant impetus to mitigate the effects of biofouling to maximize uranium uptake. Experiments by Park et al. [3] have seen a loss in uranium uptake as high as 30% due to the effects of marine biofouling. This drastic reduction in adsorbent performance results in an almost 30% increase in the unit cost of recovering seawater uranium. Therefore the aims of this research are to develop and to demonstrate a method for mitigating marine biofouling in an adsorbent similar to those synthesized by ORNL and to quantify the efficacy and uncertainty of the mitigation technique using neutron activation analysis.

The desire to mitigate oceanic biofouling is by no means unique to the uranium from seawater project, and a literature review uncovers numerous measures taken to mitigate fouling by microorganisms. These measures span many industries and applications. Various antifouling strategies were considered for the coupling with the recovery of uranium from seawater via the passive scheme but none of these strategies

could be directly applied due to either their prevention mechanisms or implementation cost. A noteworthy technique that is gaining popularity across all of these disciplines is the use of silver nanoparticles to introduce antimicrobial properties. This research aims to take advantage of the proven capabilities of silver nanoparticles and extend them to a novel application, the recovery of uranium from seawater. While nanoparticles have been placed in polymer matrices for the introduction of antifouling properties to water treatment membranes [5] [6], the application to these marine adsorbents and the method of synthesis are unique. The addition of silver nanoparticles to the polymer backbone prior to the extrusion process would result in a new marine fouling resistant adsorbent, thus achieving a higher uptake than its non-silver modified counterpart, ideally reducing the cost of seawater uranium recovery.

The novelty of this work is in the development of a method of synthesizing microbial resistant adsorbents suitable for uranium recovery at lower cost per mass of uranium recovered than previous non-resistant adsorbents. To that end, a neutron activation analysis method for quantifying the effectiveness of the uptake restoration offered by these novel adsorbents, and the uncertainty or variability, was developed. The adsorbent performance resulting from the use of this mitigation technique was considered in conjunction with the implementation cost so that recommendations regarding optimal fouling mitigation efforts and deployment parameters could be made. The capacity restoration factor performance observed in laboratory scale experiments at the Nuclear Engineering Teaching Laboratory (NETL) at the University of Texas was coupled with a cost analysis and optimization framework to arrive at fouling mitigation as well as adsorbent deployment and recycle strategies to be implemented were the deployment of the national laboratory adsorbents to be carried out on an industrial scale.

If this technique can successfully mitigate microorganism growth without hampering the ability of the polymer to be extruded, then it should be easily adaptable to all national laboratory and university adsorbent types that are melt-spun from a variety of thermoplastics. This is particularly important given the variety of adsorbent types and substrate materials under development [7][8].

To accomplish this goal the literature was first reviewed to provide more information regarding the driving mechanism of biofouling and then document the search for applicable mitigation methods as well as analytical techniques for quantifying their effectiveness. Background information on an analytical and mathematical technique frequently utilized throughout this work, neutron activation analysis and ANalysis Of VAriance (ANOVA), respectively, is then provided for reference. The remainder of this dissertation then details the steps taken toward the ultimate determination of the cost of uranium recovered by silver doped adsorbents.

This logical progression naturally started with the production of surrogate adsorbents allowing for the completion of a large number of uptake and fouling trials. Once adequate surrogate adsorbents were synthesized experiments were carried out to determine the most suitable adsorbent deployment conditions. This included the parameters necessary for both adsorbent exposure to spiked seawater as well as those capable of inducing observable losses in uptake due to biofouling. Then the details regarding the actual silver doping of adsorbents were described, most notably the determination of silver concentrations to test. The uptake restoration performance of all of the silver doped adsorbents is described in Chapter 7.1, including both the improvement in uptake as well as experiments targeting the reusability of silver doped adsorbents. The resulting performance was then incorporated into the cost model predicting the uranium production cost for the industrial scale recovery of uranium from

seawater using the ORNL adsorbents could they be analogously doped with silver to experience the same behavior observed in UT experiments. Lastly, all of the sources of uncertainty were identified, quantified, and ultimately propagated through the estimated uranium production cost.

Chapter 2: Literature Review

The literature is first reviewed to provide a brief background on marine biofouling in order to have a basic knowledge of root causes and driving mechanisms. The existing methods of mitigating marine biofouling are explored and considered for use with ORNL uranium adsorbents. Then the scope is broadened to include fouling mitigation techniques outside of a marine environment, with the aim of identifying those that may be adapted for use in recovering seawater uranium. Finally, analytical techniques for quantifying heavy metal uptake are reviewed to down select that most appropriate for this work. Neutron Activation Analysis is ultimately selected as the most appropriate procedure for reasons including: detection limit, type of sample able to be analyzed, and equipment availability.

2.1: Marine Biofouling

The literature indicates that the initial fouling sequence follows a similar pattern regardless of type of substratum, geographical region, or colonizing species. It is almost identical across various environments (seawater, human oral cavity, vertebrate circulatory systems) [9], [10]. Fouling by microorganisms begins with a chemical conditioning phase, which begins within seconds after immersion and involves the adsorption and concentration of organic molecules on the surface[10][11][12]. Even within seconds of exposure, macro-molecules and dissolved organic matter begins to adhere to a surface, forming a conditioning film and allowing for further surface settling [12] [6]. The biofilm is typically a precursor to higher order fouling [10] [11]. It is often followed by bacterial colonization, adhesion of unicellular organisms, and settlement of spores. This biofilm, colloquially referred to as slime, occurs with a growth rate on the order of hours,

or even minutes, to days [13]. Even longer exposure times can result in the settling of macroscopic species [9]. This sequence can be seen in Figure 1.

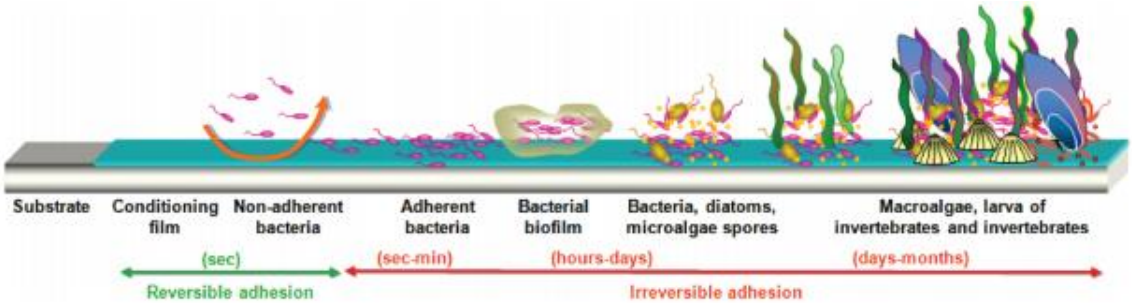

Figure 1: Evolution of surface biofouling taken from [10]

Although some of the currently available uranium adsorbents for industrial scale deployment may remain immersed for several days to weeks, the later stages of fouling will not be the focus of this work. If the early stages of biofouling can be mitigated, namely the establishment of a biofilm, then there is reason to believe this will subsequently increase uranium recovery by reducing biomass accumulation by aiding in the mitigation of large fouling. Furthermore, since a loss in adsorbent uptake was observed in seawater filtered to 150 microns it is clear that the early, micro rather than macroscopic stages of biofouling were responsible [3] for the decrease in uranium uptake. Additionally, since seawater must be removed from the ocean for experimentation, rather than adsorbents brought out to the ocean, the consistent attainability of macro-species and larvae is limited.

Although the mechanism of biofouling is broadly the same across substrate types [9] [10], the literature does suggest that the degree of biofouling may differ. Most variation in degree of fouling across surfaces can commonly be attributed to zeta potential, surface roughness and hydrophobicity [6] [14] [15]. Zeta potential, a surrogate measure of surface charge density, has been identified as an parameter influencing degree

and rate of biofouling, with some evidence indicating that negatively charged surfaces typically experiencing less fouling [14][16] . Conversely, other studies have shown that it is simply the magnitude of charge, regardless of sign, that influences biofouling propensity[15]. Increased surface roughness has been seen to enhance biofouling by both entrapment of particles and bacteria in valleys and an increase in surface area [14] [17] [18]. Hydrophobicity of surfaces is generally cited as a particularly important factor contributing to enhanced biofouling potential. Greater adhesion typically results on non-polar surfaces due to the hydrophobic nature of most cell surfaces of microorganisms. The exposure of a hydrophobic surface to water locally repels the polar water molecules, creating an accumulation of non-polar molecules enhancing the probability of the favorable hydrophobic-hydrophobic interaction between surfaces and cell walls. [14] [15] [17][6].

Two of these three factors are chemical properties inherent to the adsorbents that cannot be altered without fundamental changes to the chemistry. Similarly, the topography of the ORNL adsorbents is in some ways characteristic of its desired properties as high surface area adsorbents are believed to have a higher capacity for uranium uptake [2]. Although high degrees of grafting of a non-amidoxime functional group onto polyethylene by means of a similar radiation-induced graft polymerization shows a linear relationship between degree of grafting and surface roughness [18], it is also believed that high degrees of amidoxime grafting, around 250wt %, are required for sufficient uranium uptake[2] . Therefore, the literature is next reviewed for anti-biofouling measures which will not impede uranyl ions' access to binding sites on the ligand. In addition to not blocking the adsorption mechanism, the economic and logistical implications of implementing the reviewed techniques on an industrial scale must not outweigh the restoration of capacity offered.

2.2: Fouling Mitigation Techniques

Existing methods of mitigating surface fouling by microorganisms are considered for coupling with the recovery of uranium from seawater. Since patterns of microbial surface fouling transcend industries and even environments, fouling mitigation methods used outside the marine habitat are also explored. The primary criteria that qualify a technique as potentially suitable are: maintaining water, thus uranyl, contact with the adsorbent surface and the ability to implement on a large scale without incurring exorbitant economic logistical challenges.

2.2.1: Marine Fouling Mitigation Techniques

The issue of marine biofouling is by no means unique to the recovery of uranium from seawater. Naval ships can incur an additional operating cost, predominantly from increased fuel consumptions, of $2.3 million annually due to the increased weight and drag caused by micro-organism communities on their hulls [19]. The aquaculture industry is also afflicted by marine fouling as bacterial culture on cages and netting can interfere with both equipment operation and fish health, which has the potential to propagate up the food chain[20]. Therefore the literature is reviewed for mitigation techniques successfully employed by these industries.

Efforts to combat biofouling of ship hulls have served as the foundation for mitigation techniques on other surfaces, so it is the natural place to start when searching for the uranium from seawater application. One common strategy involves the use of antifouling paints or coatings that cover the surface area of the hull [21], some of which relied on harsh biocides and were eventually banned in many regions [22]. Although coatings are widely available for commercial uses, anything that prevents the surface of the adsorbent from contacting the surrounding seawater would block the adsorption mechanism altogether. If any such coating were to be applied to the un-functionalized

HDPE fiber prior to the attachment of amidoxime ligand and hydrophilic co-monomer, then the grafting chemistry would be altered and there would be no guarantee that radiation induced graft polymerization would still work. Therefore, surface coatings are not considered further for this application.

Some novel antifouling technologies for ship hulls include the use of silicone elastomers, which undergo topography changes weakening the adhesion of settled organisms. The drag force created by the ships motion is then enough to remove much of the fouling [23]. This however is contingent upon the high speed motion, making this approach not feasible for use with the uranium adsorbing material, at least given the current kelp field-like deployment strategy. An alternative use of dynamic topography for release of organisms uses an electric or pneumatic stress to detach biofilms from a submerged surface [24]. Although this active approach could potentially be applied to the current deployment scheme the implementation of such a system, involving active stressing of the material, would be cost prohibitive.

The aquaculture industry similarly takes advantage of the available antifouling coatings. Physical methods of fouling removal are also employed such as pressure washing of shellfish and equipment [25]. This method would likely damage the adsorbent fibers, and would only be helpful in removing rather than preventing fouling, meaning uptake would have already suffered by the time this method were to be applied. Means of biological control are also used to deter population of particular species of foulants [26]. This exposes a fundamental difference between the antifouling goals of the aquaculture industry and uranium from seawater in that aquaculture often only need to avoid pathogenic fouling while uranium adsorbents need to be free of any microorganisms.

2.2.2: Non-Marine Fouling Mitigation Techniques

Given the similarities in fouling and microbial growth behavior across environments [9][10], antifouling strategies outside marine industry are explored. Beyond aquatic applications, for instance in the medical, dental, food preparation and packaging industries, surface fouling by microorganisms colonization presents significant problems [27]. This, along with growing recent use of polymer materials, has led to an expanding body of work regarding the development of antimicrobial plastics [28]. Several mechanisms for adding antimicrobial agents to polymer surfaces have been demonstrated. Chemical modification by means of oxidation through ozonolysis or by use of a strong acid creates functional groups that can bind to antimicrobial agents such as quaternary ammonium salts[29]. Other chemical modifications include the use of ammonium persulfate and ferric nitrate mixtures to achieve nanosilver/polypropylene plastics for a variety of antibacterial applications [30]. Physical means such as UV surface grafting [31][32] or plasma induced surface grafting [33][34][35] have been proven to modify polymers for antibacterial purposes. The materials and equipment requirements for such procedures are likely to add significant capital and/or operating expenses to the adsorbent production process, and are potentially less desirable for the current application. Further review of the literature yields adsorbent modification techniques that have the potential to meet simplicity and cost requirements, notably the construction of selected polymer-metal composites.

Copper [36] [37] [38] [39] [40] [41] and silver [42] [43] [44][45] [46] [37] [40]nanoparticles are both known for their antibacterial properties for a variety of applications. Although the bactericidal properties of these metals have been known for quite some time, the specific mechanism is not fully understood, with several hypothesis having been advanced [43] [47] [37] [46]. It is believed by some that silver does not

directly kill the bacteria but rather enters the cell and interferes with bacterial growth-signaling pathways and thus hampers the cell's ability to divide and replicate [48] [43]. Others believe silver does in fact directly kill cells by adhering to the cell wall, changing the permeability of vital components of metabolism [43] [47] [46]. It is also believed that silver may bind to DNA, causing abnormalities and/or reducing replication abilities [49] [50] [43] [47]. In the case of nanoparticles it is believed that the large surface area to volume ratio allows for greater interaction with microbial cell walls, resulting in enhanced antifouling properties [37] [30] [51]. Although effectiveness may vary across bacteria species or even strain, silver has been shown to have superior inhibition qualities compared to copper [37].

In some cases silver or copper nanoparticles are attached to polymers using the aforementioned complex chemical techniques. Alternative methods relying on simpler physical means have been pursued, and these are believed to be better suited for this application as these chemical methods are more likely to result in interference with the grafting chemistry and/or significant additions to the adsorption production cost. Copper/LDPE nanocomposites have successfully been created for use in intrauterine devices using a melt and mix method followed by solidification under pressure [52]. Melt-compounding followed by extrusion has been used to construct silver/polypropylene composites to be used as antimicrobial textiles [53]. Perhaps most applicable to this research is the addition of silver to HDPE via solution-casting, melt-extrusion, and solid-state drawing techniques [54]. Although these Ag/HDPE nanocomposites were not created for their antimicrobial properties, rather their optical and semi-conductive properties, the feasibility of adding a nanoparticles into a related polymer fiber forming process has been demonstrated. Therefore, it is believed that this

extrusion method for creating silver/HDPE nanocomposites can be adapted to this project and will be the biofouling mitigation technique used in this work.

2.3: Analytical Techniques for Measuring Uptake

The proposed work depends on a reliable means of heavy metal quantification in order to precisely and repeatedly determine improvements in adsorbent uptake. Many candidate techniques exist in the field of analytical chemistry. The literature is reviewed to down select a quantification method most suitable for this work. Given the nature of this work the chosen technique must be capable of analyzing metals; also both liquid and solid state samples will need to be analyzed. A high degree of sensitivity is an important characteristic, especially given that uranium uptake by ONRL adsorbents is on the order of g/kg and the concentration in the ocean is on the order of ng/g. Lastly, the practicality of using any given technique must be considered it terms of ease of use and equipment availability.

Mass spectrometry is an analytical method of quantifying the mass of sample constituents based on their mass to charge ratio. After being subjected to an applicable ionization process the sample breaks down to charged fragments and is accelerated through an electric or magnetic field. The degree of deflection, or time of flight, can be used to sort ions by their charge to mass ratios, allowing a charge detector to determine the relative abundance of the detected ions [55]. Several variants of ionization method are explored, with a focus on those techniques commonly applied for elemental, as opposed to molecular, analysis.

Inductively Coupled Plasma (ICP) Mass Spectrometry uses a plasma to ionize samples. A high temperature plasma is typically prepared by ionizing argon gas via inductive heating by an electromagnetic coil and collision with free electrons, reaching

temperatures on the order of 10,000 K. Upon entering the chamber containing the ICP the high temperature causes the sample molecules to decompose into atoms that will lose their most loosely bound electron. In the case of time of flight mass spec these ions are then sorted and quantified in relative terms based upon the time it takes them to travel a known distance [56].

A similar technique relying upon the high temperature plasma for elemental analysis is ICP-optical emission spectrometry. The sample, typically water-dissolved, is likewise atomized and ionized in the plasma torch. This process excites electrons, elevating them to a higher quantized state. Upon decent to the ground state energy in the form of light is emitted by the electron. Given the characteristic emission spectrum known to correspond to each element, samples can then be identified by capturing the photons on a charged coupled device.

Chromatography is another commonly used analysis method for sample separation and quantification. This technique is typically used for molecular analysis but is considered given its inter-department availability. The sample is dissolved in a fluid creating a mobile phase. As the fluid travels through a stationary material, variations in component speed lead to sample partition, allowings for determination of relative abundance that can be compared to a standard reference material. Gas chromatography uses an inert gas, such as helium, as the mobile fluid that passes through a column containing a liquid or polymer stationary phase [57].

Neutron Activation Analysis (NAA) is an identification and quantification technique useful for determining trace elements by inducing nuclear reactions. Subjecting a sample to a neutron flux will cause, among other reactions, radiative capture, meaning a target nuclei absorbs a neutron, becomes excited, and sheds its excitation energy in the form of a characteristic gamma ray. Since the resulting gamma

rays are indicative of the activation products NAA can be used to identify constituents of unknown compounds and decay events can be counted to determine isotropic concentrations in the sample.

Table 1 summarizes all of the aforementioned elemental analysis techniques with respect to relevant qualities in the required down selection.

Table 1: Summary of Quantification Techniques

Analytical Technique	Form of Sample Analyzed	Type of Sample Detected	Ease of Use	Sensitivity	Equipment Availability
ICP Mass Spec	Liquid, solid (often must be dissolved in something like aqua-regia for metals)	Metals, some non-metals (biological samples)	low	pg/g	yes (other department)
ICP Optical Emission Spectrum	Liquid, solid, Gas (with perturbation)	Metals, Organics	low	pg/g	no
Gas Chromatography	Liquid, Gas	Organic compounds	high	ng/g	yes
Neutron Activation Analysis	Solid, Liquid, Gas	Metals, Inorganic non-metals	moderate	ng/g	yes

It is clear that neutron activation analysis is the most appropriate analytical technique for this work. This is due primarily to its accessibility at available facilities,

the Nuclear Engineering Teaching Laboratory, and the type of samples that can be analyzed.

Chapter 3: Background and Theory

This section describes the theory and provide supporting calculation for two mathematical techniques to be referenced throughout this document. First, Neutron Activation Analysis (NAA), the analytical method used to measure uptake, will be described. Secondly a statistical model, the ANalysis Of VAriance (ANOVA) is detailed as this technique used throughout this work to analyze differences between groups of values.

3.1: Neutron Activation Analysis Background

As mentioned previously, neutron activation analysis exposes a sample, containing nuclei, N_0, to neutron bombardment to induce radiative capture. Characteristic gamma rays of daughter product, N_1, are then analyzed to determine the isotopes present and their concentrations. Given the simple nature of the working mechanism, this section will give a more detailed explanation of the post-priori calculation of concentration. The number density of any generic isotope of interest, N_0 , which transmutes to N_1, is determined using the time rate of change of $N_1$and is described below.

First the irradiation period is considered via the differential equation governing the sources and losses, Eqn. 1. The production of N_1 is dependent upon N_0 along with the neutron flux, ϕ, and the radiative capture cross section of the parent isotope, σ_0 while the loss mechanism is radioactive decay.

$$\frac{\partial N_1}{\partial t} = \phi N_0 \sigma_0 - \lambda_1 N_1$$

Eqn. 1

The concentration of the product isotope can easily be solved for by taking into account some assumptions. First it is assumed that initially $N_1 = 0$ since the isotope does not naturally exist in the sample. Additionally, since N_0 is very large as compared to N_1 it can be treated as constant. Lastly, other loss mechanisms are considered negligible, as long as N_1 is not a significant neutron absorber. Using these assumptions, the time dependent population of N_1 can be seen in Eqn. 2.

$$N_1(t) = \frac{\phi N_0 \sigma_0}{\lambda_1}\left(1 - e^{-\lambda_1 t}\right)$$

Eqn. 2

Upon removal from the neutron flux the differential equation governing the time rate of change of N_1, Eqn. 3, simplifies as the source terms has dropped to zero ($\phi = 0$). The subsequent decay is considered to start immediately following the irradiation time, t_i.

$$\frac{\partial N_1}{\partial t} = -\lambda_1 N_1$$

Eqn. 3

Using the initial condition of $N_1(t = t_i)$ as determined above, the concentration of isotope N_1 during its decay time, t_d is seen in Eqn. 4.

$$N_1(t) = \frac{\phi N_0 \sigma_0}{\lambda_1}\left(1 - e^{-\lambda_1 t_i}\right)e^{-\lambda_1 t_d}.$$

Eqn. 4

This can be used to find the number of decays that occur during the counting time by multiplying $N_1(t)$ by the decay constant to obtain the activity. The activity is then integrated over the counting time, t_c, starting from the time the sample was removed from the reactor to start the decay process, t_d as shown in Eqn. 5

$$Decays_1 = \int_{t_d}^{t_c+t_d} \phi N_0 \sigma_0 \left(1 - e^{-\lambda_1 t_i}\right) e^{-\lambda_1 t_d} dt$$

Eqn. 5

Evaluating this integral gives the number of decays occurring during the counting period (Eqn. 6).

$$Decays_1 = \frac{\phi N_0 \sigma_0}{\lambda_1} \left(1 - e^{-\lambda_1 t_a}\right)\left(e^{-\lambda_1 t_d}\right)\left(1 - e_1^{-\lambda_1 t_c}\right)$$

Eqn. 6

The number of counts registered by the detector is also a factor of the detector efficiency, ϵ, and the decay yield, γ for the photon of interest as seen in Eqn. 7.

$$Counts_1 = \epsilon\gamma \frac{\phi N_0 \sigma_0}{\lambda_1} \left(1 - e^{-\lambda_1 t_i}\right)\left(e^{-\lambda_1 t_d}\right)\left(1 - e^{-\lambda_1 t_c}\right)$$

Eqn. 7

The count rate in the detection period can then be used to back out the activity of the desired nuclide by dividing by the detector efficiency and decay yield, and the activity be used to easily solve for the number density by dividing by the decay constant.

The software employed to carry out these calculations is Neutron Activation Data Analysis (NADA) which uses a comparator method [58] [59]. This method involves the irradiation of certified standard material with a known concentration, X_{std} and level of precision, $\sigma_{X_{std}}$. Provided the irradiation and counting conditions (time, flux/power, and detection geometry) are consistent across the known standard and unknown sample(s), the number of counts registered by the detector from the unknown sample, c_{sample}, can be compared to that of the known standard, c_{std}. The concentration of the unknown, X_{sample}, can then be determined by adjusting for the weight of the sample and standard, W_{sample} and W_{std} respectively, as seen in Eqn. 8.

$$X_{sample} = X_{std} \frac{W_{std}}{W_{sample}} \frac{c_{sample}}{c_{std}}$$

Eqn. 8

If the irradiating or counting conditions for the sample and standard are not identical then a post-priori correction factor must be applied. This correction factor is typically a ratio of the terms that are not identical from Eqn. 7. For example, if the samples were irradiated for different lengths of time and/or different powers than the standard then a correction factor of $\frac{\left(1-e^{-\lambda_1 t_{i_{standard}}}\right)}{\left(1-e^{-\lambda_1 t_{i_{sample}}}\right)}$ or $\frac{\phi_{std}}{\sigma_{sample}}$, respectively is applied to Eqn. 8 above.

Early in this work NAA was attempted on prototype adsorbents to ensure its viability in detecting metals at the concentration in which they accumulate in the deployed adsorbents. Neutron activation analysis was conducted on four different adsorbents, a sample of pure activated carbon serving as the background, and two NIST standard coal materials certified to contain manganese at known low levels. All irradiations took place at a power of 100kW for times ranging between one and three minutes and then counted on a high purity germanium detector.

In order to ensure the accuracy of concentration quantification by NAA one of the NIST standard materials was treated as an unknown so its measured concentration could be compared to the NIST published value. The other NIST standard coal material with its certified concentration and low uncertainty, was treated as the known material to which all later manganese containing samples would be compared. Table 2 below shows the results for the two standards, where 1632C was treated as the standard library material and 1632D as the unknown.

Table 2: Measured and published concentration and uncertainty values for 2 NIST standard coal materials

NIST ID	Concentration as Determined by NAA (ppm)	Uncertainty as Determined by NAA (ppm)	Known Concentration (ppm)	Known Uncertainty (ppm)
1632C	13.04	0.68	13.04	0.53
1632D	12.12	0.70	13.1	0.4

These results indicated that the NAA techniques were accurate in that manganese concentration in 1632D was within the range published by NIST and can therefore be reliably used moving forward.

3.2: Analysis of Variance Background

In trying to declare two groups of values as statistically different or equivalent there are a number of statistical tools and models available. This work will consistently rely on the method of ANalysis Of VAriance (ANOVA) for null hypothesis testing as it is known to be a more conservative approach resulting in fewer type 1 errors. The basis of ANOVA will thus be described here.

ANOVA is a statistical method used to examine differences between two or more sample populations. The validity of the null hypothesis, that the groups all cluster around the same mean, is tested by comparing the mean square error between sample groups, MSB, to the mean square error within sample groups, MSW. The calculation of the mean square error within and between groups is shown in Eqn. 9 and Eqn. 10 respectively

$$MSW = \frac{\sum_{i=1}^{n} \sigma_i^2}{n}$$

Eqn. 9

$$MSB = n\sigma_M^2$$

Eqn. 10

where σ_i^2 is the variance of each individual sample, n is the number of samples in each set, and σ_M^2 is the variance of the means between data sets.

The value of the ratio of signal to noise, or MSB to MSW is termed F and is compared to a critical value, F_{crit}. This critical signal to noise ratio is a function of the a-priori designated significance value, α, and the degrees of freedom within and between populations. In this work the α-level will always be set to 0.05 resulting in a confidence interval of 95%. If the value of F is greater than the critical value, then the null hypothesis is rejected.

Chapter 4: Adsorbent Production

Since the ORNL uranium adsorbent fibers are very costly to produce and require the use of specialized equipment, it was decided that surrogate adsorbent materials would be used. Additionally, the relatively slow adsorption kinetics of ORNL adsorbent fibers led to the decision to seek surrogate adsorbents allowing the completion of uptake and fouling trials at a much faster rate and lower cost. After a down selection of commercially available products, composites made of activated carbon in a high density polyethylene matrix were determined to be the most appropriate choice.

The initial intention was to produce adsorbent as analogous as possible to those synthesized by ORNL, polyethylene based fibers on the order of tens of microns [2]. The utilization of available scale equipment was successful in producing surrogate adsorbents with a diameter of approximately 1.75mm. Analysis of heavy metal uptake kinetics by the adsorbent filaments however observed significant variability in performance both within and across adsorbent batches.

After extensive alteration to the synthesis process rendered little success in ensuring suitable reproducibility, a method of individual adsorbent characterization by means of NAA was pursued. It was hypothesized that irregularities in adsorbent composition was responsible for variation in uptake, so adsorbents were subjected to irradiation before and after deployment in an effort to tie performance to activated carbon content. No significant correlation was observed however, leading to the conclusion that heterogeneity in adsorbent behavior was primarily a function of activated carbon aggregation and differences in exposed surface area rather than concentration.

Therefore the filament type adsorbents were replaced with adsorbent suspensions to ensure a more uniform distribution of available surface area. The kinetic performance

of adsorbent suspensions was examined and the time series data ultimately fit to a pseudo-first order kinetics model.

4.1: Adsorbent Filaments

This sub-section describes the selection of surrogate materials with regards to both the adsorbent material as well as heavy metal targeted for adsorption. Activated carbon was selected as the surrogate heavy metal adsorbent due to its ability to capture a large number of metals as well as its commercial availability. In initial uptake and fouling trials the decision was made to choose a metal other than uranium so a large number of scoping trials could quickly be completed while minimizing the creation of radioactive waste. After a down selection of metals adsorbed by activated carbon, manganese was eventually determined to be the most appropriate uranium surrogate.

The procedures for synthesizing the surrogate adsorbents is then described, as well as the refinements made in an effort to ensure adsorbent homogeneity. When the consistency of adsorbent performance could not be guaranteed, an irradiation procedure for characterizing individual adsorbent filaments was designed.

4.1.1: Selection of Surrogate Materials

The first task was to identify appropriate surrogate materials that could be used to accurately represent fouling of the organic substrate thus precluding the adsorption of heavy metals. The initial selection of surrogate materials resulted in the use of a high density polyethylene matrix with activated carbon (AC) replacing the amidoxime ligand. While there was no hope of producing ultrafine fibers on the same scale as the ORNL adsorbents, 20-30 microns [2], methods of constructing analogously cylindrical adsorbent filaments were pursued.

The benefits of activated carbon leading to its selection include, most importantly, its commercial availability. Additionally, it has the ability to remove a wide variety of heavy metals from aqueous solution, and analogous to the uranium adsorbents this selection occurs via an adsorption mechanism, as opposed to other sorption mechanisms such as ion exchange or absorption [60][61][62][63][64][65]. Although activated carbon may not be extruded easily in a laboratory setting, as its melting point is on the order of thousands of degrees, the literature reports it has been extruded successfully at 160^0C by means of a low density polyethylene (LDPE) binder[66].

Initially a surrogate for uranium was also utilized so that a large number of scoping trials could be conducted without the added complications of concentrating radioactive material and producing unnecessary amounts of Pu-239 after irradiation. Given the large number of metals that can be adsorbed by activated carbon, a down-selection of the most logical surrogate for uranium was conducted.

Firstly and most importantly, the metal had to be soluble in water in some form. Secondly since the seawater will be spiked with the metal of interest, it can't be associated with any anti-fouling properties as this would render biofouling experiments near impossible to conduct. The last and perhaps most complicated requirement is sufficient detectability by NAA.

Isotopes that can be detected via NAA with a high degree of accuracy are characterized by a few defining parameters. The natural abundance of a given isotope should be comparatively high, especially if using small sample sizes. This requirement can to some degree be circumvented however by compensating with a high neutron flux. Similarly, the radiative capture cross section for the isotope of interest must be significant. The resulting, A+1, isotope must then decay with a characteristic gamma ray energy that can be easily registered by the detector. Additionally, this gamma ray must

not be subject to interference by other isotopes that may be present in the adsorbent post deployment, most notably sodium-24 (1368 and 2754 keV) and chlorine-38 (1642 and 2168 keV). The percent yield of that characteristic gamma ray must also be non-negligible. Lastly, for practical purposes the half-life of the resulting isotope must not be so long that excessive counting times are necessary, nor so short that the sample will be too hot to handle.

Table 3 summarizes the aforementioned characteristics for each naturally occurring isotope for a representative handful of heavy metals adsorbed by activated carbon, although a larger number were analogously analyzed. Clearly manganese is the most appropriate for quantification by NAA as the single naturally occurring isotope has a comparatively high neutron capture cross-section to produce Mn-56 which decays with a detectable gamma ray in a reasonable amount of time. Since it also fulfills the solubility and lack of antimicrobial property requirements for deployment it is chosen as the most suitable element to act as a uranium surrogate.

Table 3: NAA relevant properties of naturally occurring isotopes adsorbed by activated carbon

Isotope	Abundance (%)	N-gamma X-Section (barns)	Gamma Ray Energy of N+1 (keV)	Percent Yield per Decay	Half Life of N+1
Fe-54	5.9	2.3	Electron capture (with X-ray)		2.7 years
Fe-56	91.7	2.8	Stable		
Fe-57	2.1	2.6	Stable		
Fe-58	0.28	1.2	1100 and 1291	56 and 43%	44.51 days
Zn-64	48.6	.44	1115	49%	245 days
Zn-66	27.9		Stable		
Zn-67	4.1		Stable		
Zn-68	18.8	1	318	.0012%	56.4 min
		0.1 (Zn-69m)	440	95%	13.8 hr
Zn-70	.6	.09	120, 510		2.2 min
		.09 (Zn-71m)	380,490,610		3 hr
Mn-55	**100**	**13.3** barns	**837-846**	**99**	**2.58 hrs**

4.1.2: Adsorbent Homogeneity

Reproducibility of the adsorbent is crucial to the success of this work and in the very early stages of the project homogeneity of adsorbents was identified as a potential issue, therefore many efforts were made to ensure reproducibility in adsorbent performance. In the context of these experiments there are two classifications of reproducibility that must be ensured. A batch of adsorbent refers to a mass of adsorbent prepared in a given time period and according to a set of parameters including: mass fraction of activated carbon, temperature of extrusion, number of times extruded. To ensure reproducibility, any two pieces of adsorbent from a given batch that are exposed

to identical conditions should have corresponding performance. Additionally, an analogous batch of adsorbent prepared at a later time period should perform identically to previous batches constrained by the same parameters. The ability to combine two solid inputs to produce large quantities of adsorbent with identically valued key properties (mass, diameter, activated carbon content, etc.) and resulting performance within and across batches eventually proved to be not feasible. The remainder of this section will discuss the measures taken to address this issue, before ultimately moving toward a different form of adsorbents- suspensions.

The main obstacles identified as contributing to adsorbent heterogeneity were the high viscosity of the polymer and the large particle size of the activated carbon. The easiest of these issues to address, and thus first modified, was the size of the activated carbon particles. Activated carbon granules were ground up into a fine powder for better mixing. In order to ensure an upper bound on particle size the resulting powder was sequentially sifted such that the maximum particle size retained was 250 microns.

The more difficult issue of high polymer viscosity was first addressed by turning to the literature. The previously referenced study that successfully extruded LDPE/activated carbon composites explored the use of wax as an adjuvant to decrease the viscosity; where an addition of 5% wax by weight was able to decrease the viscosity by nearly 12% [66]. A similar attempt was made with the surrogate adsorbents with varying amounts of paraffin wax. As little as 2.5% wax by weight was sufficient in observing a qualitative difference in viscosity and thus ease of adsorbent mixing. This small addition of wax however also resulted in an observable difference in adsorbent appearance and texture (shinier and smoother). The qualitatively large changes resulting from this minor adsorbent formulation adjustment, especially given the correlation between increased hydrophobicity and enhanced fouling noted in the literature review

[6][14] [15] [17], were determined to be too undesirable to outweigh the moderate gain in process-ability.

As a next attempt, rather than using additives, and moving even further away from the process of making the ORNL uranium adsorbents, the rheological properties of the polymer were considered. Although LDPE was initially chosen in lieu of HDPE due to the lower melting point, HDPE was reconsidered as it proved to be more favorable for other processing properties. The viscosity and melt flow index, a measure of a thermoplastic's ability to flow through a unit capillary under standardized conditions, of HDPE are lower and higher, respectively, for HDPE as compared to LDPE. This is due to a linear structure as opposed to the long branched chains of LDPE, which impedes its ability to flow. Given the low marginal difficulty of achieving 130^0C, the melting point of HDPE, as compared to 110^0C, the melting point of LDPE, and more importantly the observed improvement in using a HDPE matrix in suspending activated carbon, it was decided that HDPE would be used moving forward.

Even if a perfectly homogenous mixture of material could be achieved, the consistency issue still exists in that all adsorbents must have an identical size, or minimally an identical surface area to volume ratio. Since this level of precision cannot be achieved through manual means it was decided that a mechanical device would be required moving forward. A variety of pre-manufactured and DIY extrusion devices were considered and ultimately the Filastruder Kit was selected. The Filastruder Kit contains all of the necessary parts to build a single screw extrusion instrument. Although its intended use is the extrusion of thermoplastics, primarily acrylonitrile butadiene styrene, to create filaments for at-home 3-D printing, it boasts an adjustable heating element with the ability to process a variety of thermoplastics. No record of the

Filastruder being used to extrude HDPE could be found, but it was rated for use with LDPE so it was assumed HDPE would be possible as well.

Significant experimentation with the Filastruder temperature and adsorbent formulation was carried out to determine the best adsorbent synthesis procedures. High activated carbon content impedes the ability of the mixture to be extruded so various adsorbent compositions were tested. Eventually it was determined that an adsorbent consisting of a HDPE matrix with 7% activated carbon by weight was able to be consistently extruded without jamming the extruder. It was also found that using HDPE pellets in lieu of the previously used HDPE flakes also led to improved extrude-ability. A temperature of 230^0C was used to push the adsorbent through the 1.75mm nozzle. Visual inspection indicated that the surfaces of the adsorbents were uniformly coated with activated carbon but deployment experiments indicated continued variability requiring further refinement of the synthesis process. A close-up image of the extruded adsorbents can be seen in Figure 2.

Figure 2: Representative adsorbent composed of 7% activated carbon in a high density polyethylene matrix

The adsorbent filament synthesis methodology was further improved to include additional iterations of extrusion, which provides mixing, in an effort to ensure greater adsorbent homogeneity. The degree of filament homogeneity was analyzed quantitatively using NAA by examining levels of impurity. Analysis of raw activated carbon showed the presence of, among other isotopes, Mn-55. Therefore the level and variation of manganese impurity pre-existing in the activated carbon was used to determine the relative activated carbon content in adsorbents.

The degree of variation in manganese concentration in adsorbent samples was compared to the degree of variation in raw activated carbon. Since the degree of variability of manganese in activated carbon is known, any additional variability of the calculated manganese concentration in the activated carbon contained in the adsorbents can be attributed to variation in the activated carbon content. Table 4 shows the results as a function of number of extrusions.

Table 4: Analysis of adsorbent homogeneity as determined by variation in manganese pre-existing in activated carbon

Number of Extrusions	% Std. Dev. In Mn Concentration
Raw Activated Carbon	0.78%
1	60.%
2	47%
3	35%
4	12%
5	6.7%
6	1.1%
7	2.7%

It is clear that additional extrusions of the adsorbent filaments provide better mixing, leading to more homogenous adsorbents. Therefore adsorbents were extruded 7 times before being exposed to metal spiked solution. The slightly lower deviation observed in the adsorbents taken out after only 6 extrusions as compared to 7 is believed to be the result of chance and small sample size rather than an optimal number of extrusions after which heterogeneity increases. With this confirmation of consistency of material composition, the adsorbents were next analyzed for reproducibility in performance.

Time series data for adsorbent filaments exposed to DI water spiked to 1,000 μg/g uranium was collected. The uptake of individual adsorbent samples can be seen in Figure 3. These batch experiments were conducted at room temperature with constant circulation of the deployment tank to ensure adequate mixing and flow.

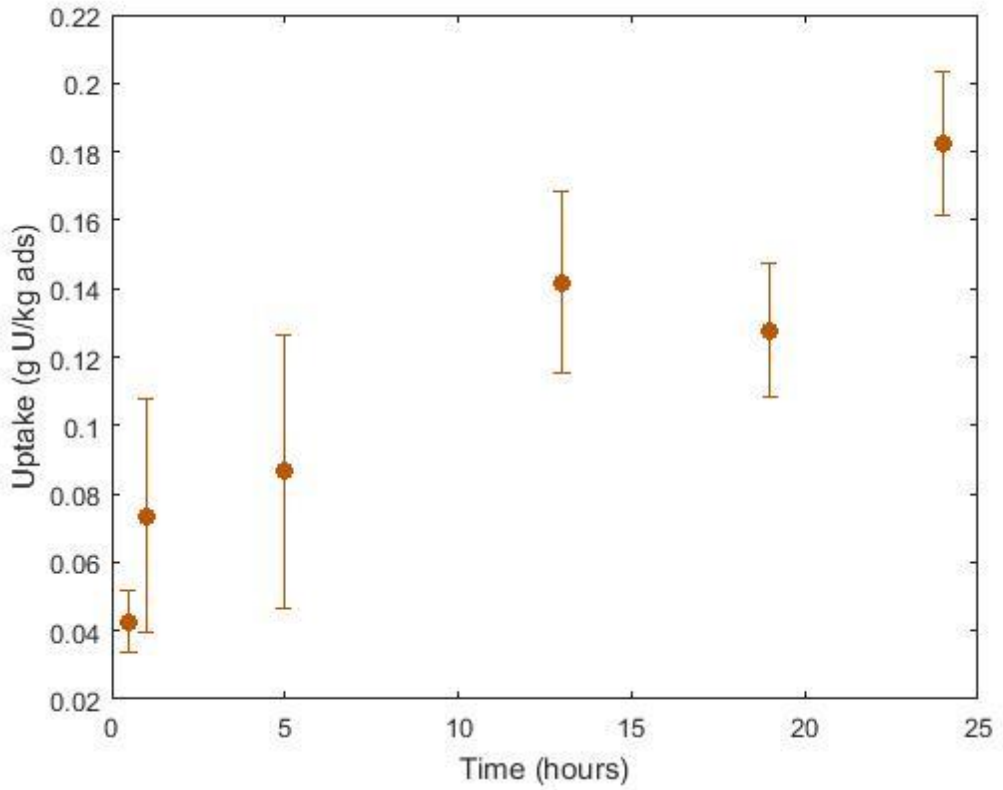

Figure 3: Uptake of uranium by adsorbent filaments as a function of exposure time to deionized water spiked to 1,000 µg/g uranium

As would be expected, the uranium uptake increases with exposure time. Also, as expected, relative standard deviation among sets of adsorbents decreases with increasing exposure time, which can be seen more clearly in Table 5. The moderate standard deviation across adsorbent samples achieved at soaking times of 24 hours was determined to be satisfactory for further experimentation.

Table 5: Deviation in uptake performance of adsorbent filaments as a function of exposure time

Hours of Exposure	% Std. Dev. In Uptake
0.5	22
1	47
5	46
13	19
19	15
24	11

The most important conclusion to be drawn from this analysis however is the suitability of NAA for the quantification of low concentrations of uranium. This was evident given that the NAA-inherent uncertainty for individuals samples, on the order of 1-2% of the measured concentration, was found to be trivial as compared to the deviation within sample populations [67]. Additionally, the experimentally measured concentrations were consistently higher than both the lower limit of detection and quantification.

The detection, L_D and quantitative L_Q limits were computed according to Currie's method in order to determine the smallest metal concentrations that could reliably be measured using NAA [68]. The massL_D, calculated using Eqn. 11, is defined to be the lowest true net signal level expected to lead to detection at the desired confidence level.

$$L_D(g) = \frac{k_c^2 + 2k_c\sqrt{\mu_B + \sigma_B^2}}{K}$$

Eqn. 11

The mass L_Q calculated using Eqn. 12, is the minimum net signal level required to obtain an accurate quantitative result.

$$L_Q(g) = \frac{\frac{k_Q^2}{2}\left(1 + \sqrt{1 + \frac{4(\mu_B + \sigma_B^2)}{k_Q^2}}\right)}{K}$$

Eqn. 12

Both limit values are tied to the blank signal reading, μ_B and, the variance of the blank signal, σ_B^2. The blank signal reading was quantified using trials in which identical adsorbent samples were analyzed prior to exposure to the metal spiked solution. Because the background was not well-known, calculations were performed with the paired observation assumption that $\mu_B = \sigma_B^2$. The confidence level was set to 95%, at which the tolerance factor, k_c is defined to be 1.645. The requisite relative standard deviation was set to 10%, so k_Q = 10 for L_D calculations. The overall calibration factor K, in units of counts per gram, was calculated for each sample using the variable parameters defined by Currie [68]. All of the deployed adsorbents, both those exposed to manganese and uranium spiked solution, were observed to have a concentration greater than the detection and quantification limits. Therefore the investigation of conditions required to induce biofouling, to be discussed in more detail in Section 5.2, was initiated.

Additional exposures of adsorbents prepared by identical means resulted in significant variation in uptake across samples. The observed standard deviation for fouled and unfouled adsorbents was as high as 30 and 27%, respectively. While it could be conceived that variability in adsorbent performance would increase in the presence of biofouling, the unfouled adsorbents were treated analogously to those in Table 5 and Figure 3 and should thus have similar behavior. Therefore further investigation was

carried out in an attempt to reconcile uptake inconsistencies, first by considering differences in adsorbent surface area.

Although forcing the same homogenously mixed material through a single nozzle at a constant temperature would be expected to result in adsorbents of uniform diameter, visual inspection has shown that there is a degree of variation. This could be an important parameter as it affects the surface area to volume ratio, which could manifest itself in deviations of uptake between samples, or even within samples if the diameter is not consistent along a given adsorbent filament. It would of course be ideal to quantitatively correlate the effect of diameter to resulting uptake. This could be done by holding the mass fraction of AC in the adsorbent fixed and observing the variation in uptake as a function of diameter. It has been demonstrated however that maintaining a very precise activated carbon content and/or consistent diameter are some of the notable obstacles in adsorbent preparation. Therefore non-uniformities in adsorbent diameters, if not substantial, will simply have to be accepted as a contributor to variation in uptake per unit mass of adsorbent. That being said attempts can be made to correct for the differences by measuring the diameters and calculating the exposed surface area for each mass of adsorbent.

Since the diameter can of course not be measured at all points along the adsorbent, the average diameter of each adsorbent was used to compare across samples. The average diameter of each adsorbent was calculated by measuring the adsorbents length and mass, given that the density is assumed to be consistent and a function of the known composition.

Given that uranium binds to activated carbon using an adsorption mechanism, only the exposed surface of the adsorbent is relevant for uptake performance. Therefore the uptake per unit mass of adsorbent, determined via NAA, was considered in light of

surface area such that the performance parameter of interest became the uptake per unit surface area. This area dependent uptake of uranium by activated carbon, ϒ, was determined using the measured mass dependent uptake, U, filament weight, w_{ads}, and surface area, SA_{ads} of a given adsorbent (Eqn. 13)

$$\Upsilon = \frac{U}{SA_{ads}} * w_{ads}$$

Eqn. 113

A population of 20 adsorbents analyzed for both uptake and surface area was seen to have a standard deviation in surface area of 7%. The incorporation of this variation in surface area did act to reduce the deviation across replicate samples, from 29% to 20%. Additional trails however testing the consistency of uptake per unit surface area resulted in trivial decreases, or in some cases even increases, of the standard deviation of the sample set, indicating that non-uniformity in filament surface area was not the driving factor of irreproducibility.

Given the very large surface area of individual activated carbon granules, on the order of thousands of meters per gram [69], it is possible that the variation in surface area of the adsorbent filaments does not significantly affect the equilibrium between uranium ions in suspension and availableactivated carbon sites. It was next hypothesized that the seemingly small differences in activated carbon content existing amongst adsorbent filaments, shown previously in Table 4 as a function of extrusion number, may drive non-trivial differences in adsorbent performance. Therefore a NAA methodology was developed to better characterize the make-up of individual filaments.

4.1.3: Characterization of Individual Adsorbent Filaments

Having concluded that variation in adsorbent behavior may stem from heterogeneous composition across adsorbent samples, a method of using NAA to trace individual adsorbent performance back to its specific composition was designed. Two separate implementations of NAA were used to characterize each filament before and after exposure to uranium spiked solution. The objective of this method was to determine the uptake of uranium per unit activated carbon, rather than per unit adsorbent, in hopes of achieving a more Gaussian distribution.

As was discussed previously, the Mn-55 impurity pre-existing in the activated carbon was used as a surrogate for activated carbon content in the polymer matrix. Previously, however, the standard deviation across the entire sample set was used to simply determine the degree of mixing to broadly characterize homogeneity of the entire adsorbent population. Using this method of individual filament characterization, the Mn-55 content of each adsorbent filament to be deployed was quantified prior to exposure so the level of uranium uptake could be correlated to the relative activated carbon content. The two different NAA techniques used to characterize adsorbent filaments before and after exposure to uranium spiked solution are outlined in Table 6 and will be descried in further detail below.

Table 6: Neutron Activation Analysis used for the characterization of individual adsorbent samples

	Pre-deployment Characterization	Post Deployment Performance
Activation Reaction of Interest	${}^{55}_{25}Mn + n \rightarrow {}^{56}_{25}Mn$	${}^{238}_{92}U + n \rightarrow {}^{239}_{92}U$
Decay Observed for Counting	${}^{56}_{25}Mn \rightarrow {}^{56}_{26}Fe + \beta$	${}^{239}_{93}Np \rightarrow {}^{239}_{94}Pu + \beta$
Gamma Ray Counted	847 keV	278 keV
Detector Used	HPGe	HPGe with Compton Suppression System
Neutron Energy	Thermal	Epithermal
Power Level (keV)	400	500
Irradiation Time (s)	1,800	120
Sample Delivery System	Rotary Sample Rack	Epithermal Pneumatic Tube

While NAA is often considered a non-destructive technique, the specific implementation of NAA used at the Nuclear Engineering Teaching Laboratory in previously discussed analyses of adsorbent filaments for both Mn-55 and U-238 uptake left filaments unsuitable for deployment post analyses. The use of the existing pneumatic system to insert and retrieve samples to and from the reactor core requires that each sample be contained in a polyethylene vial of height 5.5cm. Furthermore, use of the HPGe detector to count the irradiated samples again requires the use of the small polyethylene vials. Once the filaments have been divided into these small pieces they are too small for deployment in the current system. While the deployment system could be altered to accommodate the very small adsorbent pieces, this was assumed to exacerbate variation within adsorbent samples. Therefore the means of both irradiating and counting

were altered to be able to analyze filaments on the order of 15-20 cm weight around 0.3 grams.

The rotary sample rack, RSR, at NETL allows for up to 30 samples to be co-irradiated as they circle around the outside of the core. The primary benefit of the RSR, for this application, is the larger size of the sample vessels, which are capable of housing an adsorbent sample of the aforementioned size in its entirety. Use of the RSR did present an obstacle with regards to the longer sample retrieval times. Unlike the pneumatic system, which automatically returns samples to the experimenter for counting within seconds after irradiation, the RSR requires manual unloading of the entire sample batch at once taking on the order of 30 minutes. This typically does not pose a problem as the RSR is intended for analysis of isotopes requiring long irradiation and counting periods. In this instance however, the 30 minute delay time is somewhat of a nuisance, albeit non-insurmountable, given it is a non-trivial fraction of the ~2.5 hour half-life of Mn-56. Additionally, the irradiation of all samples at once further extended the decay time between irradiation and counting, at least of the latter counted samples, as compared to the method of sequential irradiation followed by immediate counting of filaments, which was used previously with the pneumatic system. Therefore calculations, and a trail experimentation, of the necessary power level and irradiation time were performed in order to secure a sufficient number of decays could be observed for the last sample counted.

Documentation on the TRIGA Mark II reactor indicated that the neutron flux experienced by samples inserted into the core at full power is approximately 2.7 $x10^{12}$ $n/cm^2/s$ while those irradiated via the RSR are subjected to 2.0 $x10^{12}$ $n/cm^2/s$. Although movement around the circumference of the core acts to ensure all samples achieve the same flux, the non-trivial flux differences occurring during start up and shut down favor

longer irradiation periods in order for the average flux experienced by all samples to approach that of when operating at the desired power level.

Post irradiation the samples are counted on an HPGe detector and in order to prevent contamination of the detector it is standard practice that the radioactive samples are placed in a clean small polyethylene vials. Therefore it was necessary to create a custom sample holder in which whole adsorbent filaments could be counted. This was accomplished by 3-D printing a trough-like structure atop the appropriate size ring to fit the detector. This piece can be seen in Figure 4.

Figure 4: Custom sample holder used for post-irradiation analysis of adsorbent filaments

In the case of uranium uptake quantification a uranium daughter, Np-239, is used due to the very low energy, 74.7 keV of gamma rays emitted by U-239, which are subject to high background noise. The gamma rays emitted by Np-239 are still relatively low energy, 277.6 keV, and are thus counted using a Compton suppression system. The manganese content can be quantified directly however by means of its single naturally occurring isotope, Mn-55. The high energy gamma emitted by the resulting Mn-56, 846.7 keV, does not require counting with a Compton suppression system. Interference however was observed at this energy due to what appeared to be Mg-27 at 843.7 keV present in the activated carbon; therefore the less abundant but still sufficiently present 1810.7 keV gamma ray was instead counted [67] and still did not require use of the Compton suppression system.

After the long thermal irradiations and counting of a set of 60 adsorbent samples, half the filaments were fouled and subsequently exposed to simulated seawater spiked o 500ppm uranium for 2 days to examine uptake behavior. Post deployment adsorbent filaments were again irradiated, this time with epithermal neutrons using the pneumatic tube system to quantify the presence of uranium so the uptake could be considered in light of the initial activated carbon content.

Epithermal neutrons are generally preferable for the detection of low concentrations of U-238, as the metal has large epithermal resonance integral of 278 barns. Using epithermal neutrons thus provides enough feedback to properly detect uranium, while also decreasing the background interference from Cl-38 and Na-24. This can significantly increase sensitivity, as chlorine atoms have been observed to cause a six-fold detection limit increase in organic samples when using thermal NAA [70]. The small epithermal cross-sections of both Na-24 and Cl-38 thus make low detection limits achievable, despite the prevalence of the two ions in seawater samples.

The uranium uptake and pre-existing manganese concentration, acting as a surrogate for activated carbon content, for two sets of adsorbent samples can be seen in Figure 5 and Figure 6.

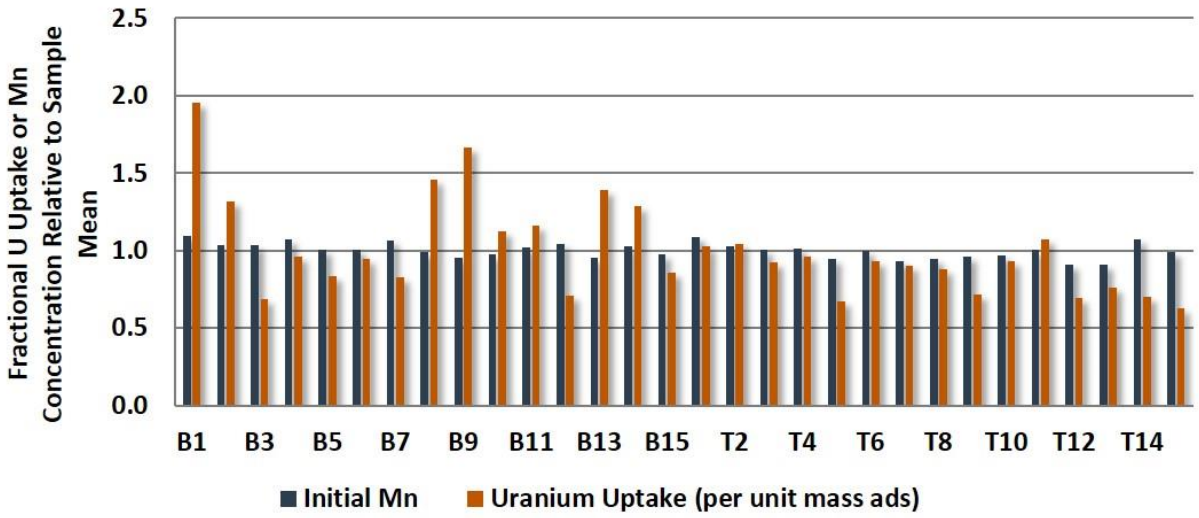

Figure 5: Characterization of pre-existing manganese content in adsorbent filaments and observed uptake under non-fouling conditions. Adsorbents were stacked and numbered (positions 1-15 on Top and Bottom) in a rotated tank with uranium spiked DI water.

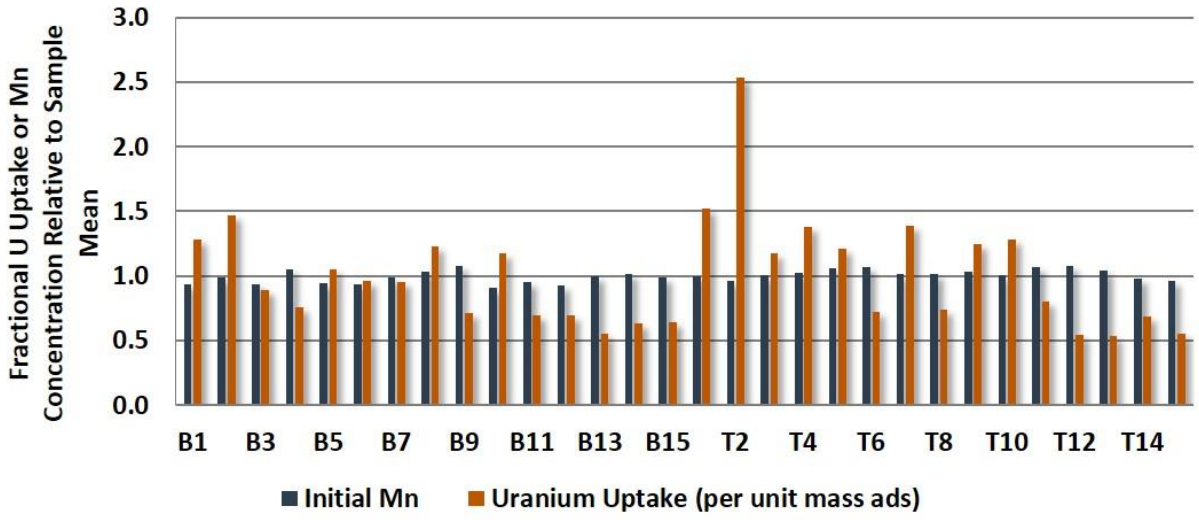

Figure 6: Characterization of pre-existing manganese content in adsorbent filaments and observed uptake under pre-fouling conditions. Adsorbents were stacked and numbered (positions 1-15 on Top and Bottom) in a rotated tank with uranium spiked DI water.

Each pair of bars represents an individual adsorbent sample where in both cases the uranium uptake and initial manganese concertation are plotted as a fraction of the sample mean. The labels on the x-axis refer to the adsorbents position in the deployment tank, which consists of a top, T, and bottom, B, row of 15 adsorbents each.

It is clear that the initial Mn-55 concentration of any individual adsorbent sample does not deviate far from the mean. The uranium uptake however varies significantly with sample standard deviations of 42 and 31% of the mean for the fouled and unfouled adsorbent sets, respectively. Considering uranium uptake on a per unit initial Mn-55 concentration basis does little to alleviate this issue, changing the standard deviations to 44 and 30% of the sample means.

If the variation in uptake performance across adsorbent samples was in fact caused primarily by differences in activated carbon content then it would be expected that adsorbent filaments with higher than average manganese concentrations would

correspond with higher observed uranium uptake. This does not however appear to be the case simply by visual inspection of Figure 5 and Figure 6 where only 33 of the 60 adsorbents analyzed were observed to have a manganese concentration and uranium uptake that both varied in the same direction of the mean, i.e. both greater than or both less than the mean. Further absence of a positive correlation between activated carbon content and uranium uptake can be seen in Figure 7 where the initial manganese concentration and uranium uptake for each adsorbent filament are plotted against each other and the Pearson correlation coefficient is displayed. The low yet negative value for the Pearson correlation coefficient, -0.37, suggests there is no statistical correlation between initial activated carbon content and uranium uptake performance.

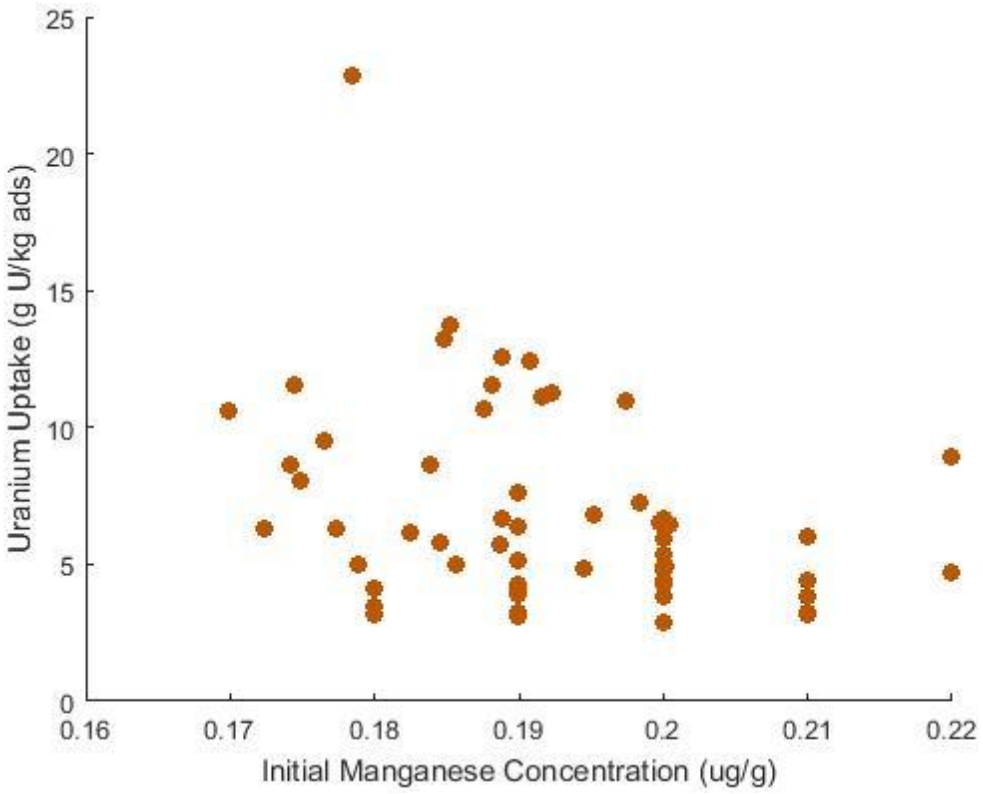

Figure 7: Investigation of correlation between uranium uptake and initial activated carbon content of adsorbent filaments as determined by pre-existing manganese content in the activated carbon.

It is clear that this lengthy analysis and evolving methodology of adsorbent production were unsuccessful in producing homogenous adsorbent filaments with reproducible behavior. While variation in activated carbon content across samples was successfully reduced, it appears as though aggregation of activated carbon particles presented a larger obstacle which could not be surmounted by the aforementioned production means. Therefore a new form of adsorbent, neither fibers nor filaments, but suspensions, was utilized.

4.2: Adsorbent Suspensions

In an effort to ultimately eliminate reproducibility issues across adsorbent performance, the form of the adsorbent was changed. Having concluded from the previously discussed characterization of individual adsorbent filaments that the presumed main source of variation was aggregation of activated carbon in the polymer matrix, the use of high density polyethylene and the extruder were discontinued. Instead, granules of activated carbon were placed directly in solution allowing equal surface area to volume ratios of activated carbon to be exposed to uranium spiked solution in all experiments. The resulting performance of these adsorbent suspensions is discussed in the remainder of this section.

4.2.1: Adsorbent Suspensions Kinetics

Time series data for adsorbents in suspensions was collected in order to quantify the relationship between uranium uptake and length of soaking campaign as seen in Figure 8. Granules of activated carbon were suspended in deionized water spiked to 500 ppm uranium. The uptake data for each time point was collected via a batch experiment such that all solutions were initialized to 500 ppm uranium and the concentration was not adjusted until the conclusion of the time trial in which the entire mass of adsorbent was removed rather than removing components of the suspension over time as to not perturb the system.

Following the methodology applied to the ORNL adsorbents, the time series data was first fit, using an ordinary least squares regression, to the one site ligand saturation model seen in Eqn. 14 where U is the time dependent uranium uptake, $B_{\max}$ is the theoretical saturation capacity and K_D is the time required to reach half of that saturation capacity. [71].

$$U(t) = \frac{B_{max} t_i}{K_D + t_i}$$

Eqn. 14

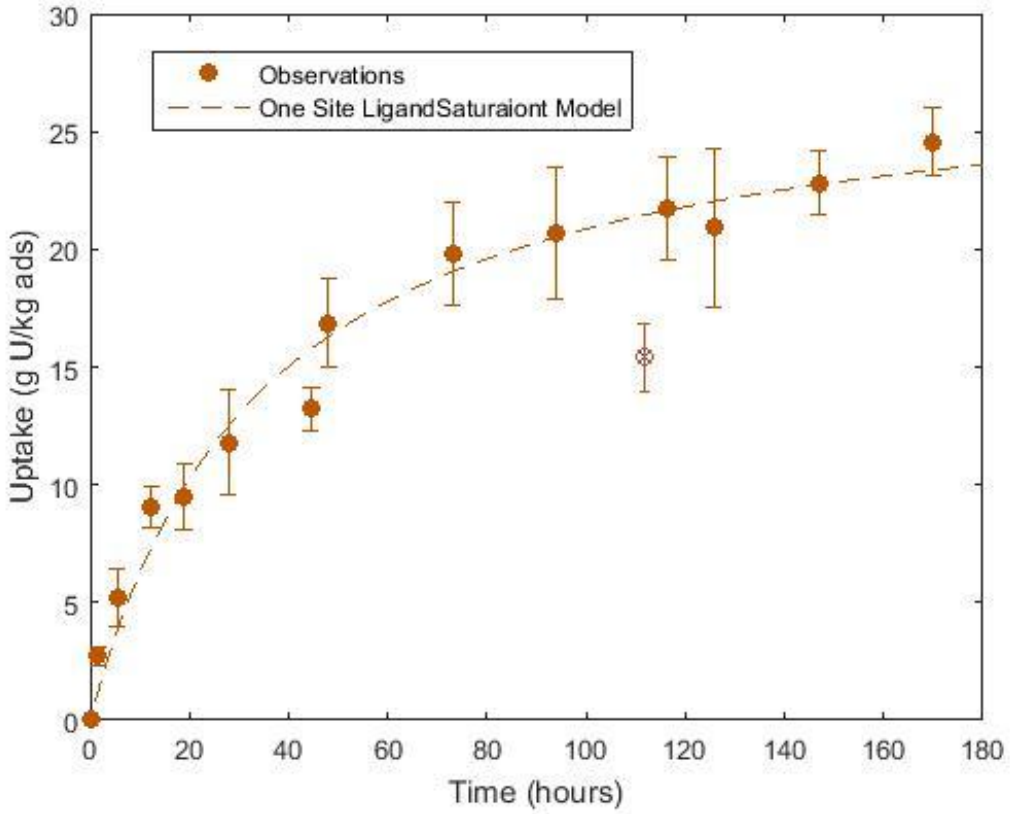

Figure 8: Time series data of suspended adsorbent fit to the one site ligand saturation model

Visual inspection of Figure 8 suggests that the one-site ligand saturation model does not appear to be a good fit at small soaking times. The goodness of fit was thus explored by residual analysis, depicted in Figure 9 and quantitatively in Table 7.

Table 7: Kinetic parameters of the one-site ligand saturation model

	Value	Sigma	% Sigma	Residual Sum of Squares
B_{max}	28.1	1.4	4.9%	1.5
K_D	35	5.3	15.1%	

The uncertainty on the kinetic parameters is higher than desired, especially when considered in light of the uncertainty surrounding the ORNL adsorbents: 3% of the saturation capacity and 7% of the half saturation time.

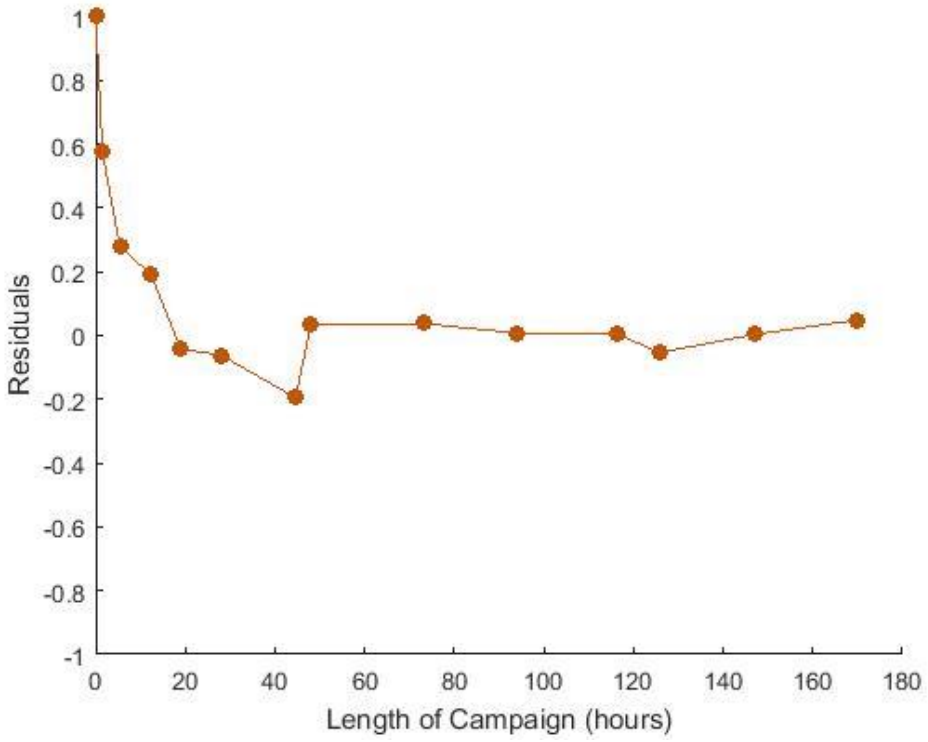

Figure 9: Evidence of heteroscedasticity of adsorbent suspension uptake performance

The residuals are examined as fraction of the time dependent uptake to account for the increase in the absolute value of the residuals with soakinging time, which is not

necessarily indicative of the goodness of fit. The non-random scatter of the residuals suggests that the one site ligand saturaiton model is systematically underestimating adsorbent uptake for short exposure campaigns. This is particularly important given that, in the interest of time, short uranium exposure periods are desired for the majority of experimentation. This dependence of the variance of the errors of sub-populations on the predictor variable commonly appears in econometrics and is referred to as heteroskedasticity.

Formal tests have been developed for the detection of heteroskedasticity in linear regression models, notably the Breush-Pagan test [72]. The Breush-Pagan test can be applied generally to a linear model $y = \beta x + u$ by examining the residuals vector, u. A subsequent regression can be performed on the residuals over the independent variable: $u^2 = \alpha x + v$. If the value of the coefficient α is statistically different from 0 then the null hypothesis of homoskedasticity may be rejected. Use of the Breush-Pagan test on the time series uptake data with the one site ligand saturation model yields a p-value of $1.03x10^{-4}$ on the coefficient α confirming the presence of heteroskedasticity with respect to soaking campaign.

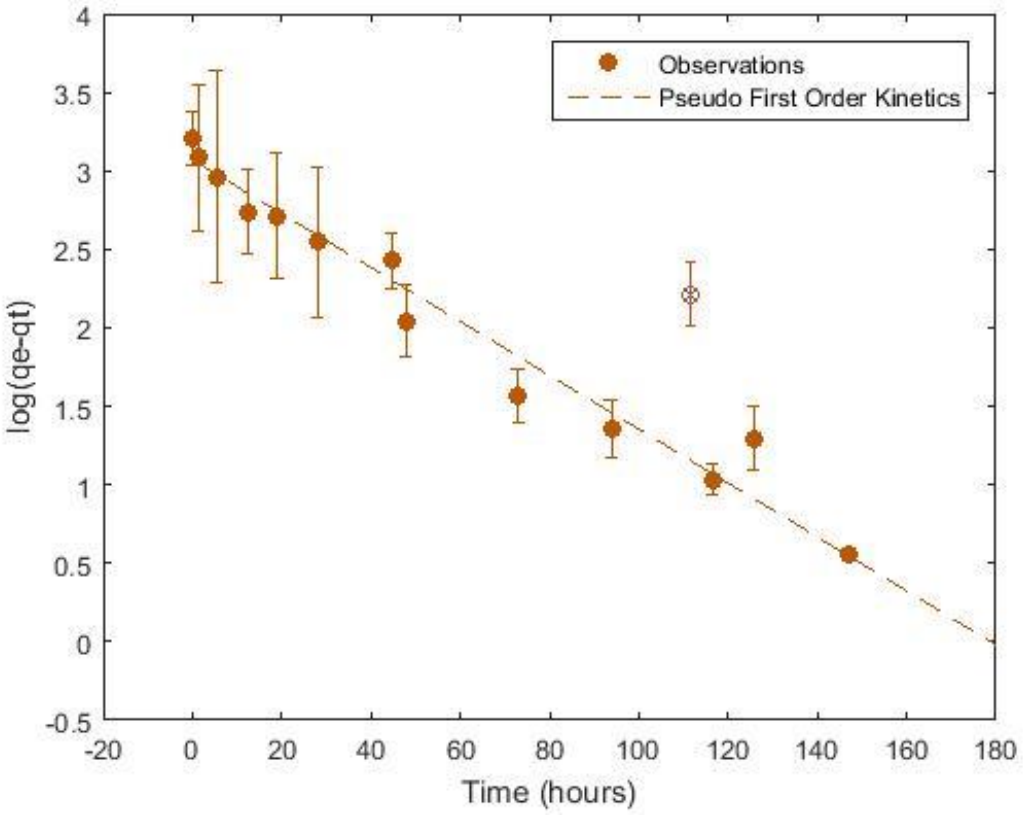

Figure 10: Adsorbent suspension uptake performance fit to pseudo first order kinetics model

Common methods for addressing heteroscedasticity in data include the transformation of the dependent variable. This procedure, and the use of a log transformation specifically, is further supported by review of the literature for alternative adsorbent uptake models. Previous publications examining the viability of coconut shell activated carbon for uranium removal from radioactive waste streams have investigated adsorbent kinetics and found a pseudo first order kinetics model to most appropriately characterize the adsorption of uranyl ions onto activated carbon sites [73] [74]. The first order pseudo

model, seen in Eqn. 15, is a function of the Lagergren rate constant, K_1, and the adsorbent capacity at equilibrium, q_e.

$$\frac{dU_t}{dt} = K_1(q_e - U_t)$$

Eqn. 15

Integration and application of the initial condition $q_{t(0)} = 0$ yields the following prediction for time dependent uptake (Eqn. 16). The data is plotted using this model in Figure 10. A linear least squares regression is used to determine the coefficients dictating adsorbent performance, the results of which can be seen in Table 8.

$$\log(q_e - q_t) = \log(q_e) - \frac{K_1}{2.303}t$$

Eqn. 16

Table 8: Kinetic parameters of the pseudo first order kinetics model

	Value	Sigma	% Sigma	Residual Sum of Squares
q_e	22	1.4	4.9%	0.14
K_1	.039	.002	6.6%	

It is evident that the pseudo first order kinetics model is a better fit for the observed data. The residual sum of squares resulting from the first order model is much lower than the one site ligand saturation model, indicating the predicted uptakes are closer to the observed data points. When analyzing both models the residuals were considered relative to the time depended uptake to counter act the absolute increase in residual value with increasing soaking time as well as decrease resulting from the log

transformation. Additionally the standard error on the regression coefficients is lower in the case of pseudo first order kinetics model indicating it is a better fit for the data.

Upon further consideration, the unsuitability of the one site ligand saturation model can likely be attributed to experimental design. The availability of laboratory equipment and the nature of these studies resulted in the use of batch experiments as opposed to the flow-through style column and flume experiments conducted at PNNL with the amidoxime-based polymeric adsorbents. This difference is significant because in the PNNL studies once the seawater has come into contact with the adsorbents it is either not disposed of or is recirculated along with a constant supply of fresh seawater. The ability to maintain a constant ambient seawater concentration justifies the use of the one site ligand saturation model which assumes the uranium concentration remains constant in the bulk solution.

In the case of the batch experiments conducted with the surrogate adsorbents, however, the concentration of uranium in the bulk solution did not remain constant over time. Instead the concentration of uranium in solution was initially fixed, in this case spiked to a level of 500 ppm, and then decreased over time as uranyl ions are removed from solution by adsorption onto the activated carbon sites. In the case of the longest time point analyzed in the experiments pictured in Figure 10 and Figure 11, approximately 1 week, the mass of uranium adsorbed onto the activated carbon was on the order of 3.7 mg. When considered in light of the approximately 25mg of uranium added to each solution and the one site ligand saturation model assumption that the uranium concentration in the bulk solution remained constant, this value is not necessarily negligible but also not so large as to completely invalidated the one site ligand model. This likely explains why the model is apoor, although not completely erroneous, fit for the observed data, and sees the most significant deviation at short

exposure cycles where the uranium concertation in the bulk solution is seen to decrease at the most dramatic rate. The first order rate expression, on the other hand, depends upon the uranium concentration, which is assumed to decrease with time.

It is also worth pointing out that in fitting both models to the observed data, one data set was excluded. The set of adsorbents exposed to the uranium spiked solution for 5 days (112 hours) was observed to have uncharacteristically low uptake. This can be visualized in Figure 8 and Figure 10. The removal of this set can be justified mathematically by first solving for the expected uptake, $q_t(112hrs)$, by rearranging Eqn. 16 to yield Eqn. 17.

$$q_t = q_e(1 - e^{-K_1 t})$$

Eqn. 17

The standard propagation of uncertainty is then used to find the uncertainty in the predicted uptake value seen in Eqn. 18.

$$\sigma_{q_t} = \sqrt{(1 - e^{-K_1 t})^2 \sigma_{q_e}^2 + (-q_e t e^{-K_1 t})^2 \sigma_{K_1}^2}$$

Eqn. 18

Using Eqn. 17 and Eqn. 18 to predict adsorbent behavior at 112 hours yields an uptake of 20.8 ± 1.1 g U/kg adsorbent, while the adsorbent set in question was observed to have an uptake of 15.4± 1.4 g U/kg adsorbent. Given the goodness of fit of all other points and the deviation of observed data by more than 3 standard deviations from the predicted value, this set can be assumed to be an outlier and is thus removed from the model formulation process. Given the small relative standard deviation within this sample set it is likely that some systematic error arose, potentially even a clerical error with regards to time records of the adsorbents exposure.

4.2.2: Polyethylene Suspensions

Further deviation from the adsorbents produced by the national laboratory was introduced by the absence of polyethylene in moving away from the filament type adsorbents. While it was assumed that all of the uptake capabilities, in both the national laboratory adsorbent and the surrogate adsorbents used in this work, are provided by the ligand as opposed to the polyethylene, experimentation was carried out to prove this assumption. Time series uptake trials of adsorbent suspensions were conducted, as described above, but with the addition of polyethylene.

In determining the ratio of polyethylene to activated carbon the ORNL adsorbent type that has been most frequently analyzed for economics [75][76][77][78][79][80], AF1 type adsorbents, was referenced. The degree of ligand grafting, DOG, as defined by Eqn. 19, compares the weight of adsorbent before and after radiation induced graft polymerization, w_{before} and w_{after}, respectively.

$$DOG = \frac{w_{before} - w_{after}}{w_{before}} * 100\%$$

Eqn. 19

Although variations exist in degree of grafting across individual AF1 adsorbent formulations, 250% DOG has historically been used as a representative value [2][75][76][77][78][79][80]. Therefore the adsorbent suspensions tested here were formulated to analogously contain weight ratios of polyethylene and activated carbon such that the achieved DOG would be 250%. While it is presumed that the ratio of ligand to polymer backbone impacts uptake abilities with regards to surface area rather than mass, the degree of grafting as measured by mass is the only currently existing means of quantifying this relationship in both the national laboratory and UT surrogate adsorbents was thus utilized.

The results of these adsorbent suspensions containing polyethylene can be seen in Figure 11, with the previously analyzed activated carbon suspensions plotted for reference.

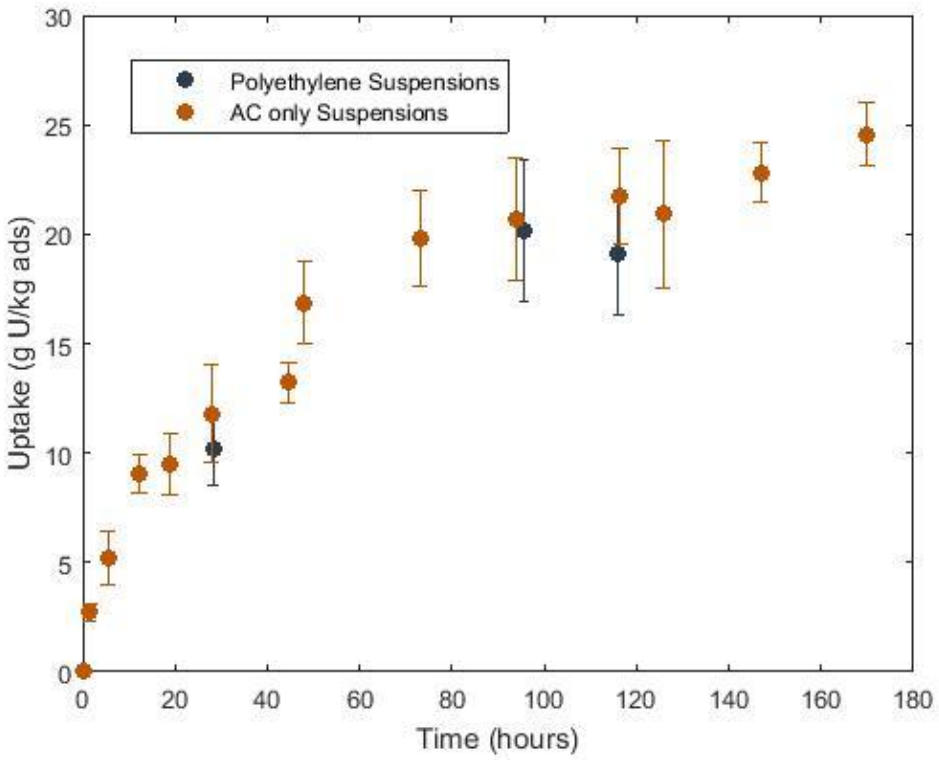

Figure 11: Uptake performance of adsorbent suspensions, including both activated carbon and polyethylene, exposed to deionized water spiked to 500 ppm uranium

As expected, it is appears as though the presence of high density polyethylene does not impact the ability of the activated carbon granules to adsorb the suspended uranyl ions. The presence of polyethylene does, however, slightly increase the degree of performance variation across adsorbent samples in a given batch. This was presumed to be a result of differences in composition of adsorbent suspension samples analyzed for

uptake as there was no way of ensuring homogeneity of each portion of suspension mixture fractionated from the greater adsorbent suspension population. In an effort to avoid the introduction of another source of variation across adsorbents, coupled with the conclusion that the presence of polyethylene does not impact adsorbent performance, it was decided to proceed with suspensions of strictly activated carbon.

Chapter 5: Adsorbent Deployment

An important step in quantifying the effectiveness of silver nanoparticles was the determination of conditions to be used for adsorbent deployments and those required to induce biofouling that would be impactful enough to observe a statistically significant drop in uptake ability. The details of establishing both of these experimental parameters are discussed here.

Experimental procedures were built up in order of appreciating complexity so adsorbent exposure to metal spiked solution, absent any fouling, was first established followed by the implementation of biofouling capable of inducing a statistically significant drop in uptake.

5.1: Exposure to Metal Spiked Solution

In an effort to reduce the potential for introduction of additional variability most adsorbent deployments were conducted using uranium spiked DI water as opposed to real or simulated seawater. Analogous to experiments conducted using the national laboratory adsorbents [2], [8], the solution was spiked with uranium in the form of the uranyl ion, UO_2^+. Unlike the national laboratory experiments, however, this was introduced in the form of uranyl acetate rather than uranyl nitrate, which poses an increased safety risk due to its toxicity and risk of fire.

The screening solution used to down-select promising national laboratory adsorbents based on capacity is spiked to 8 µg/g uranium [2], [8]. Given the lower affinity of activated carbon for uranium as compared to amidoxime, along with instances in the literature of coconut shell activated carbon adsorbing uranium from aqueous solutions with uranium concentrations on the order of 100 µg/g [81],[73], [74], a higher concentration was preferred. In order to reach the equilibrium point quickly enough to

efficiently conduct multiple experiments, a concentration of 500 µg/g was selected; the resulting uptake for this test can be seen in Figure 10 where the kinetics were discussed. These experiments were conducted by exposing suspensions consisting of 0.5 grams of activated carbon to 50mL of uranium spiked solution, in triplicate, at room temperature under constant stirring.

Before the decision was made to conduct uptake and fouling trials utilizing uranium, adsorbents were exposed to solutions spiked with manganese to avoid the superfluous creation of radioactive waste, as previously discussed. Time series experiments were likewise conducted in solutions of DI water spiked with varying concentrations of manganese sulfate monohydrate salt, purchased from Sigma Aldrich as well as Instant Ocean, a commercially available sea salt mixture for simulating seawater in aquariums. The uptake of adsorbents exposed to manganese spiked simulated seawater can be seen in Figure 12.

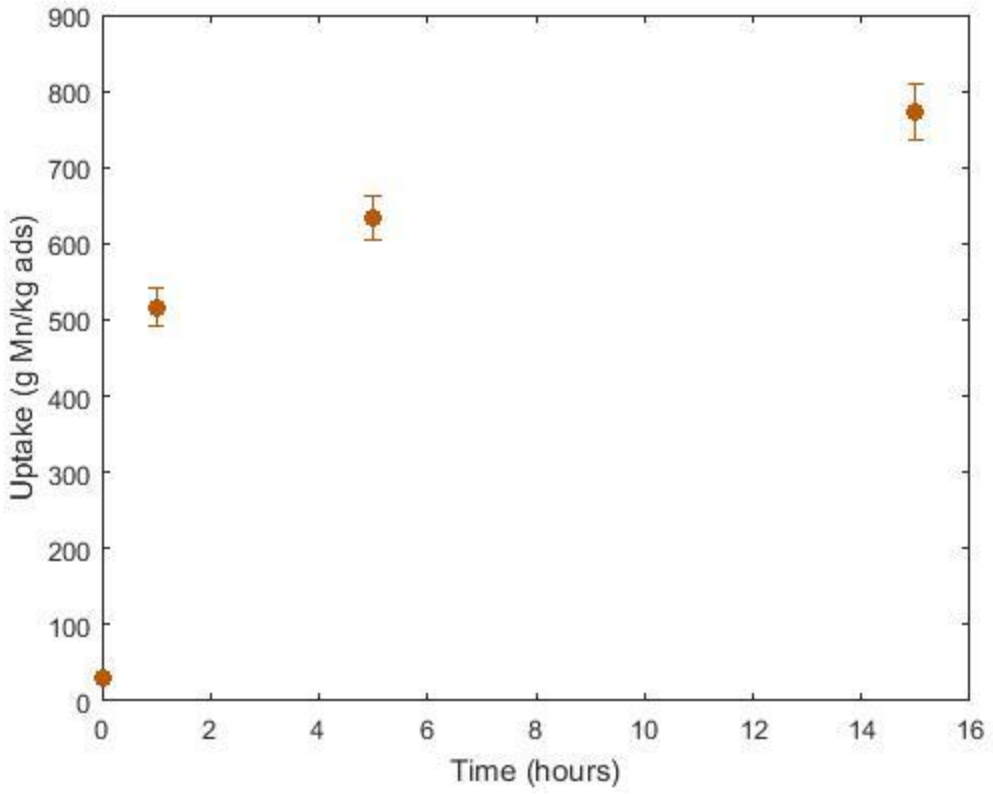

Figure 12: Uptake of early adsorbent exposed to simulated seawater spiked to 1,000 ppm manganese

The uncertainty on these uptake data points corresponds to the measurement uncertainty resulting from NAA concentration quantification and is thus much smaller, in relative terms, compared to the deviation across sample sets displayed in previous adsorbent loading curves. It is also worth pointing out that although it appears there are no error bars on the zero time point adsorbents, those which were never deployed in manganese spiked seawater, the same approximately 1% uncertainty is likewise present but too small to visualize.

The faster uptake kinetics observed for uptake of aqueous manganese as compared to uranium matches experimentation of activated carbon performance in the literature [82][75][76][85].

5.2: Adsorbent Fouling

Before carrying out further experimentation to test the antifouling capabilities of silver nanoparticles it was necessary to first identify the conditions in which marine biofouling had a non-negligible effect on the uptake of uranium by adsorbent samples. To expedite the fouling process and mimic the pre-fouling carried out by PNNL, a biphasic deployment process was used where in adsorbents were subjected to a pre-fouling stage, before being exposed to the uranium spiked solution. The literature was reviewed to identify a fouling agent most appropriate for experiments moving forward and ultimately *Vibrio fischeri*, a bioluminescent marine bacteria, was selected.

In order to ensure reproducible inhibition of uptake on these adsorbents the literature was reviewed in search of commercially available microorganisms possessing specific relevant properties. Since not all organisms contribute to biofouling equally and given that the primary goal of this mitigation technique is to prevent the initial biofilm phase of fouling, a microorganism known for creating biofilms is most suitable. Growth on activated carbon should also be possible in order to impede uptake. To ensure translation of the effectiveness of this mitigation technique as tested in laboratory conditions to marine environments, the fouling agent must be a natural inhabitant of marine ecosystems. Lastly, and perhaps most importantly, the safety of the experimenters must be considered so any species known to cause severe human health issues should be avoided. Table 9 shows some of the results of the down selection process. From this review it has been decided that the commercially available*Vibrio*

fischeri will be used in future experimentation. This choice is further supported by the fact that this is a bioluminescent species. Given the dark appearance of activated carbon and thus the adsorbents, the observation of biofilm formation will not be easily observable by color change.

Table 9: Microorganism species considered for use in pre-fouling of adsorbents

Microorganism	Growth on Activated Carbon	Biofilm Forming Organism	Notes or Hazards	Natural Habitats
Flavobacterium johnsoniae	yes[84]	yes[85]		Soil and Freshwater[86]
Vibrio vulnificus		yes[87]	Highest death rate of any food-borne disease agent[87]	Marine Environments[87]
Navicula pelliculosa		yes[88]		Freshwater Diatom[88]
Ulva fasciata		Later stage of biofouling[89]		Marine Environments [90]
Pseudomonas fluorescens	yes[84]	yes[91]		Marine Environments[92]
Vibrio fischeri	AC Promotes growth[93]	yes[94]	Bioluminescent [94]	Marine Environments [94]

A pure stock culture of plated *Vibrio fischeri* (ATCC 49387) was obtained from PNNL. The culture was maintained in solutions of nutrient rich AB media [95] and on AB agar plates. From the variety of media suitable for bacterial growth availableboth as published recipes and commercially prepared off-the-shelf products, AB media was selected due to the initiation of the master *Vibrio fischeri* culture using that particular

media. Additionally, this particular nutrient rich media has a relatively high salt content, which aids in the avoidance of contamination by providing harsher growth conditions for other bacterial strains less apt for growth in such high salt environments. Pre-mixed and autoclaved AB media was provided from PNNL. The received culture was maintained at 4^0C while plates and/or media solutions were re-cultured every 1-2 weeks to ensure viable cells would always be available for experimentation.

Following selection of the most appropriate fouling agent, the particulars of the pre-fouling stage were determined through experimentation, notably time of fouling and composition of fouling solution. To determine these parameters a series of small scale fouling control experiments, of the form displayed in Figure 13, were conducted. These five conditions were tested at multiple time points and the adsorbent performance analyzed.

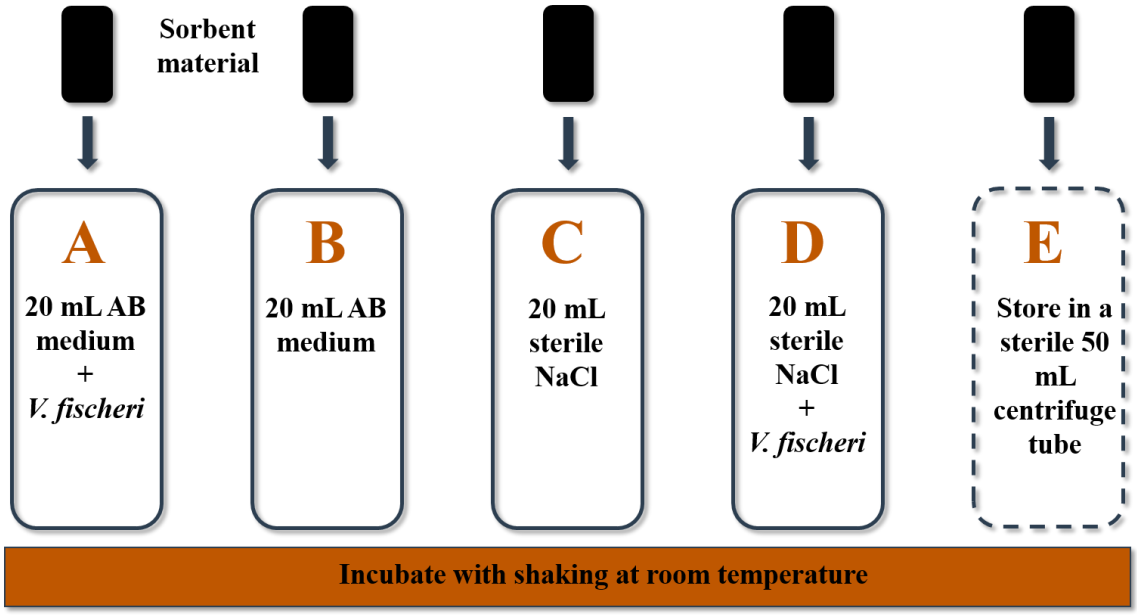

Figure 13: Visualization of degrees of fouling conditions tested in fouling control experiments

Condition A was included in the fouling control experiments as this procedure most closely resembles those used by PNNL in the pre-fouling of the ORNL adsorbents [3]. Condition B was included as it also mirrors pre-fouling procedures conducted by PNNL (unpublished) in an effort to isolate the effects of biofouling resulting directly from the growth of *Vibrio fischeri* as opposed to simply the abiotic conditioning film created from the macromolecules in the media. Conditions C and D were included to examine the effects of fouling by the abiotic condition film and the competition of some other ions that will be present in real seawater. The use of a 3% NaCl solution was selected because that was the buffer used for resuspension of *V. fischeri* cells. Lastly, condition E served as the negative control to represent the behavior of unfouled adsorbents, to which all other conditions would be compared.

The preparation of conditions A and D were carried out as follows in order to be certain bacterial growth was occurring. Most importantly however, an aseptic technique was implemented to avoid contamination, thus ensuring the bacterial growth was in fact the desired *Vibrio fischeri,* as opposed to other bacteria existing anywhere in the laboratory. A single colony of *V. fischeri* (ATCC 49387) was obtained using a sterile inoculating loop from the master culture provided by PNNL and immersed into a sterile 50mL centrifuge tube containing 20mL of either autoclaved AB media or vacuum sterilized 3% NaCl. After inoculation of the respective fouling solution the culture was incubated overnight with shaking at room temperature under aerobic conditions. Once growth was observed in condition A, as denoted by transformation of the media from transparent to opaque, equivalent masses of adsorbent were added to centrifuge tubes representing each condition.

Fouling control experiments using the aforementioned conditions were conducted at a variety of time points to determine an appropriate length of time for the pre-fouling

stage. In the PNNL procedures the length of the fouling stage could be quantified by the observation of growth on the adsorbent fibers, indicated by a color change. The dark appearance of the activated carbon however renders the use of visual inspection of color change less effective. The bioluminescent ability of *V. fischeri* was targeted with the hopes of being able to observe growth on the adsorbent surface upon examination in a dark room. When adsorbent material was viewed in the absence of light a glow could be observed, indicating the presence of viable cells. The presence of *V. fischeri* in aqueous form however resulted in light emanating from the entire solution, so it was not possible to differentiate between cells that had established a biofilm on the surface of the adsorbent from those suspended in solution. Therefore a series of time points were tested so the uptake performance could be compared and used for determination of the conditions to be used moving forward.

A variety of incubation time points were selected in order to both allow sufficient time for the formation of a biofilm as well as including incubation times short enough to attempt to isolate the growth of *Vibrio fischeri* as opposed to any slower growing contaminants. Short fouling periods, on the order of several days were included with the hopes of providing enough time for colonization of *Vibrio fischeri* while ending the pre-fouling period before slower growth organisms that may have found their way into the media, originating from the surface of the non-sterile adsorbent or simply the surrounding air, would compose a significant portion of the population. Observation of the non-cultured media after periods as short as 3 and 4 days indicated growth of other organisms, as noted by opacity of the media. Therefore even shorter fouling periods, one and two days, were attempted so that the media that had not been inoculated with *Vibrio fischeri* was still transparent at the conclusion of the pre-fouling phase, suggesting minimal bacterial growth had occurred. At the other extreme, longer pre-fouling periods were

explored by continually observing media for additional signs of growth. After observing inoculated media for a week, what appeared to be macroscopic signs of fouling, a free floating film appeared in the media, and so fouling periods on the order of seven days were also explored.

Each fouling period was ended by carefully drawing the fouling solution away from the adsorbent using a sterile serological pipette. A volume of 50mL of uranium solution, either DI water, simulated or in later cases real seawater based, spiked to 500 ppm uranium was then added to all adsorbent conditions for the exposure period. It is recognized that this method would not be sufficient in removing the entirety of the fouling solution and some would thus become mixed into the uranium spiked solution. This was by design as it is believed to best represent the true deployment conditions of the ORNL adsorbents when placed in the ocean where the fouling and exposure to uranium will in fact occur simultaneously.

Each set of adsorbents was exposed to uranium spiked solution for a period of approximately 48 hours as determined from the previously conducted kinetics study. Although the equilibrium point is not reached until closer to 1 week of uranium exposure, the 48 hour exposure cycle was selected in the interest of time, while maintaining an acceptable deviation within sample sets.

Figure 14 depicts the uptake performance achieved by adsorbents exposed to each condition, from which several important conclusions can be drawn. Broad conclusions regarding the objective of these control experiments can be made by simply comparing the behavior of adsorbents in conditions A and E, as denoted in Figure 13. Perhaps the most apparent, and most important, is that pre-fouling of adsorbents can in fact lead to a statistically significant decrease in uranium uptake as compared to unfouled adsorbents,

as noted by the large drop in uptake suffered by adsorbents pre-fouled in media with *V. fischeri* as compared to the negative exposure control.

Furthermore, it appears as though the effects of biofouling on adsorbent uptake are independent of the length of fouling time. While this may at first seem to be counter intuitive given the time dependent nature of bacterial growth, this agrees with the observations made in the PNNL biofouling experiments[3]. This is further supported by insight gained from the literature review that the initial stages of biofouling occur within seconds to minutes of immersion of a surface into the ocean.

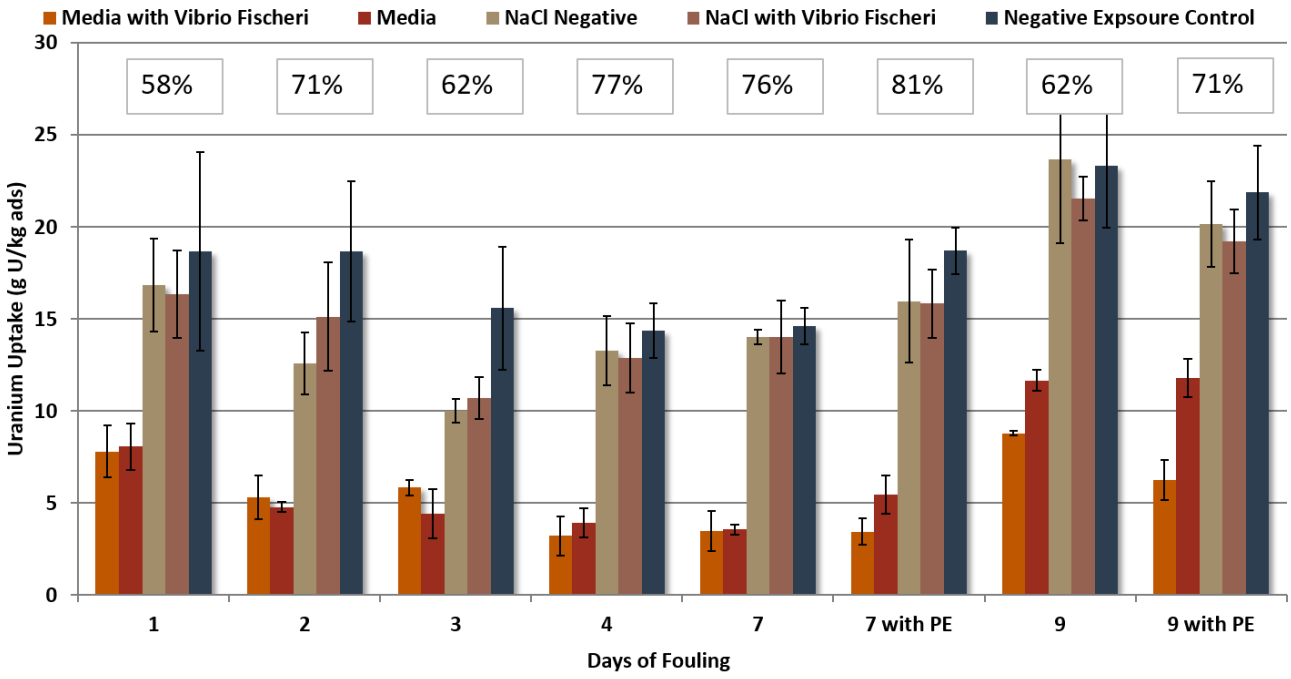

Figure 14: Resulting uptake performance from adsorbents used in fouling control experiments

Additional, more subtle, conclusions can be drawn upon further examination of the results. Comparison of the uptake of the negative exposure control adsorbents

(condition E) to those exposed to conditions C and D yield no significant difference. This indicate that the 3% NaCl solution cultured with *Vibrio fischeri* is not sufficient to cause notable effects from fouling, likely because a simple salt solution cannot sustain bacterial growth. Considering the performance of condition C adsorbents in light of the negative control adsorbents however allows for speculation of performance in the presence competing ions. In all but one experiment the average uptake achieved by adsorbents in condition C was lower than, but could not be declared statistically different from that achieved by adsorbents in condition E, as determined by the use of ANOVA. This suggests that while adsorption of competing ions present in real seawater may have some impact on uranium uptake, it is not likely to dramatically decrease performance ability of the activated carbon adsorbents tested here, although this may not necessarily be true with a binding ligand like amidoxime. Furthermore, this supports the conclusion that the loss in uptake observed by condition A is in fact a result of marine biofouling rather than simply the effects of competing ions.

The observation of similar uptake performance by conditions A and B may at first appear troublesome. Given the lack of a statistical difference in all but one experiment, with 9 days of fouling being the exception, between adsorbents fouled in media with and without *Vibrio fischeri* may seem to suggest that adsorption of competing ions rather than marine biofouling is the cause of the hampered uptake. This unlikely conclusion is not supported however by the literature reports of marine biofouling beginning with the establishment of a macronturient conditioning film. Rather it is likely that the very nutrient rich media in which the adsorbents were submerged resulted in significant portions of the adsorbents surface becoming coated with the abiotic macro-nutrients that make up the media and contribute to the earlies stage of fouling, the abiotic conditioning film as discussed in the literature review.

It is also possible that adsorbent exposed to the less severe fouling conditions, trail B, still experienced bacterial growth. Even though no *Vibrio fischeri* was intentionally added to those volumes of media and aseptic technique was carried out to the best of the experimenter's ability, the possibility of contamination still exits. In addition to any ambient airborne bacteria that could have found its way into the media, the introduction of the adsorbent material itself, which was not sterilized prior to being added to the rich media could have likely introduced contamination. This however was believed to be sufficient in representing the deployment of the ORNL adsorbents in true marine conditions as those adsorbents will also be placed in the ocean with ambient bacteria already existing on the surface.

Analogous experiments conducted at PNNL (unpublished but results shared via personal communication) using a media only control similarly noted little difference in adsorbents subjected to pre-fouling in media with and without culture of a microorganisms known to contribute to the production of marine biofilms. Therefore, these fouling control experiments were still considered successful in identifying conditions adequate to induce a quantifiable loss in uptake due to biofouling.

Lastly it is worth pointing out that some fouling experiments were conducted with polyethylene present. This, analogous to the polyethylene deployments included in the kinetics study, was to confirm that the presence of polyethylene would not drastically alter the results. Given that the trend, a loss in uptake suffered only in conditions A and B, follows that of the adsorbents without the added polymer, it was concluded that the presence of polyethylene is not a necessary component in simulating marine fouling and can be eliminated to reduce variability.

Therefore the optimal conditions for promoting biofouling, which would be used in later experiments, were determined to be the biphasic exposure of activated carbon to

AB media, which has been cultured overnight with *Vibrio fischeri*, for a period of at least one day before subsequently exposing to metal spiked solution. Although little quantitative difference was observed in the uptake performance of adsorbents exposed to AB media with and without *Vibrio fischeri,* it was decided to nonetheless culture all media to be used in the pre-fouling of adsorbents to test the biofouling inhibition capabilities of silver nanoparticles against bacterial colonization as opposed to strictly the formation of the abiotic conditioning phase.

Chapter 6: Silver Doping of Adsorbents

This section describes the implementation of the adsorbent doping procedures. Most notably, the determination of the range of silver nanoparticle concentrations to be tested is outlined.

The goal of this work is to restore adsorbent performance to that of adsorbents deployed under bio-actively inert conditions in an effort to lower the uranium production cost. Therefore the fouling mitigation technique must not be so expensive as to offset the economic gains made by increased uranium recovery. The equipment cost associated with implementation of adsorbent doping with silver nanoparticles is expected to be negligible given that the synthesis of the reference national laboratory adsorbents begins with melt extrusion of polymer resins [96], thus the addition of silver nanopowder to the feed would not require any additional capital expenditures. Material costs however of silver nanoparticles would add a very non-trivial component to the raw material and operating costs.

Given the cost considerations it is thus desirable to add as little silver to the adsorbents as possible. Contrastingly, the quantity of silver present must be sufficient to ward off enough biofouling to result in measurable gains in uptake performance. Therefore preliminary research was conducted to determine an appropriate range of silver concentrations for adsorbent doping. This section will first describe the brief literature review as well as the toxicity experiments carried out to determine the lower bounds and breakeven cost calculated to determine the upper bound prior the preparation of silver doped adsorbents.

6.1: Literature Review

The literature was first reviewed in an attempt to identify the minimum possible silver nanoparticle concentration capable of introducing antimicrobial properties. The literature shows that even below 1 wt% silver is satisfactory to cause observable bacterial growth inhibition [30] [97] [98]. This literature value was used as a starting point. Additional silver concentrations were likewise explored in order to determine the relationship between restoration of uptake and addition of silver nanoparticles, as it is assumed these two quantities would be positively correlated. This quantification would thus allow for optimization of adsorbent formulation in order to minimize resulting uranium production cost.

It has also been reported that using stronger Ag concentrations in chemical preparation methods of doping polypropylene with silver nanoparticles leads to slower bactericidal effects as compared to an optimized lower concentration; this was presumed to be due to greater aggregation of larger silver particles [30]. Therefore it is important to explore silver concentrations below which a bio-inhibitory effect is observed.

6.2: Toxicity Experiments

Due to the time intensive nature of constructing and deploying even the surrogate adsorbents used in these experiments the toxicity of silver nanoparticles was tested before synthesizing the doped adsorbents. These microtox experiments were conducted collaboratively at the PNNL Marine Science laboratory under the instruction of Dr. Jiyeon Park.

A microtox test is a standard laboratory practiced utilized by microbiologist to test toxicity by measuring the bioluminescence of bacteria [99]. Bacterial cells, known to be luminescent, are analyzed with and without exposure to test material. The correlation between luminescence and bacterial metabolism can then be used to determine the

toxicity of the sample material on the given bacteria strain. A material is determined to be toxic at an effective concentration, EC_{50} if the luminescence is reduced by 50% after exposure.

These toxicity experiments used *Vibrio fischeri* culture (ATCC 49387), the same strain selected for use in later adsorbent fouling experiments, that had been grown overnight in ALNa [95] broth at 22^0C with shaking. The overnight culture was then used to inoculate 40mL of sterile ALNa broth, which was allowed to incubate until the optical density of 0.25 at 590nm was achieved. Cells were collected via a 5 minute centrifugation at 4150 rpm for washing with 40mL of sterile 3% NaCl solution (pH 7.0). The cells were then re-suspended in 40mL of sterile 3% NaCl solution.

These cell solutions were exposed to varying concentrations of silver micro-particles. Regulations imposed by Battelle national laboratory restricted the use of silver nanoparticles so silver micropowder was instead analyzed. The bacterial luminescence was measured before and after a 30 minute exposure using a Synergy HT microplate reader (Biotek, VT, USA). This analysis was conducted with varying silver concentrations, with each condition in triplicate. An overview of this process can be seen in Figure 15.

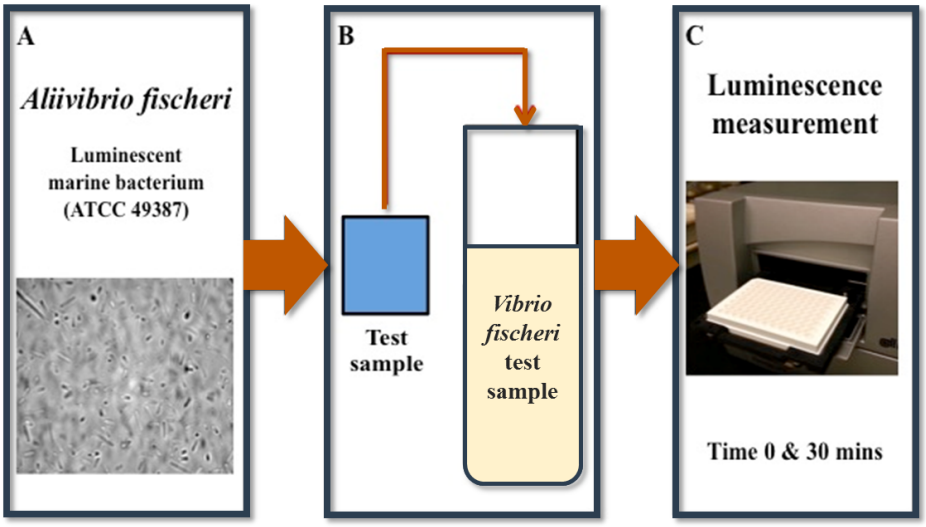

Figure 15: (A) Luminescent marine bacterium *Vibrio fischeri* (ATCC 49387) was used for the test. (B) Testing sample was exposed to *V. fischeri* cell suspension for 30 minutes. (C) Cell suspension samples were collected at Time 0 and after 30 minute of incubation

The luminescence of each test sample was represented as a percentage of the control value, with 100% defined at the luminescence from a sample containing only cells with no silver. It is anticipated however that over the 30 minute period between luminescence readings there will be some natural decay of cells. This correction factor, KF, is simply the ratio of the luminescence of the control sample at the end of the 30 minute exposure as compared to the initial reading. The decrease in luminescence (INH %), and thus toxicity, is then determined using this correction factor as well as the initial luminescence of the sample and control cell population, IT_0 and IC_0 and luminescence after 30 minute exposure to the proposed toxin, IT_{30} as can be seen in Eqn. 20

$$INH\% = 100 - \left(\frac{IT_{30}}{IT_0 * KF}\right)100$$

Eqn. 20

The viability of this methodology was verified using a known toxic solution, $ZnSO_4$, as a positive control. The decreasing luminescence of cell samples exposed to this solution can be seen in Figure 16. As expected, toxicity to the *Vibrio fischeri* population increases as $ZnSO_4$ concentration increases as indicated by the decreases luminescence.

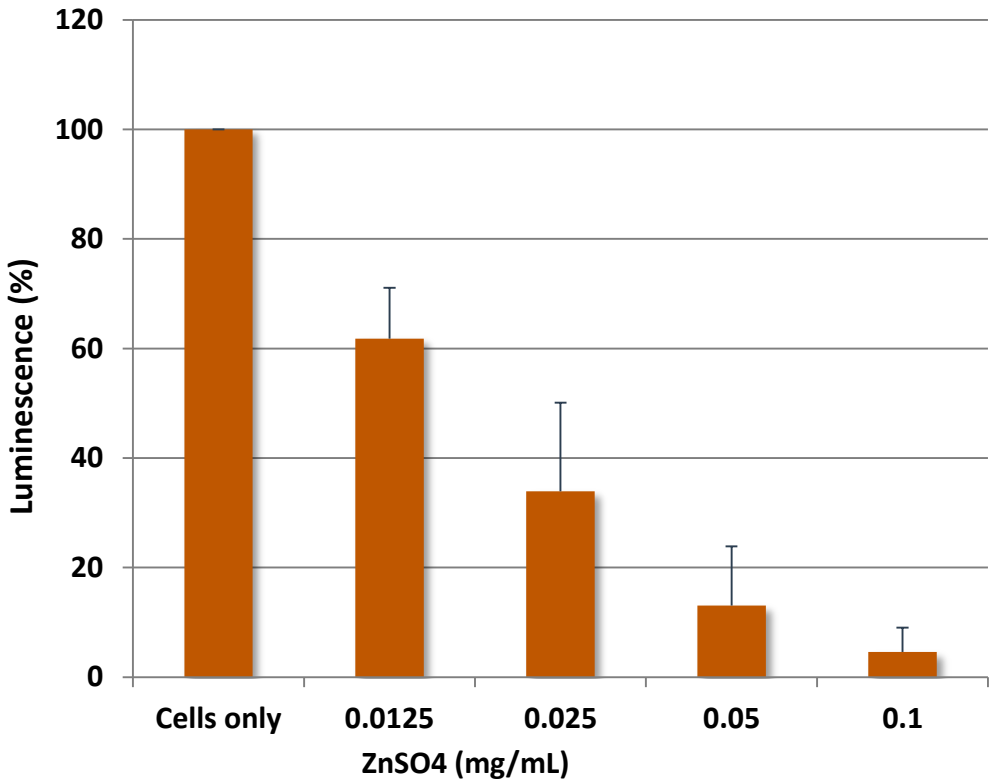

Figure 16: Positive control experiment on *Vibrio fischeri* using known toxin, zinc sulfide, to verify viability of microtox assay

An array of silver concentrations was likewise examined for toxicity; the resulting decrease in bacterial luminescence can be seen in Figure 17 as a function of silver content added.

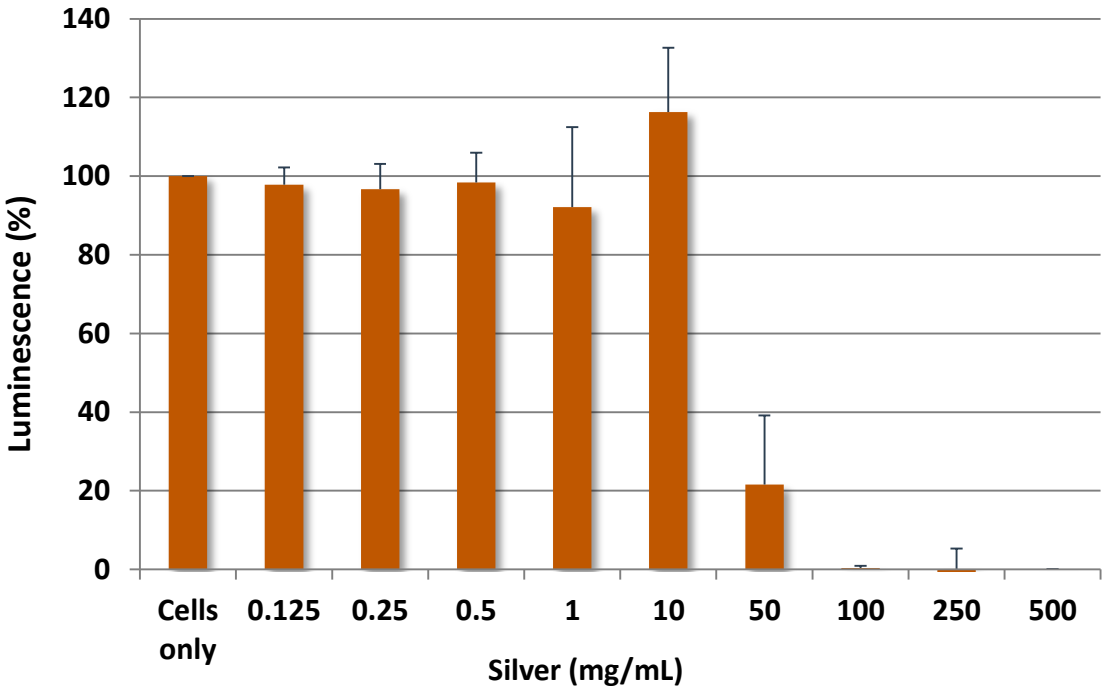

Figure 17: Toxicity of silver microparticles to *Vibrio fischeri* as measured by observed luminescence

These results indicated that the effective concentration for toxicity of silver micropowder, or EC_{50} is 5% by weight. Given the difference in size between micro and nanoparticles is three orders of magnitude coupled with the observations in the literature that decreasing particle size is correlated with increased bio-inhibitory effects [97], some adsorbent formulations with slightly less than 5 wt% silver would still tested in hopes of observing at least partial restoration of capacity. Additionally, the aforementioned toxicity results were for a 30 minute exposure period but adsorbents will be exposed for 10s or hours to days and it is possible that toxicity could increase with exposure time.

6.3: Preliminary Breakeven Calculation

It is important to determine the point at which the mitigation cost exceeds the savings achieved by increasing uptake in order to avoid experimenting with adsorbent formulations that would never be economical to produce. This preliminary breakeven analysis does just that by comparing the uranium production cost of ONRL adsorbents retaining full capacity, but doped with varying levels of silver nanoparticles, to the cost of adsorbents suffering a loss in uptake due to marine biofouling. All uranium production costs were calculated using discounted cash flow methodologies, adsorbent performance, and deployment parameters utilized in previously published systems analyses [78][79][75][96][80]. Additional details regarding the calculation of the final uranium production cost resulting from the reference ORNL adsorbents doped with silver nanoparticles is discussed in Chapter 8.1.

Recent experimentation by PNNL [3] indicates that adsorbents subjected to true marine conditions would result in uranium uptake 30% lower than those placed in bio-actively inert seawater. The cost of seawater uranium collected via adsorbents suffering this 30% loss is displayed as the dotted line in Figure 18 as it represents the upper bound for the uranium production cost associated with silver doped adsorbents.

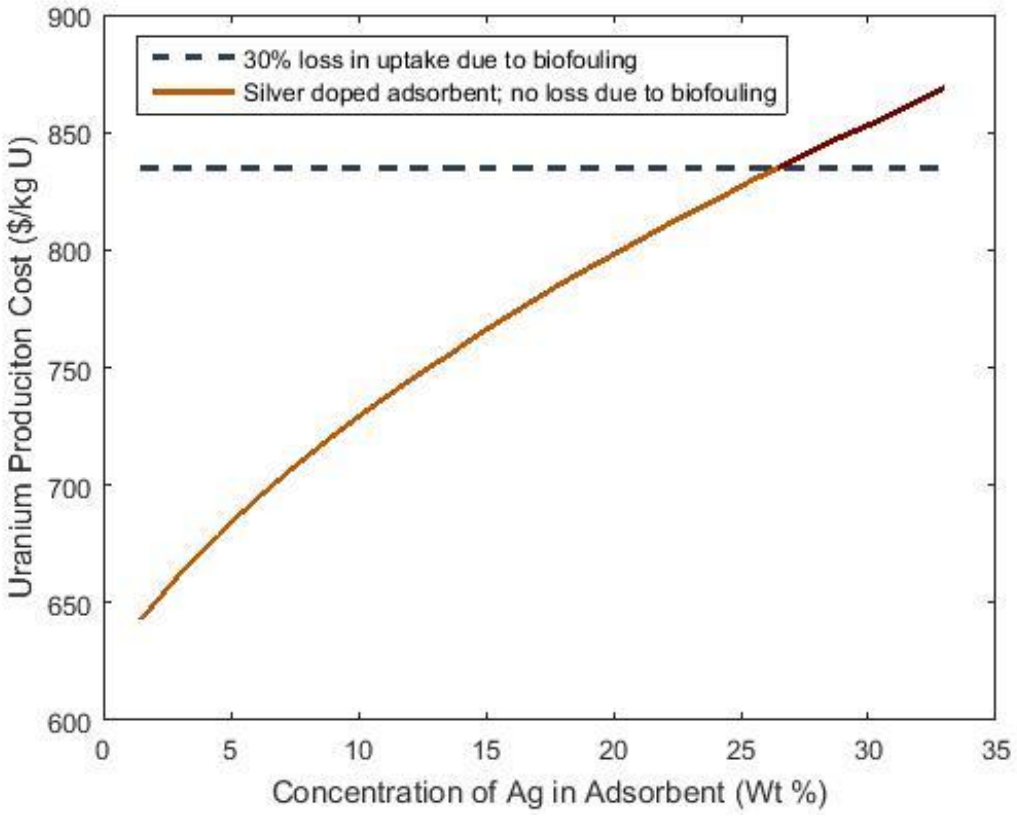

Figure 18: Initial break-even analysis of silver content for determination of upper bound to be empirically tested. The cost of recovering seawater uranium using reference ORNL adsorbents retaining full capacity with varying levels of silver concentration was compared to that of the umodified adsorbents suffering the full loss due to biofouling to determine the point at which mitigation cost exceeds the potential savings offered by increased uptake.

This analysis identifies an adsorbent formulation of approximately 25 wt% silver nanoparticles as the highest silver concentration worth exploring; above this point the cost of producing silver doped adsorbents would result in a uranium production cost greater than the use of unmodified adsorbents that had suffered the effects of marine biofouling.

6.4: Implementation of Adsorbent Doping

A benefit of this biofouling mitigation technique is its simplicity with regards to implementation and applicability to national laboratory and other university adsorbent production. Given that a variety of the currently available amidoxime-based polymeric adsorbents are melt-spun from polymer resins, the extrusion process used in the synthesis of the surrogate adsorbents is analogous to the hypothesized industrial scale production of ONRL adsorbents, which are the sole variety analyzed here for cost savings. Therefore the silver nanoparticles were simply added to the surrogate adsorbent feed material and extruded using the single screw extrusion instrument constructed from the commercially available Filastruder kit.

The silver nanoparticles were purchased in powder form from Sigma Aldrich (CAS Number 7440-22-4). The material was certified to have a particle size less than 150 nm and a purity of 99% and was used as received.

The diminished mixing ability of the laboratory scale Filastruder as compared to the industrial scale extrusion equipment used in the hypothetical scale-up of ORNL and PNNL adsorbent production required additional repetitions of the extrusion process [96]. Following the analysis of adsorbent homogeneity with respect to activated carbon discussed previously in Chapter 4.1.2 the silver doped adsorbents underwent a total of 7 iterative extrusions. In the case of the adsorbent suspensions, the silver nanoparticles were simply mixed with the activated carbon prior to exposure to the pre-fouling solution and/or uranium spiked solution.

It is important to point out however that the presence of the silver nanoparticles in no way hampered the ability of the thermoplastic to undergo the extrusion process. Therefore it was concluded that this mitigation technique would in fact be easily

reproduced in and scale-able to the reference ORNL adsorbents, as well as any of the other existing, or even future adsorbent, variants melt-spun from polymer resins.

Chapter 7: Performance Quantification of Silver Doped Adsorbents

The uptake of uranium by silver doped adsorbents was compared to the unmodified adsorbents to quantify the extent to which the uptake of the silver doped adsorbents was higher than the negative control adsorbents. Adsorbents were first tested in the fouling conditions described previously using the marine bacterium *Vibrio fischeri*. Results were then verified by exposing modified and unmodified adsorbents to real seawater spiked with uranium.

To ensure that any observed improvement in adsorbent capacity was in fact a result of biofouling mitigation, the accumulation of biologically active material on the adsorbent surface was investigated. This chapter describes the quantitative and qualitative methods for analyzing bioaccumulation on the silver doped adsorbents as compared to the negative control adsorbents after deployment.

In addition to the uptake restoration capabilities offered by the silver doping of surrogate adsorbents, the reusability was examined. The current scheme for the industrial scale recovery of seawater uranium includes multiple re-uses of the national laboratory adsorbent fibers, thus requiring the biofouling mitigation capabilities of the modified adsorbents to be retained over time. Given the inability to elute and re-use surrogate adsorbents, the reusability of the silver doped adsorbents was quantified by examining the rate at which silver nanoparticles leached out of the surrogate adsorbent material. The use of NAA and ANOVA on the surrogate adsorbent filaments before and after deployment is described here.

7.1: Capacity Restoration

The effectiveness of the mitigation method will be measured by how closely the presence of silver nanoparticles restores adsorbent uptake to that of the un-fouled

adsorbents,$U_{unfouled}$. The determination of this capacity restoration factor, R, can be seen in Eqn. 1.

$$R = \frac{\mathrm{U}_{Ag} - \mathrm{U}_{control}}{\mathrm{U}_{unfouled} - U_{control}}$$

Eqn. 21

The capacity restoration factor is used in lieu of the mathematically simpler but less informative increase in uptake performance by silver doped adsorbents, U_{Ag} relative to the negative control adsorbents, $U_{control}$, which were likewise exposed to fouling conditions. While a relative increase in uptake would be sufficient in characterizing the efficacy of silver doping in these specific adsorbents under laboratory fouling, in order to apply the observed trends to national laboratory adsorbents the performance improvements must be normalized to the severity of biofouling endured. The denominator in Eqn. 21 serves thus as the normalization factor by considering the performance enhancement from the silver in light of the degree of loss due to biofouling.

The uptake restoration factor was determined for a variety of different fouling conditions. In all performance analysis trials ANOVA was used to test the statistical significance of the capacity recovery factor by determining if uptake achieved by the silver doped adsorbents was in fact statistically higher than that of the unmodified control adsorbents.

7.1.1: Analytical Procedures: NAA

The quantitative analysis of uptake performance by adsorbents doped with silver nanoparticles required slightly different procedures as compared to the irradiation of unmodified adsorbents utilized in the investigation of uptake kinetics. The simple presence of silver in the adsorbents necessitates extra caution with regards to irradiation

due to the highly absorbing nature of naturally occurring silver isotopes. Furthermore, characteristic differences between silver and uranium isotopes require different decay and counting procedures for effective quantification.

The epithermal irradiation of silver nanoparticle doped adsorbents presents challenges due the large resonance integrals of both of the two naturally occurring isotopes of silver, Ag-107 and Ag-109 at 94 barns and 1,112 barns, respectively. Therefore in the interest of ALARA (As Low As Reasonably Achievable) radiation safety practices the irradiation time and power were both reduced, to 10 seconds and 100kW, in an effort to reduce the dose rate of the sample immediately following irradiation. When uranium was the only isotope to be quantified, dose exposure to the experimenter was further minimized by utilizing decay periods sufficiently long enough for the longer lived Ag-108 (2.37 minute half-life) to decay away before the samples were handled manually.

The quantification of silver concentration was eventually desired, in some instances in conjunction with the quantification of uranium uptake, in which case it was not possible to wait for all of the Ag-108 to decay away. The Ag-110, with a 24.6 second half-life, was however allowed to decay away in order to both minimize radiation exposure to the experimenter as well as to allow the dead time to fall below 10%.

When the analysis of both silver and uranium concentrations was sought samples underwent two separate counting periods. The short half-life of Ag-108 required that samples be counted shortly following irradiation, within approximately 20 minutes to avoid allowing all of the Ag-108 to decay prior to counting. A decay time on the order of several minutes was still incorporated to allow the Ag-110 to decay away, reducing dose exposure. This did not exceed the 20 minute window allowed between irradiation and

culmination of counting as the high radioactivity allowed for very short count times, on the order of 60 seconds to achieve 10,000 counts.

The 2.36 day half-life of Np-239, which was used to quantify uranium as previously discussed, however requires much longer count times as well as an approximately 3 hour decay time to allow U-239 to decay into Np-239. Therefore adsorbent samples whose both silver and uranium content were desired were each counted twice: one short count occurring minutes after irradiation followed by a later longer count, on the order of hours.

7.1.2: Restoration Performance Analysis Trials

The performance of the silver doped adsorbents was first tested using populations of adsorbents doped with varying degrees of silver, each subjected to pre-fouling by AB media cultured with *Vibrio fischeri*. At the conclusion of the pre-fouling phase the media was removed using a serological pipet. DI water spiked to 500µg/g uranium was then introduced, initiating the two day exposure period. After two days of shaking at room temperature the adsorbents were removed from solution and dried via vacuum filtration. The adsorbent drying method of vacuum filtration was selected in an effort to systematically remove any uranium that may have dissolved in water simply residing on the adsorbent surface so as to prevent these ions from being counted as actually adsorbed when the sample undergoes irradiation. Uranium uptake from both populations, U_{Ag} and $U_{control}$, was determined using NAA. The population means for each adsorbent formulation was used to calculate the capacity restoration factor to quantify the effect of silver nanoparticles on uptake. Figure 19 shows the capacity restoration factor as a function of silver content in the adsorbent for this performance analysis trial.

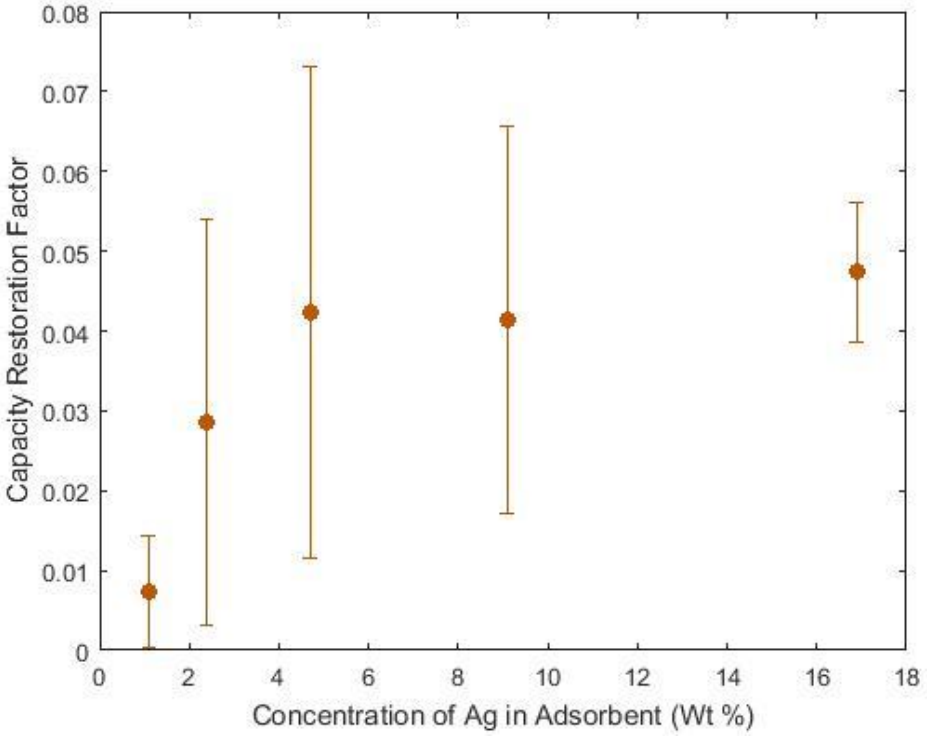

Figure 19: Observed capacity restoration factor as a function of silver content in adsorbent for adsorbents pre-fouled in AB media cultured with *Vibrio fischeri*

As hypothesized, the capacity restoration factor increases with increasing silver concentration. The value of the capacity restoration factor however is lower than anticipated, or hoped for. Given the very extreme fouling conditions these adsorbents were subjected to additional experiments were carried out with the dual aim of providing conditions that would more closely reflect reality and increase the value of the capacity restoration factor.

The large uncertainties will be discussed in further detail in the chapter on uncertainty quantification. In summary, however, the major contributor to the very large relative uncertainty values was identified as the non-trivial variation in adsorbent

performance in the extreme fouling conditions, which is exacerbated by the very low restoration values.

The same AB media used in the pre-fouling phases of the aforementioned trail was originally selected because it is a very rich media that was hypothesized to provide conditions adequate to induce enough biofouling to cause a measurable decrease in uptake. While this initial aim was certainly achieved, the use of the nutrient rich AB media culture with *Vibrio fischeri* may have had the unintended consequence of sustaining biofouling conditions that were too severe to be mitigated by silver nanoparticles, and more importantly, were not reflective of true marine conditions. Therefore a second performance analysis of silver doped adsorbent was conducted with altered pre-fouling conditions.

A mixture consisting of 25% cultured AB media and 75% sterile NaCl by volume was used to pre-foul adsorbents with varying degrees of silver. After a period of 18 days the fouling solution was removed and the adsorbent exposed to the uranium spiked solution for two days. Upon completion of the exposure period the adsorbents were again all vacuum filtered and their uranium uptake measured by NAA. During the pre-fouling period the adsorbents were monitored via visual inspection for signs of impeded growth. Figure 20 depicts the qualitative difference in opacity of the pre-fouling solution for the negative control (left) as compared to silver doped adsorbents (right).

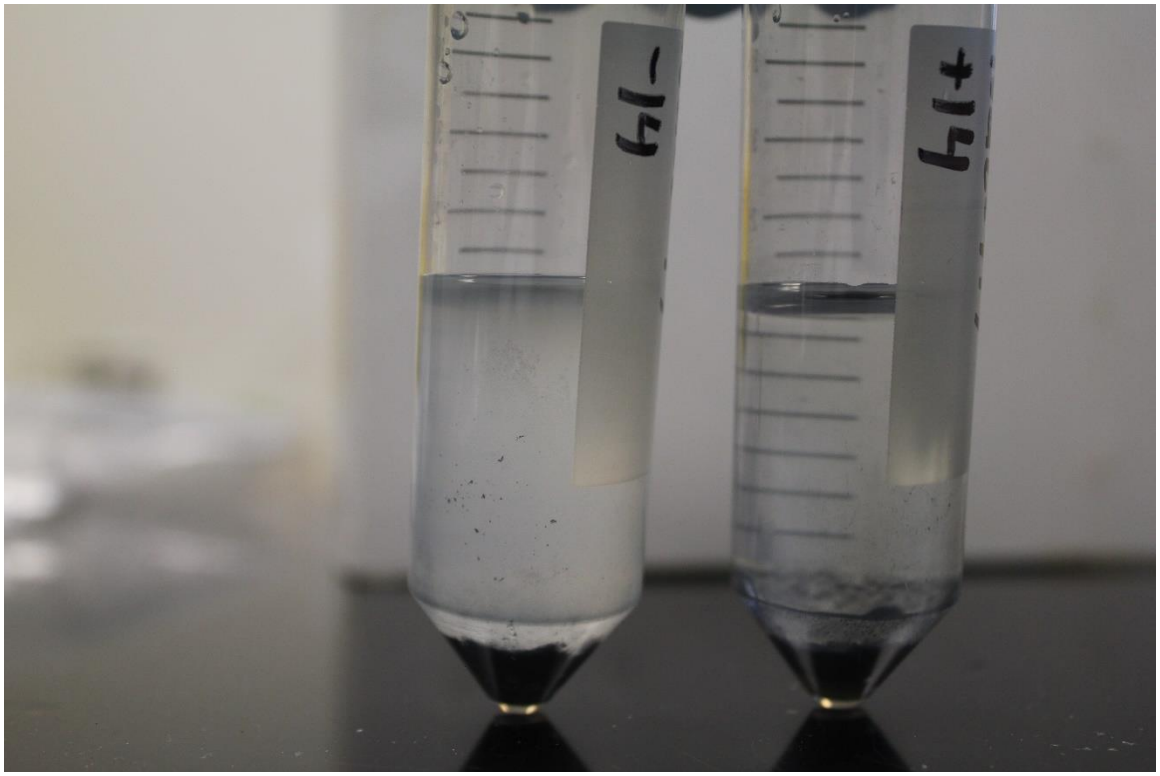

Figure 20: Comparison of bacterial growth occurring in pre-fouling solution during deployment of negative control (left) and silver doped adsorbents (right)

The capacity restoration factor for these adsorbents can be seen in Figure 21, again as a function of silver concentration in the adsorbent.

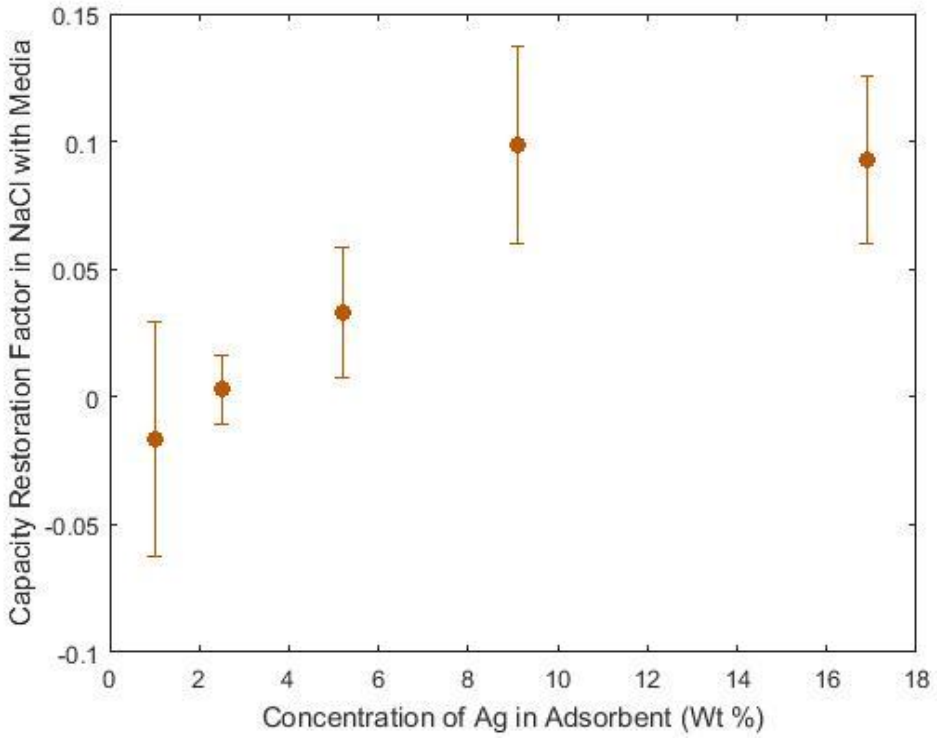

Figure 21: Observed capacity restoration factor as a function of silver content in adsorbents pre-fouled in 25% media cultured with *Vibrio fischeri* and 75% NaCl solution by volume

As predicted, the capacity restoration factor exhibits a similar trend to that of the adsorbents exposed to the very extreme fouling conditions, but with moderately higher values. The qualitative observations made in Figure 20 however would suggest that the quantitative values in Figure 21 would be even higher. Continuing to operate under the assumption that the laboratory fouling conditions were still significantly more extreme than that of true marine conditions, a third performance analysis was conducted.

The capacity restoration factor resulting from adsorbents doped to contain 1 wt% silver warranted further consideration as it seemed to imply the silver nanoparticles may present a mechanism that interferes with uranium uptake. The large uncertainty surrounding this value however makes this conclusion unlikely. Statistical analysis of

both the 1 and 2.5wt% silver adsorbent formulations, using the confidence intervals on the capacity restoration values along with ANOVA on the uptake observed by the modified and unmodified adsorbent populations, suggests that there is in fact no statistical difference between the negative controls and adsorbents doped with this level of silver. Therefore it was decided that moving forward fewer adsorbent formulations would be tested in this region of the domain.

The negative restoration value was also an enlightening result in identifying another potential improvement to be made in future experiments. Given the small quantities of silver being added to the adsorbent, there exist greater potential for relative variation in actual silver content across different adsorbent samples and batches. An attempt was made to revisit the spectra recorded for the adsorbent samples pictured in Figure 21 to see if variation in silver content could partially explain the observed results. Unfortunately, however, since the irradiation and counting parameters used in this experiment were established with the exclusive intention of detecting and counting Np-239, the amount of silver detected, by means of the Ag-110m, was never above the quantification limit. It was thus decided that moving forward the analysis of silver content would likewise be conducted using NAA. Given the significant differences between uranium and silver isotopes activation and decay behavior, irradiated samples were counted twice, according to both of the parameters described previously in the subsection detailing the NAA method used for these experiments.

In an effort to most closely replicate true marine conditions in a laboratory setting, real seawater provided by PNNL was next used to test the efficacy of silver nanoparticles for biofouling mitigation. In order to ensure the presence of biofouling a biphasic approach consisting of a pre-fouling stage was again utilized; the pre-fouling solution consisted of real seawater, enhanced with 5% by volume cultured AB media. In all other

respects the adsorbent preparation, fouling, exposure, and analysis methods were analogous to the previous trials. The capacity restoration factor for varying adsorbent formulations can be seen in Figure 22 with both x and y error bars.

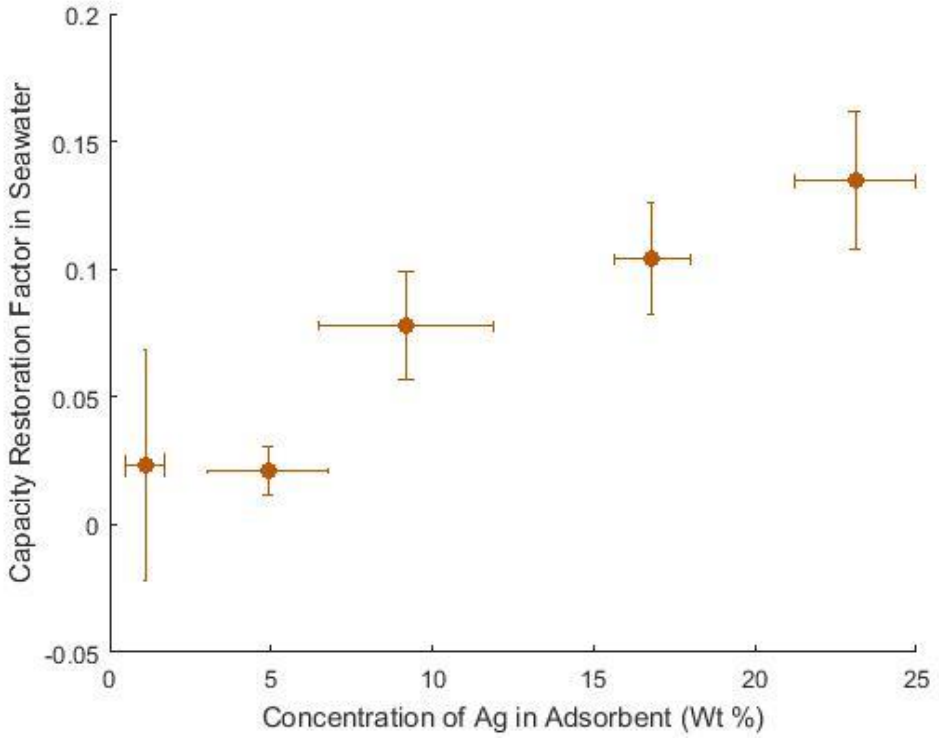

Figure 22: Observed adsorbent capacity restoration factor as a function of silver content in adsorbents pre-fouled in seawater enhanced with 5% media cultured with *Vibrio fischeri*

As expected the capacity restoration factor again exhibits a similar trend to that of the less sever biofouling conditions but with slightly higher values. The restoration factors observed however are still not as large as was hoped for to achieve the ultimate goal of providing a notable cost savings. The presence of an abiotic conditioning film was again suspected to have acted to decrease uptake while withstanding any biocidal effects introduced by the silver nanoparticles.

It was also observed that silver content of adsorbent as determined from the post-deployment NAA was lower than expected by the weight of silver intended to be added to the adsorbent. The loss mechanism of the silver nanoparticles was assumed to be, in part attributed to the use of the biphasic deployment approach; when pre-fouling solution was removed from adsorbent it was evident that some silver nanoparticles dissolved or suspended in solution could be removed.

Additionally, the capacity restoration factor calculated in all additional trials was determined using the uptake of unfouled adsorbents predicted by the kinetic model discussed in the previous section on adsorbent exposure. In the case of adsorbents exposed to real seawater spiked with uranium it is possible that other mechanisms, such as competing ions, could reduce uptake. Therefore a final performance trial was conducted in an attempt to alleviate these issues.

Adsorbents doped with varying degrees of silver, including a negative control, were fouled and exposed to real seawater in a single phase. While seawater was again spiked to achieve 500μg/g uranium, no pre-fouling was conducted and no media was added, thus closely approximating the experience of adsorbents placed in a true marine environment. Instead of comparing adsorbent performance to that predicted by the kinetics model for unfouled adsorbents in DI water, a sample of adsorbents were likewise exposed to spiked real seawater, but efforts were made to eliminate or reduce fouling as much as possible. Following methodologies used in PNNL fouling experiments [3] the seawater was sterilized using a 0.22μm vacuum filtration unit and not exposed to light to limit photosynthetic growth. The resulting uptake and capacity restoration factor for adsorbents subjected to these conditions can be seen in Figure 23 and Figure 24.

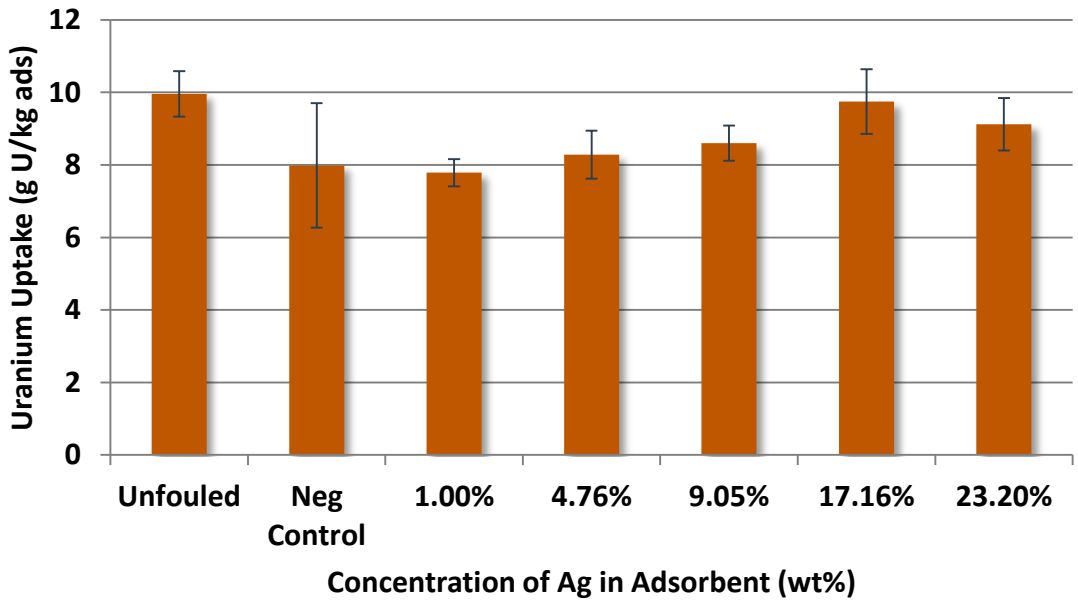

Figure 23: Uptake for adsorbents deployed in spiked seawater, without a pre-fouling treatment

It is first important to note that the difference in uptake between the unfouled adsorbents and negative control adsorbents was in fact statistically significant, as determined by ANOVA. Although the error bars appear to overlap, the single factor ANOVA test conducted yielded a P-value of 0.0017 and an F statistic of 11.4 with an F critical of 4.1, allowing rejection of the null hypothesis that the two groups can be characterized by the same mean. This contrasts with previous experiments using the adsorbent filaments, results not show here, where statistically significant biofouling was not observed using real seawater with the light and sterilization procedures described above.

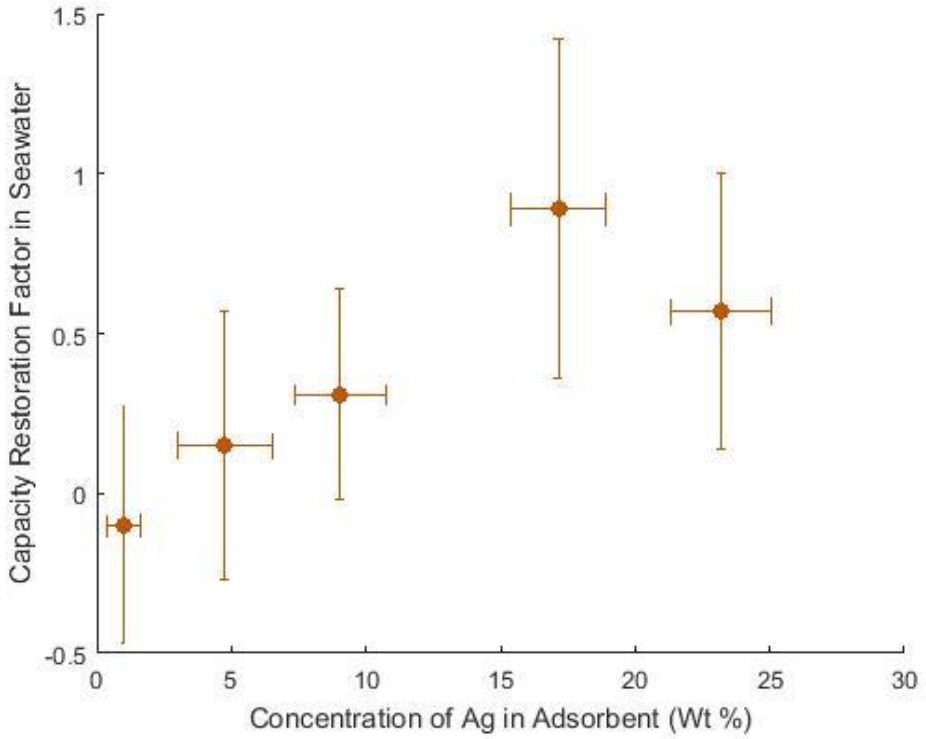

Figure 24: Observed capacity restoration factor for adsorbents deployed in spiked seawater, without a pre-fouling stage

The trend in capacity restoration factor as a function of silver content in adsorbent again aligns with previous trials but with restoration factors of much greater magnitudes. Higher capacity restoration factors will propagate to more favorable economics, but the large uncertainty bars on each point must be propagated as well, and will be discussed in a later chapter on uncertainty quantification. The increase in uncertainty on capacity restoration factor was a result of increased standard deviation within each set of adsorbent samples. This variation in adsorbent performance should not be surprising given the use of real seawater which likely introduces more inconsistencies and complexities as compared to spiked DI water.

7.2: BIOACCUMULATION

In an effort to ensure that the differences in uptake observed were in fact due to the inhibition of biological growth, experiments were conducted to quantify the mitigation of growth directly. Given the difficulty in accurately quantifying such small changes in weight and isolating the weight gain due to microorganism growth as opposed to adsorbed metals and water logging, multiple methods were explored. First the simple weight gain of silver doped adsorbents was compared to that of the negative control adsorbents. Additionally, viability of continued growth on the adsorbents post deployment was examined by placing adsorbents in a nutrient rich environment.

It is worth noting however that instances were seen in the literature of uranyl ions adsorbing onto silver nanoparticle surfaces [100][101]. Therefore it is entirely possible that a degree of the enhanced uptake achieved by the silver doped adsorbents resulted from uranyl adsorption to the silver nanoparticles directly. This mechanism of capacity increase can be considered a desirable by-product of silver nanoparticles as it still works toward the overarching goal of decreasing the production cost of seawater uranium by improving adsorbent efficiency.

Activated carbon adsorbent samples were weighed prior to and following deployment so that the weight gain could be assessed. Since it is impossible to track the weight of any individual adsorbent granule, the weight of the total adsorbent population was recorded before being subjected to the pre-fouling phase. Following the uranium exposure the population is then split up into a collection of smaller samples, in part so the variability across subsets of the population could be analyzed, and the weight of each sample recorded. The sum of the weight of all samples is then compared to the weight of the population prior to deployment. The resulting weight gain, as a fraction of initial

adsorbent weight, for the series of adsorbent formulations fouled in cultured AB media and discussed previously in section 7.1 can be seen in Figure 25.

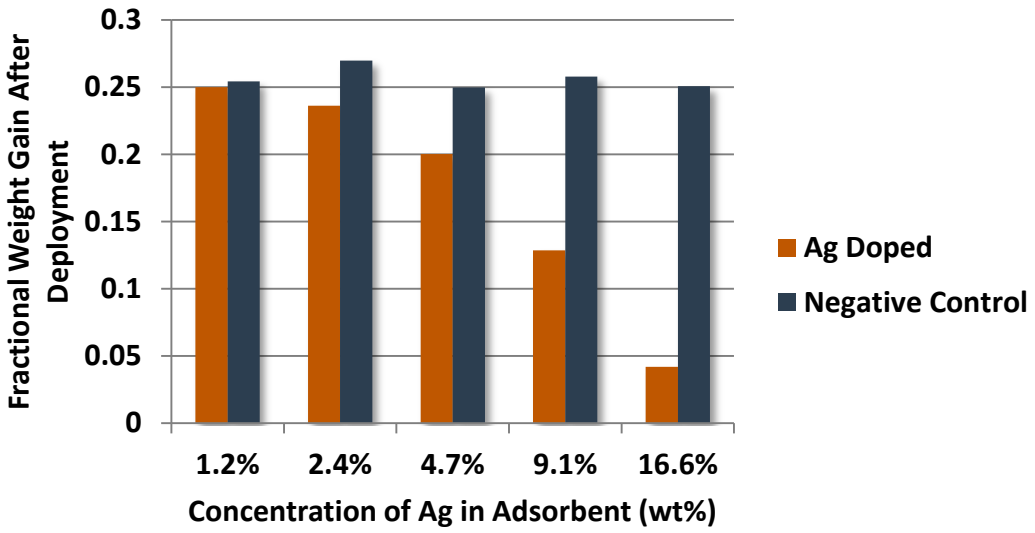

Figure 25: Quantitative analysis of bioaccumulation mass on adsorbent surfaces pre-fouled in diluted AB media cultured with *Vibrio fischeri* as a function of silver content tin adsorbent

It is clear from these results that the silver doped adsorbents experience a lower degree of bioaccumulation than their non-doped counter parts. One exception may be present however in the case of the adsorbent population doped with 1.2% silver by weight. Although the fractional increase in weight gain is in fact lower for the silver doped population, it does not differ by more than the standard deviation of all negative control adsorbents, which in theory should have identical performance. Therefore, while it appears that increasing the silver content of adsorbents does enhance the bio-inhibition abilities, this effect does not necessarily extend down to very low silver contents, on the order of 1% by mass.

Upon first observation difficulty may arise in reconciling the large decrease in bioaccumulation experienced by the doped adsorbents, especially with high silver contents, as compared to the smaller increase in restoration of capacity. It is thus worth pointing out that experiments by PNNL also observed what may appear as a discrepancy between mass of accumulated biofouling material and loss in uptake, where fouled adsorbents increased in mass by 80% relative to their initial weight while only reducing uranium uptake by 30%, as compared to the unfouled adsorbents, which gained 20% of their initial dry mass [3]. The substantial weight gain by the fouled PNNL adsorbents may be expected to observe a more severe loss due to biofouling, indicating that while bioaccumulation is correlated to loss in uptake, the two are not linearly proportional. It is instead possible that the establishment of a very low mass conditioning film composed of the macronutrients present in the media, causes a non-trivial component of the capacity loss due to biofouling while the silver nanoparticles prevent further bacterial growth outward of the filmed surface.

To further conclude that the effects observed in uptake restoration are in fact a result of biofouling mitigation, the viability of microorganisms existing on the adsorbent post-deployment was explored. After adsorbents had been deployed and analyzed for uptake they were placed in sterile AB media and incubated for 2 days in an effort to analyze the viability of *Vibrio fischeri* growth. The observed opacity of the AB media in Figure 26 shows significantly more growth resulting from the negative control adsorbents (left) as compared to the silver doped adsorbents (right).

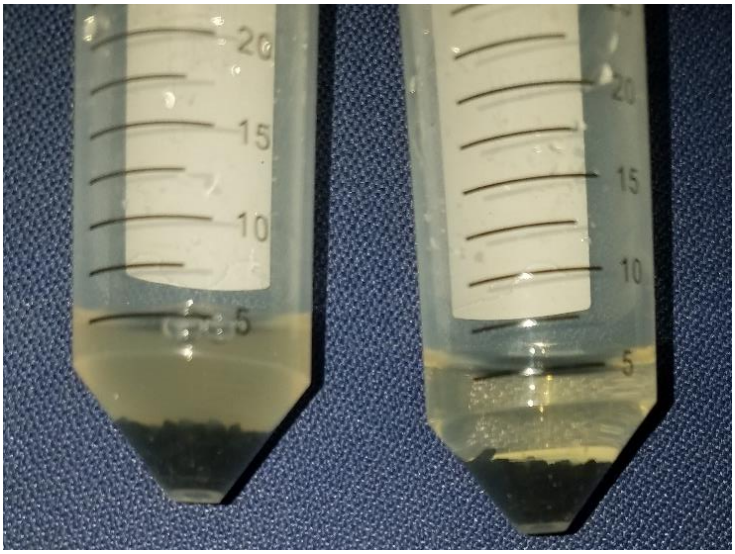

Figure 26: Qualitative analysis of bioaccumulation on the negative control adsorbent (left) as opposed to silver doped (right) adsorbent surfaces post-deployment

The extent of these growth differences was quantified using a technique common in microbiology to evaluate the number of Colony Forming Units (CFU) of bacteria present in solution. Given the difficulty of manually counting bacteria in solution, even under a microscope, agar plates and a serial dilution were used in order to count cultures.

A serial dilution was conducted on the solutions pictured in Figure 26 in order to isolate a collection of bacterial colonies small enough to be accurately counted. The methodology for a serial dilution can best be described pictorially by Figure 27.

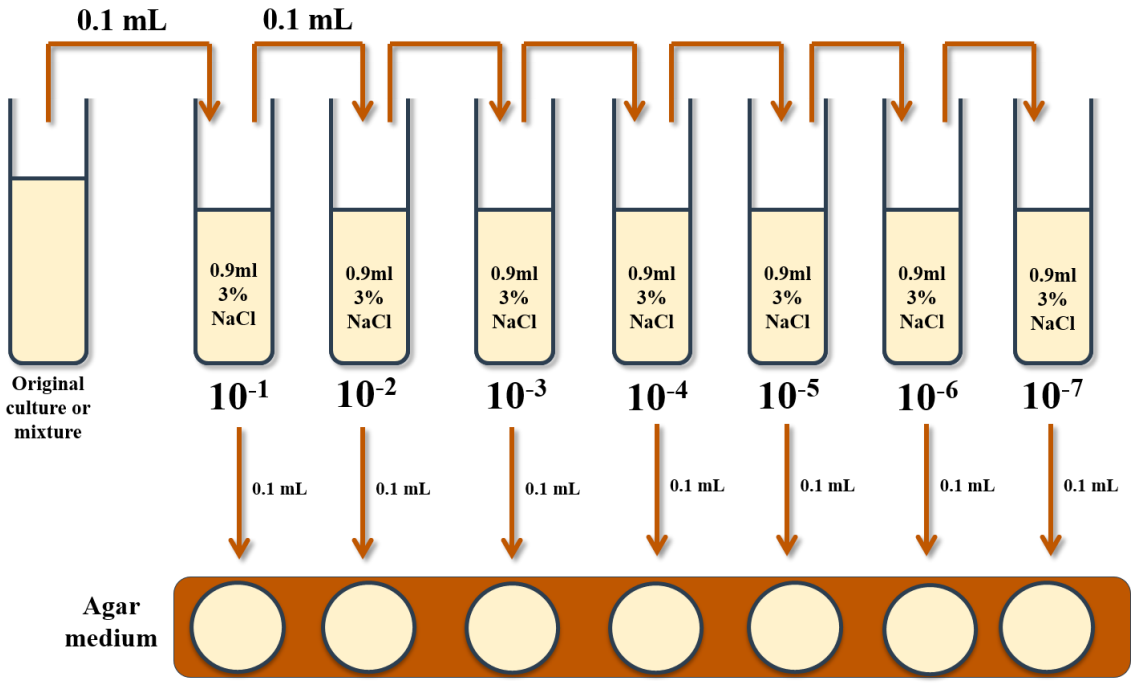

Figure 27: Visualization of protocol used in serial dilution for quantification of bioaccumulation

The initial cultured solution is diluted 10-fold multiple times, in sequences, in sterile 3% NaCl solution; the salt solution was selected as the diluent because that was the buffer solution used to re-suspend cell pellets of the master cell culture after washing. Each resulting solution is spread onto an AB agar plate for incubation at room temperature. After a sufficient incubation time has passed, as determined by the observation of bacterial growth, all of the plates are inspected. The three plates that have observable colony formation most suitable for manual counting are selected for analysis.

Counting the number of visible colonies on a given plate allows for calculation of the number of colony forming units in the original solution given that the volume of solution added to the plate and level of dilution of the plated solution are known. Three plates are selected for quantification so that an average may be taken, although an order

of magnitude approximation is typically sufficient, given the inherent variability of microorganism growth. As with all handling of microorganisms, it is very important to use proper sterile technique as to not contaminate the cultures. In many cases contamination of the cultures can be detected by the appearance of the resulting growth as compared to the known appearance of the desired *Vibrio fischeri* cultures.

In the growth analysis carried out to analyze growth resulting from the adsorbents post deployment, a 2.5 day incubation period was determined to be suitable. In the case of the negative control adsorbents the last three solutions were used for colony quantification. The AB agar plates spread with these solutions after the incubation time can be seen in Figure 28. From the analysis of these plates it is evident that the AB media exposed to these negative control adsorbents, pictured in Figure 29, contained approximately $3.5x10^{8}$ CFU/mL.

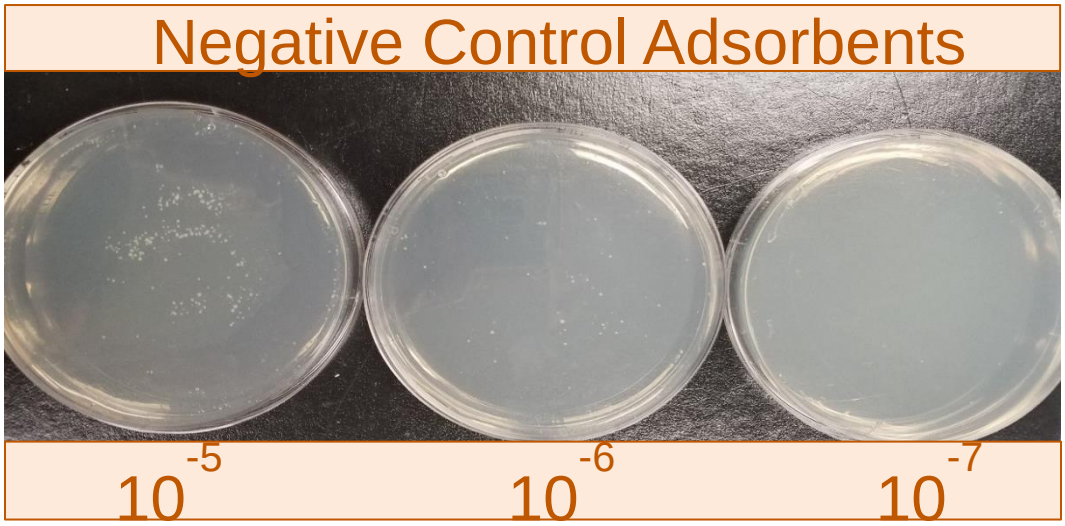

Figure 28: Observed bacterial growth from serial dilution of sterile media exposed to the negative control adsorbents after deployment

Analysis of the plates spread with varying dilutions of the media exposed to silver doped adsorbents was likewise carried out after an incubation period of 2.5 days. Unlike the negative control adsorbents however, growth could only be observed on the plates spread with the initial media exposed directly to the adsorbents and the first diluted solution. These two plates can be seen in Figure 29. The concentration of *Vibrio fischeri* contained in the original solution was calculated to be 375 CFU/mL, a much lower value than that of the negative control adsorbents. It should be noted that the bacterial colonies identified on the plate are not guaranteed to all be *Vibrio fischeri* given that the exposure of the non-sterile adsorbents to the media potentially introduced any ambient bacteria species already present on the non-sterile adsorbent.

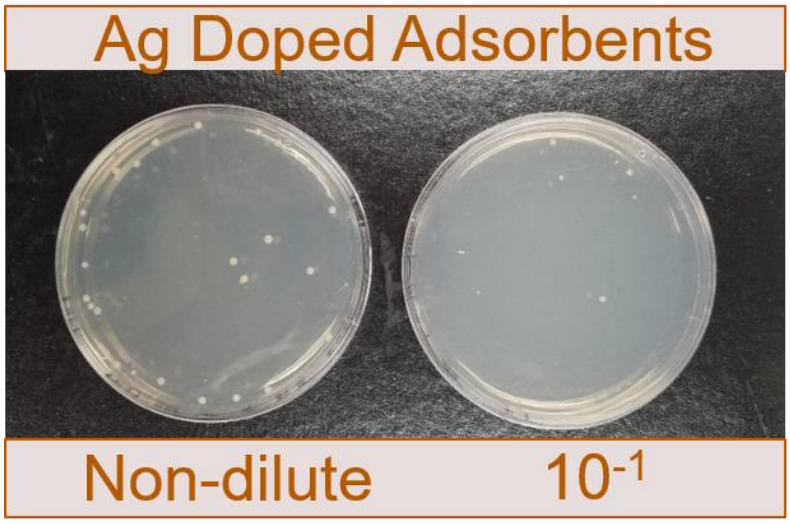

Figure 29: Observed bacterial growth from serial dilution of sterile media exposed to the silver doped adsorbents (containing 10% Ag by weight) after deployment

It is clear from both these qualitative and quantitative analyses that the presence of silver nanoparticles has hampered the ability of *Vibrio fischeri* to grow on the surface

of the activated carbon adsorbents. These observations, coupled with the increased uptake characteristic of the silver doped adsorbents certainly indicate that the silver nanoparticles were acting to mitigate the effects of marine biofouling.

These results may also help to explain the lower than expected capacity restoration factor values observed. The confirmed presence of biofouling hampered uptake and subsequent impeded growth of marine bacteria in the presence of silver nanoparticles suggests that the primary contributor to loss in uptake is the abiotic conditioning film, against which silver nanoparticles provide little relief.

As was discussed earlier in the literature review, biofouling begins with the establishment of a chemical conditioning film before the colonization of micro-organisms [10][11][12]. While there are many literature references confirming the antibacterial characteristics of silver nanoparticles [42][43][44][45], none could be found that specifically addressed the propensity of silver nanoparticles to prevent or eliminate the presence of macromolecules.

The quantitative divergence between capacity restoration factor and bioaccumulation as a function of silver doping could likewise be explained by the notion that the loss in uptake observed is dictated by the presence of the chemical conditioning film. If microorganism growth was in fact the primary cause of uptake degradation, as was originally suspected, then increasing silver concentrations in adsorbent would correspond with decreased bioaccumulation and increased capacity recover factors. Additionally, the rate at which these two phenomena were observed would expected to be quite similar if a decrease in bacterial growth correlated directly with enhanced uranium recovery. While the first criteria of qualitative agreement of trends is met, the latter is not, thus indicating some other, potentially abiotic, factor must be governing the loss due to biofouling experienced by adsorbents deployed in nutrient rich media.

7.3: REUSABILITY

Since the currently proposed deployment technique for recovering uranium from seawater involves the recycle of adsorbent, it is also important to examine the re-usability of the silver doped adsorbents. While there is no heuristic evidence as to why the addition of silver nanoparticles would degrade the adsorbents durability, there does exist the potential that the silver nanoparticles dissolve or are physically removed from the adsorbent, diminishing the biofouling mitigation capabilities upon reuse. Since the elution process is assumed to remove all or a majority of the microorganisms such that the loss due to biofouling starts at or near 0% with each reuse, it could then be reasonably concluded that the biofouling mitigation capabilities would be present on subsequent reuses of the adsorbent so long as the silver nanoparticles remain present.

Unlike the true uranium from seawater adsorbents, no elution method is used to remove adsorbed metals from the adsorbent. Since the only concern of this particular project is uptake ability, and not actual collection of adsorbed material, the concentration of uranium is tested while still on the adsorbent. Therefore, reuse studies cannot be conducted by simply removing uranium and redeploying adsorbents. Instead the rate at which silver nanoparticles have dispersed into ambient seawater was examined.

Given the high radiative capture cross section of naturally occurring silver isotopes, silver, even at the small concentrations used in these adsorbents, is a good candidate for quantification via NAA. This method of testing reusability was conducted using the filament type adsorbents, rather than suspensions. Although the filament adsorbents were not ultimately analyzed for capacity restoration they were believed to be better suited for these reusability experiments given that their form was more reflective of the adsorbents described in the literature to be used for industrial scaled seawater uranium recovery. Some number of silver ions will presumably be lost via the biofouling

mechanisms, either by attaching to or entering bacterial cells. It is hypothesized however that the overwhelming majority of silver nanoparticles would be embedded in the polymer matrix and thus not vacate the adsorbent filament, or national laboratory fibers, above levels on the order of ions.

The concentration of Ag in a given population of adsorbents was analyzed before and after deployment in uranium spiked real seawater. The average silver concentrations for the adsorbents can be seen in Figure 30 where the uncertainty bars are seen to overlap.

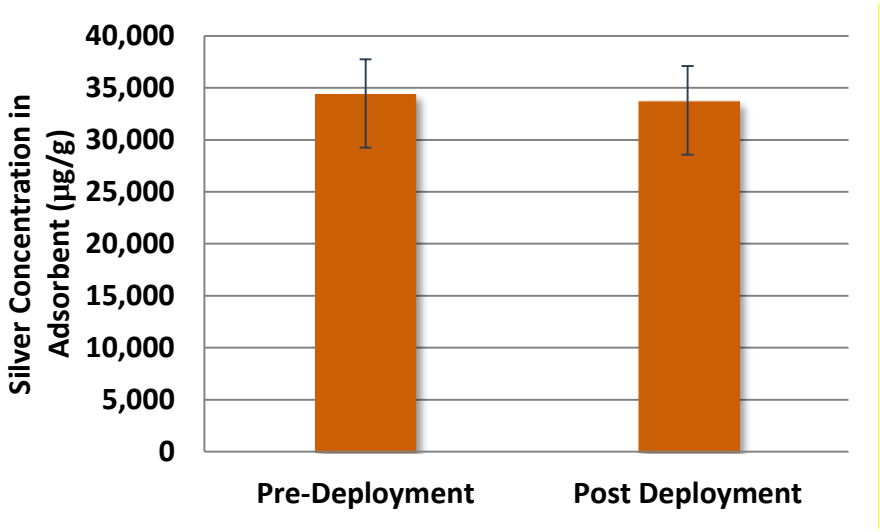

Figure 30: Analysis of silver concentration in adsorbent before and after deployment

The statistical method of ANOVA was used to test the null hypothesis that the two sets of samples could be characterized by the same mean silver nanoparticle concentration. Using a 95% confidence interval, the F statistic was not found to be greater than the F_{crit} value and the p value was found to be 0.6. Both of these

observations forbid the rejection of the null hypothesis, thus indicating that any change in concentration of silver nanoparticles was not statistically significant.

To err on the side of conservatism however, rather than assuming all of the silver nanoparticles are retained in the adsorbents, the small loss observed was incorporated into the cost model. The rate of loss of silver nanoparticles from adsorbents was assumed to be constant over deployment time. Therefore the 1.9% loss observed in Figure 30 above was averaged over the 21 days for which the adsorbents were deployed to yield a leaching rate of 0.1% of initial mass of silver per day.

To incorporate this data into the cost analysis it is necessary to be able to calculate the weight of silver nanoparticles remaining in the adsorbent at any given time. This was done by first establishing the differential equation governing the time rate of change of weight of silver content in the adsorbent, $w(t)$. This can be seen in Eqn. 22 to be a function of the rate of silver leaching, L, determined experimentally as compared to the initial weight, w_0, used to dope the adsorbent.

$$\frac{dw(t)}{dt} = -Lw_0$$

Eqn. 22

Integration and implementation of the initial condition, that $w(t = 0) = w_0$, yields the time dependent silver concentration of adsorbent as seen in Eqn. 23.

$$w(t) = w_0(1 - Lt)$$

Eqn. 23

In the cost calculation, it is necessary to determine the uptake achieved during each deployment. Therefore, it is the average capacity restoration, as dictated by the remaining silver nanoparticles, over an interval rather than at a single point that is of

interest. The average mass of silver nanoparticles remaining in the adsorbent over any n^{th} exposure cycle of length t_i is given by Eqn. 24

$$\overline{w_n} = \frac{1}{t_i}\int_{t_{n-1}}^{t_n} w_0(1 - Lt)dt$$

Eqn. 24

where t_{n-1} and t_n are the cumulative days of seawater exposure experienced by the adsorbent at the initiation and termination of the n^{th} exposure campaign, respectively. Evaluation of this definite integral yields the formula, Eqn. 25, for remaining silver content that will be incorporated into the cost model for the prediction of ultimate uranium uptake experienced by the ORNL adsorbents.

$$\overline{w_n} = \frac{w_0}{t_i}\left(t_i + \frac{L(t_{n-1}^2 - t_n^2)}{2}\right)$$

Eqn. 25

This formula for the weight of remaining silver nanoparticles at any given time will be addressed later in the cost implementation section as it will be used to predict the restoration capacity experienced by the adsorbent over time.

Chapter 8: Effects on Uranium Production Cost

Like all other perturbations made to the uranium recovery process, the cost of incorporating this biofouling mitigation strategy into industrial seawater uranium production must be determined. In some previous analyses of alternative adsorbents [8], for example, the cost associated with increased chemical consumption was shown to have outweighed the benefits of moderate improvements in capacity, and the same could be true for mitigating biofouling by means of silver nanoparticles. Therefore the uranium production cost was calculated for a variety of adsorbent formulations and corresponding capacity restoration factors to determine which combinations of parameters lead to a cost savings.

This section first describes the methodology for calculating the cost to produce uranium recovered by silver doped adsorbents. By building off of previously published methods for modeling seawater uranium production cost [80], [96], the implementation cost of synthesizing silver nanoparticle doped adsorbents can be incorporated. The capacity restoration factors observed and discussed in the proceeding results section are then used to derive an empirically based model for capacity restoration factor experienced and subsequent uranium production cost realized. Finally the break-even analysis is described to examine potentially favorable adsorbent formulations.

8.1: Implementation Cost

The methodology to calculate seawater uranium production using the reference ORNL adsorbents, as well as several other variant technologies, coupled with a passive collection scheme has been detailed in previous publications[96][80]. The same discounted cash flow techniques following a unit mass of adsorbent through-out its life time (adsorbent synthesis, mooring and deployment, and elution) were likewise used in

the cost analysis of recovery via silver doped adsorbents. Since it was assumed that the presence of silver nanoparticles in the adsorbent polymer matrix does not interfere with the ability of the adsorbent fibers to be deployed or eluted, changes in cost calculation were made only to the adsorbent production module of the cost calculation. Theoretically the addition of silver nanoparticles will add a non-zero cost to the deployment and mooring phase of the adsorbent lifecycle given the added weight of adsorbent. The total fuel cost for all ships required for the deployment and retrieval of adsorbents moored to the sea floor however makes up on the order of 1.5% of the final uranium production cost; therefore any additional fuel cost required to handle the silver doped adsorbents was assumed to be negligible and thus was not considered.

The simplicity of the biofouling mitigation technique proposed here was reflected in its incorporation to the cost estimate. The existing adsorbent synthesis process already involves the extrusion of high density polyethylene [96], meaning no, or very minimal, additional equipment costs would be required. The material cost of the silver nanoparticles would however need to be considered with regards to the newly added component to the operating cost. Additionally, the capital cost would be slightly elevated due to the 1 month supply of initial inventory required of all chemicals. Like other material inputs, the cost was determined using vendor quotes obtained from Alibaba, an e-commerce company supporting bulk purchases.

Given the growing use of silver nanoparticles in a variety of applications, the effects of economies of scale were applied to account for the increase in demand that will result from future commercial consumption, including the recovery of uranium from seawater. Independent estimates suggest that improvements in the manufacturing methods of nanomaterials will result in increased throughput, and subsequent demand, leading to an approximately ten-fold increase in production volume [102]. Estimates of

the current world market for silver nanoparticles, M_0 [$\frac{tonnes}{yr}$] were collected from the literature [103] [104] so the total industry value could be determined using the current price, P_0. The rule of six tenths, commonly used in capital cost estimations [105], was applied to the growing silver nanoparticle industry, shown in Eqn. 26, to determine the value of the future industry, I'.

$$I' = P_0 M_0 \left(\frac{M'}{M_0}\right)^{.6}$$

Eqn. 26

This calculation of economies of scale clearly accounts for the fact that as the industry grows the total value of the industry does not grow linearly, meaning the price of silver nanoparticles must decrease with market growth. The depressed price in the new industry, P', can then simply be derived using this new industry value as seen in Eqn. 27.

$$P' = \frac{I'}{M'}$$

Eqn. 27

The size of the new industry, M', is known both from the literature projections and the additional demand were seawater uranium to be harvested on an industrial scale using silver doped adsorbents, where the demand added from uranium adsorbents is a dynamic value calculated on the fly in the cost analysis.

8.2: URANIUM PRODUCTION COST

This material cost was incorporated to the existing cost analysis tool along with the capacity restoration offered by the silver nanoparticles. It was assumed that the ORNL adsorbents could be doped with the same concentration of silver nanoparticles, by weight, as the surrogate adsorbent tested here and experience the same capacity

restoration factor and silver nanoparticle leaching rate. The cost of producing seawater uranium using ORNL adsorbents was calculated for each of the silver contents, and corresponding capacity restoration factors, tested and described by Figure 24, with the exception of the adsorbent with 1% silver content by weight due to its assumedly non-physically relevant results.

The uranium production cost for each adsorbent formulation is displayed in Figure 31, with the cost of unmodified adsorbents suffering the full 30% loss in uptake due to biofouling included for reference.

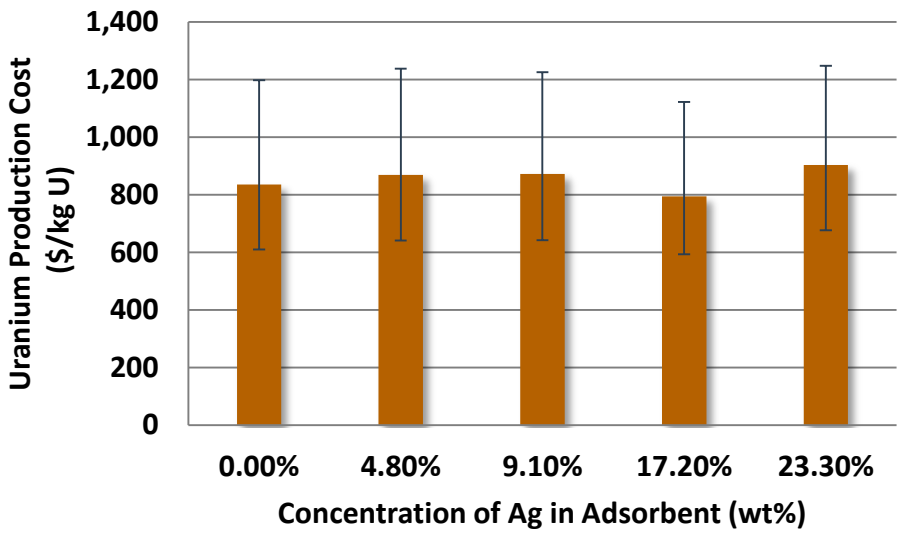

Figure 31: Projected uranium production cost for ORNL adsorbents could they achieve the capacity restoration factor observed in surrogate adsorbent formulations

In each case the uranium production cost is minimized using a previously established optimization framework that tunes deployment parameters, specifically the days of seawater exposure per cycle and number of adsorbent uses prior to ultimate

disposal [80] . The optimal deployment parameters leading to each of the costs pictured in Figure 31 are shown in Table 10.

Table 10: Production cost for seawater uranium recovered via the ORNL adsorbents should they experience the performance observed by the adsorbents utilized in this work

Silver Content	Uranium Production Cost	Optimal Number of Adsorbent Uses	Optimal Days of Seawater Exposure	Capacity Restoration Factor
0%	$835/kg U	13	12	0
4.8	$870/kg U	14	11	0.15
9.1	$870/kg U	14	12	0.31
17.2	$795/kg U	15	11	0.89
23.3	$905/kg U	15	11	0.57

In addition to changing the resulting uranium production cost, the alteration of adsorbent formulation and uptake performance also affects the optimal deployment parameters. Increasing the silver content in the adsorbent acts not only to increase the capacity restoration factor, but also the cost of producing a unit mass of adsorbent. These two factors both have the effect of increasing the optimal number of adsorbent recycles. A more expensive adsorbent favors a greater number of adsorbent exposures in an effort to recoup the higher synthesis cost. An increase in the capacity realized on each deployment cycle allows for a greater number of economical reuses. The optimal days of soaking campaign was affected little by the presence of silver nanoparticles given that this parameter is dominated by the time dependent degradation of amidoxime groups due to seawater exposure.

It is also worth noting that the one of the tested adsorbent formulations, adsorbents doped with 17% silver nanoparticles by weight, was successful in lowering the cost of seawater uranium as compared to the unmodified fouled fibers due to the large capacity restoration factor offered. Given the large uncertainty bars observed on this data point, and all capacity restoration factor data points as well as what may appear to be a deviation from the observed trend, caution is taken with regards to claiming the cost savings of this technique. The remainder of this section will explore the trends in capacity restoration performance to gauge the likelihood of adsorbents of this formulation again achieving the observed performance. A more comprehensive analysis of the many sources of underlying uncertainty will be discussed further in Chapter 9.

It is clear that a trade-off exists between the cost savings offered by the restoration of capacity and the increased material cost of adding of silver nanoparticles of appreciating masses. To find the optimal adsorbent formulation it is necessary to derive a predictive formula for capacity restoration for any given silver content.

The observed data was used to construct an empirically derived formula for the capacity restoration factor as a function of adsorbent formulation. Given the lack of an underlying physical mechanism driving this relationship a variety of candidate models were explored. In all cases the model parameters were determined utilizing a weighted orthogonal distance regression of the observed capacity factor, R, over the weight content of silver in adsorbent, w [106].

The decision to use an orthogonal, or total least squares method comes from the observation that non-trivial uncertainty existed in the silver content of adsorbent samples. Much like the more ubiquitous linear least squares regression analysis, the total least squares regression technique aims to minimize the residual distance between the model predictions and measured data. Being an error-in-variables type of regression, however

the observational errors in both the dependent and independent variables are considered by using the perpendicular distance to calculate the residuals, rather than simply vertical differences. Thus the residuals are the orthogonal distance, D calculated at each point, i, as shown in Eqn. 28.

$$D = \sqrt{(w_i - \widehat{w_i})^2 + \left(R_i - \widehat{R_i}\right)^2}$$

Eqn. 28

such that the coefficient(s), β can be determined by solving Eqn. 29.

$$\hat{\beta} = argmin \sum_{i}^{N} \sqrt{(w_i - \widehat{w_i})^2 + (R_i - f(\widehat{w_i}, \beta)^2}$$

Eqn. 29

This minimization for the determination of function parameters for each of the candidate models was conducted using an orthogonal distance regression package availablethrough ScriPy, scipy.odr. This package uses a Levenberg-Marquardt-type algorithm to find the optimal value(s) of the regression coefficients for a user supplied function [107][108]. Each of the candidate models subjected to this procedure is described here along with a rationale for their inclusion followed by an analysis of their statistical significance.

For the sake of simplicity a linear model is first applied as seen in Figure 32 and described by Eqn. 30. Given the non-physicality of a non-zero restoration factor for an unmodified adsorbent, the model is forced through the origin.

$$R = 0.032w$$

Eqn. 30

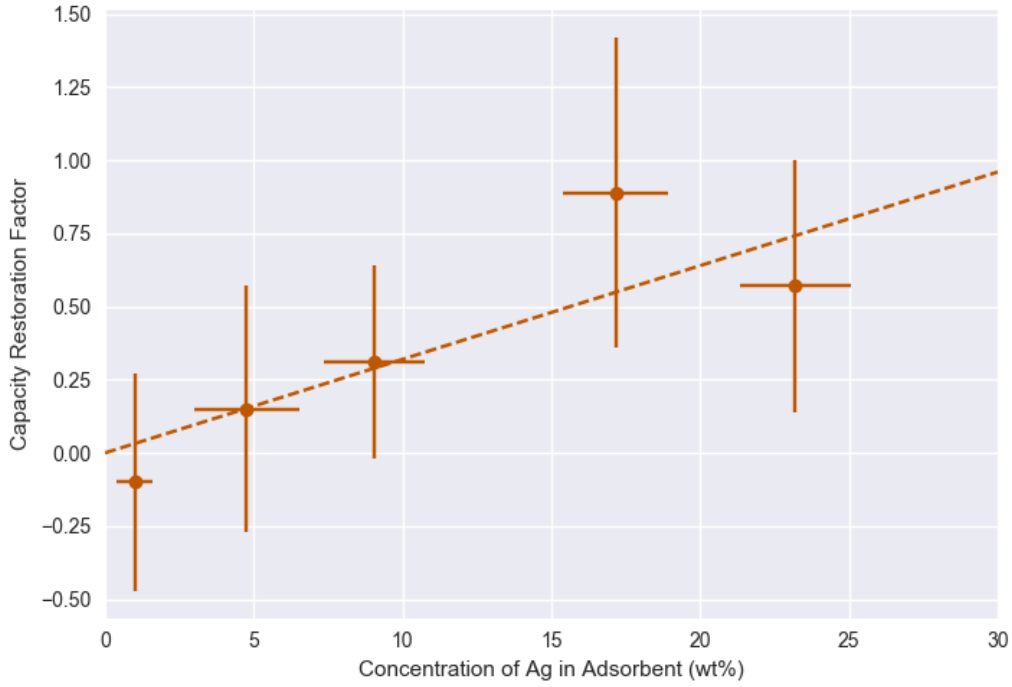

Figure 32: Linear fit for capacity restoration factor as a function of adsorbent formulation

The low p value associated with this model coefficient, 0.005, can be somewhat misleading as it indicates the model should have at least one non-zero coefficient for weight of silver. While this notion is supported heuristically, visual inspection of the plots of capacity restoration factor as a function of adsorbent formulation for all performance analysis trials suggest the data may have a curved pattern. Therefore a logarithmic model is next applied as seen in Figure 33.

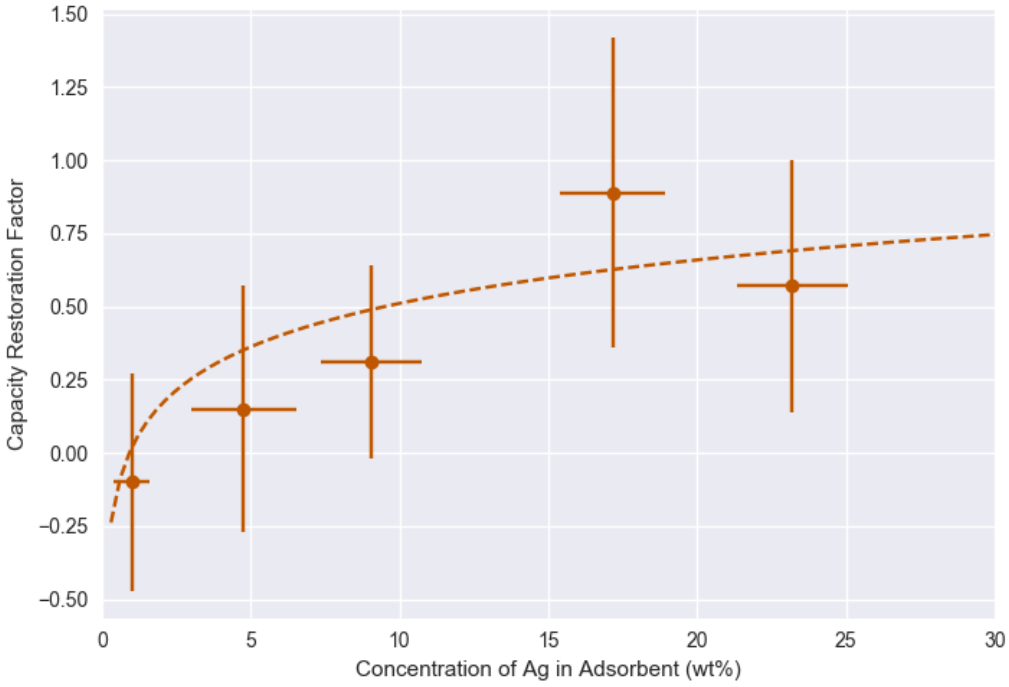

Figure 33: Logarithmic fit for capacity restoration factor as a function of adsorbent formulation

The function arising from this intuition based model can be seen in Eqn. 31.

$$R = 0.21 \ln(w) - 0.018$$

Eqn. 31

An attempt was next made to derive some aspects of the driving mechanism of capacity restoration factor from the literature. The literature was reviewed for instances of a quantified relationship between silver nanoparticle concentration and cell death rates, but such a model could never be found. Instead functions simply describing cell growth and death rates generally were explored. The most closely related function found was the Malthusian generic death rate [109] [110], given by Eqn. 32, which predicts cell population, P, at any given time, t.

$$P(t) = P_0 e^{-\beta t}$$

Eqn. 32

where specific death rate, β, is a model parameter representing the rate of bacterial die-off with no limits imposed such that the population eventually reaches 0. Since the loss of uptake due to biofouling does not appear to be dependent upon time, this predictor variable was simply replaced with the weight concentration of silver nanoparticles present in the adsorbent. Additionally, given that capacity restoration is assumed to increase with decreasing bacterial population, the capacity restoration factor was modeled as the initial population, P_0, minus the rate of population die-off as seen in Eqn. 33 and compared to the observed data in Figure 34.

$$R = 0.697(1 - e^{-0.156w})$$

Eqn. 33

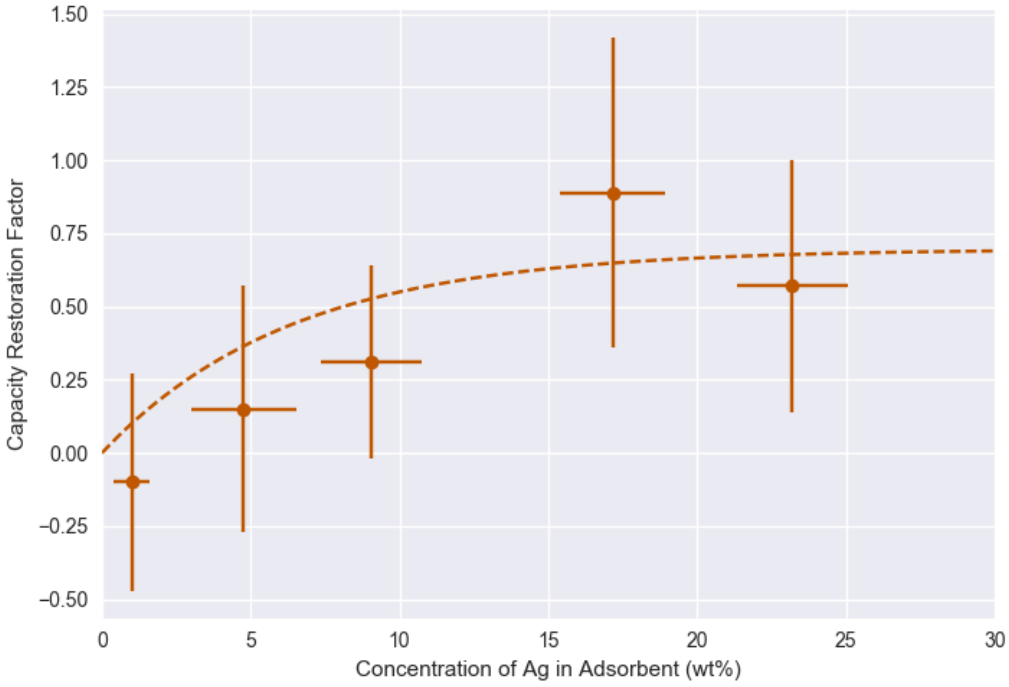

Figure 34: Exponential fit for capacity restoration factor as a function of adsorbent formulation

The generic exponential growth and death curves assume there is no limit on growth or death respectively, which may not always be reflective of reality. If the rate of growth is limited by some external factor then the growth curve becomes logistic to reflect the proportionality to population size as well as the additional growth factor [110]. This logistic growth curve can likewise be used to model a logistic death curve, where a single stress factor limits the death rate, by changing the sign in the differential equation governing the time rate of population change seen in Eqn. 34.

$$-\frac{dP}{dt} = \frac{\beta}{k}P(k - P)$$

Eqn. 34

Integration yields the remaining bacterial population as can be seen in Eqn. 35.

$$P(t) = \frac{k}{1 + e^{-\beta(t-\tau)}}$$

Eqn. 35

where β is the maximum specific death, rate in an unlimited scenario, k is a parameter related to initial population size by $k = P_0\left(1 + e^{-\beta\tau}\right)$, and τ is the time when $P = k/2$. The surviving bacterial population is again considered in light of the initial population to determine the inhibition caused by the silver nanoparticles, believed to be indicative of the capacity restoration factor. The resulting model is shown quantitatively in Eqn. 36 and depicted with the observed data in Figure 35.

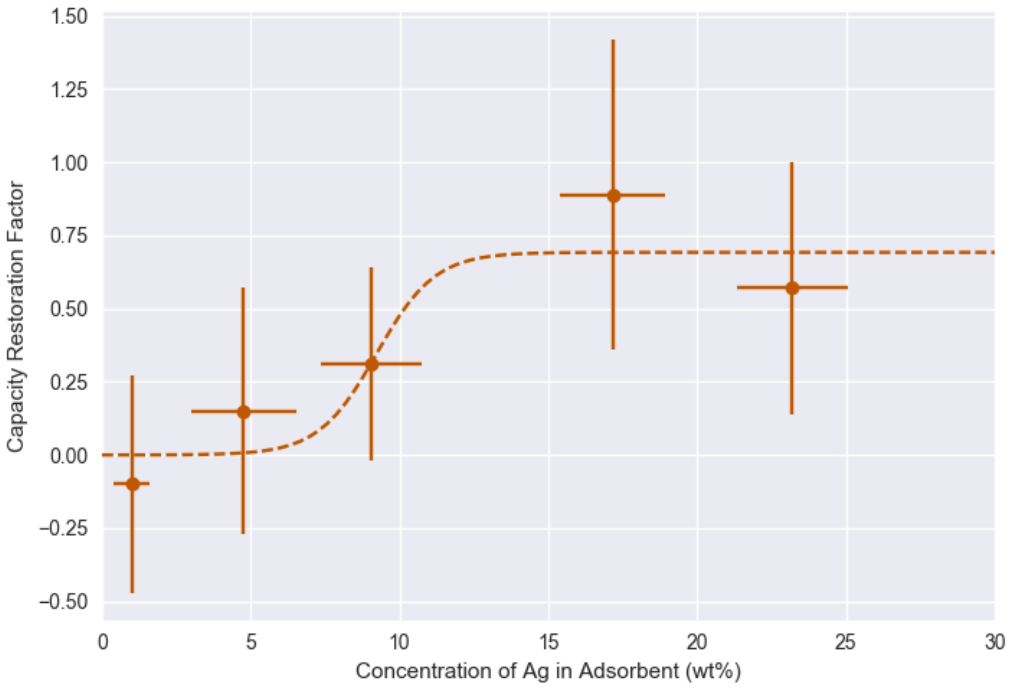

Figure 35: Logistic fit for capacity restoration factor as a function of adsorbent formulation

$$R = 0.692\left(1 - \frac{1 + e^{-1.02*9.23}}{1 + e^{1.02(w-9.23)}}\right)$$

Eqn. 36

Lastly, a quadratic model was considered. In addition to the obvious justification that simply moving from a linear to higher order polynomial model will improve model accuracy, some physical basis exists. While increasing silver nanoparticle concentration is believed to increase bio-inhibition, presumably restoring capacity, it also increases the weight of the adsorbent. At some point the additional mass of silver nanoparticles, which takes away surface area of the ligand capable of adsorbing uranium, will out-weigh the capacity improvements offered to the remaining ligand such that the uranium uptake on a per unit mass of adsorbent basis will decrease. This inverted parabolic model is seen in Figure 36 and defined in Eqn. 37.

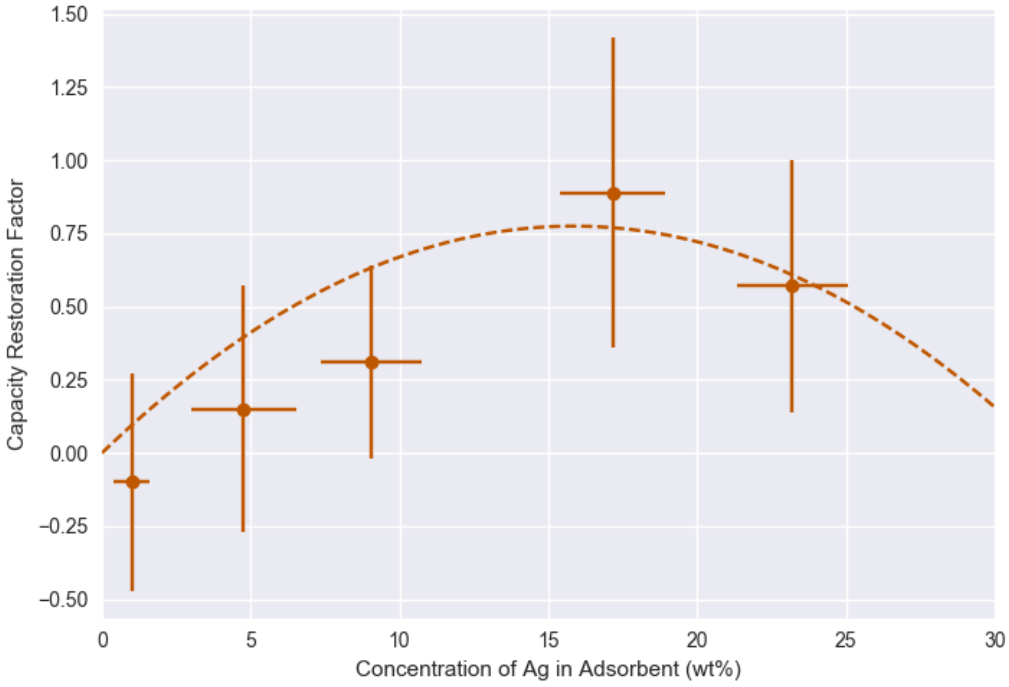

Figure 36: Quadratic fir for capacity restoration factor as a function of adsorbent formulation

$$R = -.00309w^2 + .0979w$$

Eqn. 37

In down-selecting the most appropriate empirically derived model there exists no universally accepted standard procedure. Therefore several different factors used for model selection are considered and displayed in Table 11 for each of the aforementioned fits. First the sum of squares error is used as a simple measure of deviation between the predicted and observed value. The variance of the residuals is also considered as non-uniformity of the residuals suggests that there may be additional patterns in the data that

are not reflected by the model. Lastly, the quality of the models is considered using the Akaike information criterion (AIC) [111].

The AIC attempts to quantitatively determine the relative appropriateness of each candidate model. Although the absolute value of the AIC provides little indication of whether any given model accurately represents the data, comparing AIC values across a collection of models provides a means to compute the trade-off between goodness of fit and model complexity. This can be seen in the formula for AIC seen in Eqn. 38.

$$AIC = 2p - 2\ln(\hat{L})$$

Eqn. 38

where p is the number of model parameters and $\ln(\hat{L})$ is the maximized log likelihood function. Assuming the errors of each model have a normal distribution and mean of 0 then the likelihood function for each model is given by Eqn. 39.

$$\hat{L} = \prod_{i}^{N}\left(\frac{1}{\sqrt{2\pi\sigma^2}}\right)\exp\left[\sum_{i}^{N}\frac{\left(R_i - \widehat{R_i}\right)^2}{2\sigma^2}\right]$$

Eqn. 39

where N is the number of observations and R_i and $\widehat{R_i}$ are the capacity restoration factors observed in the data and predicted by the model respectively. It is clear from Eqn. 39 that the likelihood function is a measure of goodness of fit; more specifically this function can be thought of as the likelihood of observing the data given the model. The AIC is thus essentially a measure of how much information is lost by approximating the true function using the model while penalizing model complexity to avoid overfitting.

When the sample size is small relative to the to the number of parameters, $N/p < 40$, a corrected version of the AIC, the AICc, should be used instead [112] [113].

The AICc provides further penalty for a large number of parameters as can be seen in Eqn. 40, where it can be seen that the AICc approaches the AIC as the number of samples grows.

$$AICc = AIC + \frac{2p(p+1)}{N-p-1}$$

Eqn. 40

Given the small sample size available for capacity restoration factor as a function of silver nanoparticle concentration, a low AICc was used as a means of model selection. This value, along with all of the other criteria considered in the model selection can be seen in Table 11.

Table 11: Analysis of all fits considered for the model of capacity restoration factor as a function of silver content in adsorbent

Fit	Formula	Coefficient Values	Standard Error on Coefficient (%)	Sum of Squares Error	Residual Variance	AIC	AICc
Linear	$R = \beta_1 w$	0.032	0.006	14.93	3.732	21.658	22.991
Logarithmic	$R = \beta_1 \ln(w) - \beta_2$	0.2	0.3	9.979	3.326	21.645	27.645
		0.0	0.8				
Exponential	$R = \beta_1(1 - e^{-\beta_2 w})$	0.7	0.2	8.994	2.998	21.125	27.125
		0.16	0.01				
Logistic	$R = \beta_1\left(1 - \frac{1 + e^{-\beta_2 * \beta_3}}{1 + e^{\beta_2(w-\beta_3)}}\right)$	0.7	0.1	6.194	3.097	21.260	45.260
		1	20				
		9	5				
Quadratic	$R = -\beta_1 w^2 + \beta_2 w$	0.003	0.001	4.782	1.594	17.966	23.966
		.10	.03				
3rd Order Polynomial	$R = -\beta_1 w^3 + \beta_2 w^2 - \beta_3 w$	0.00044	$5x10^{-5}$	0.1198	0.05992	1.5339	25.534
		.0132	$2x10^{-3}$				
		.046	$2x10^{-2}$				
4th Order Polynomial	$R = \beta_1 w^4 + \beta_2 w^3 + \beta_3 w^2 - \beta_4 w$	0.2	80	0.06183	0.03091	-1.7749	$\rightarrow \infty$
		0.2	80				
		.007	$5x10^{-3}$				
		.02	$4x10^{-2}$				

It appears, from a purely mathematical perspective, that a linear model is most appropriate given the limitation of data points. Were the data set more robust then a quadratic fit could arguably be selected, but instead a conservative approach to avoid overfitting was selected by using the AICc. The utilization of the corrected AIC was justified by the investigation of higher order polynomials seen in Table 11, but plots not displayed. Although the residual variance and sum of squares continues to decrease for higher order polynomial fits as expected, the AIC likewise diminishes. This suggests that the penalty for additional model parameters was not harsh enough, especially in the case of the 4th order polynomial where the AIC still favors increasing complexity as k approaches N such that the AICc approaches infinity given the $N - k - 1$ term in the denominator.

It is however very likely that over the entire x domain the capacity restoration factor does conform to an inverted parabola since approaching the edge case of 100% silver nanoparticles is presumed to see a decrease in uranium recovery as silver nanoparticles fully replace the more uranium affinitive-amidoxime. Given however that silver has been reported in the literature to adsorb uranium, the recovery would presumably be non-zero [100][101]. Approaching this boundary is however non-physical as structural issues would of course arise as the amount of polymer matrix required to hold the adsorbent material together diminishes. Therefore the capacity restoration factor model determined experimentally here can only be used for interpolation within the range of adsorbent formulations tested.

It could also be argued that the logistic model most accurately reflects the underlying mechanism. The toxicity profiles pictured previously in Figure 37 indicated the potential presence of a threshold silver concentration, below which the cell population quickly drops off, followed by a plateau region where increasing silver concentration has little effect on cell population. Therefor if insight to the process were given more weight

than statistics, then a logistic or potentially even exponential model would be selected. The inability to quantitatively weigh these two factors as well as the uncertainty in the physical insight, coupled with a tendency toward the statistical methods results in the use of the linear model in further quantitative analyses, although it can not necessarily be declared to be the best representation of the true underlying function.

Given that the silver nanoparticles were seen to evacuate the adsorbent over the soaking campaign, the capacity restoration factor must account for the time dependence of the silver nanoparticle concentration. Therefore the capacity restoration factor experienced by a unit mass of adsorbent on its n^{th}deployment cycle is a function of the average remaining silver content, determined previously in Eqn. 25, and the coefficient determined from the weighted orthogonal least squares fit, and can be seen in Eqn. 41 below.

$$R(n) = \frac{0.032 w_0}{t_i}\left(t_i + \frac{L(t_{n-1}^2 - t_n^2)}{2}\right)$$

Eqn. 41

It is clear that given the slow leaching of silver out of the adsorbent the restoration capacity factor will decrease with increased seawater exposure such that the uptake will begin to eventually approach that of the unmodified fouled adsorbents.

This time and weight dependent capacity restoration factor formula was incorporated into the cost model to determine the uranium production cost as a function of initial silver nanoparticle concentration. These results can be seen in Figure 37 where the uranium production cost recover by both unmodified adsorbents subjected to a 30% loss in uptake due to biofouling and silver doped adsorbents experiencing full capacity restoration are provided for reference.

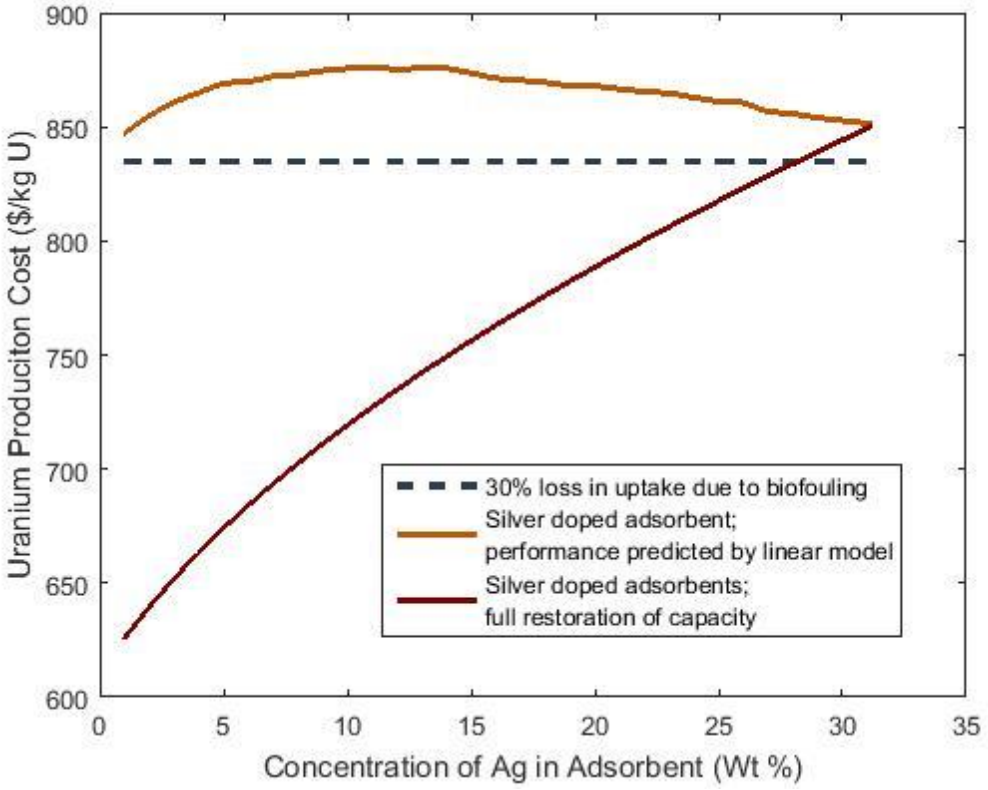

Figure 38: Uranium production cost as a function of adsorbent formulation for both the linear trend for capacity restoration factor, indicated by the burnt orange line, and the full restoration of capacity, indicated by the maroon line, for reference.

It is clear that the performance trends observed in the surrogate adsorbent models would not act to successfully lower the uranium production cost. Given the close proximity of projected costs however, it is worth determining the performance parameters that would be successful to perhaps someday improve the performance of silver doped adsorbents.

8.3: Sensitivity and Break-Even Analyses

It is worth exploring the point at which the addition of silver nanoparticles becomes economically advantageous. Therefore a break-even analysis was conducted to determine

the performance parameters required of the silver doped adsorbents to offer a cost savings as compared to the unmodified control adsorbents subjected to a 30% loss in uptake due to biofouling. The uranium production cost was calculated for a range of scenarios by adjusting the weight content of silver, initial capacity restoration factor, and rate of silver leaching. The resulting trends can be seen in Figure 38.

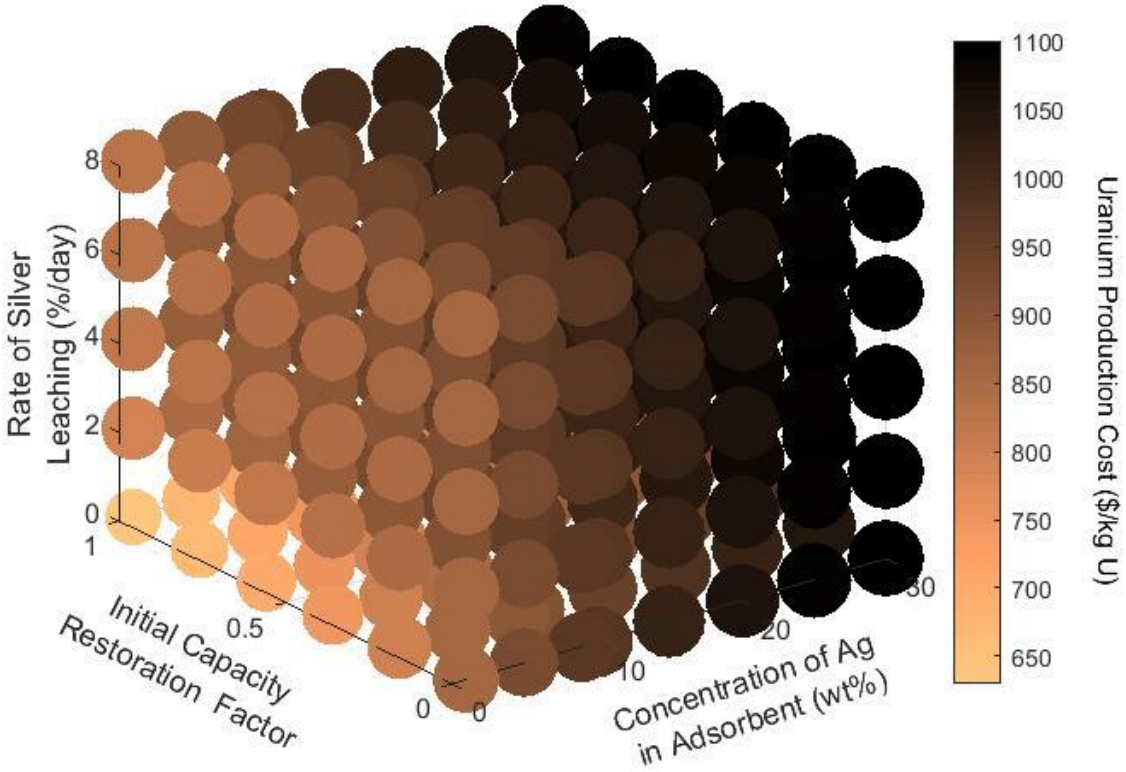

Figure 39: Hypothetical uranium production cost by modified ORNL adsorbents achieving a variety of uptake performances

As expected the projected uranium production cost increases with silver nanoparticle content due to the increased production cost and with the rate of silver leaching due to the resulting decrease in capacity restoration factor over time. The higher capacity restoration factors however act to decrease the uranium production cost by increasing lifetime uranium recovery of each unit mass of adsorbent. Additional data was

collected over a finer range of silver nanoparticle leaching rates surrounding the leaching rate observed in the surrogate adsorbents as can be seen in Figure 39.

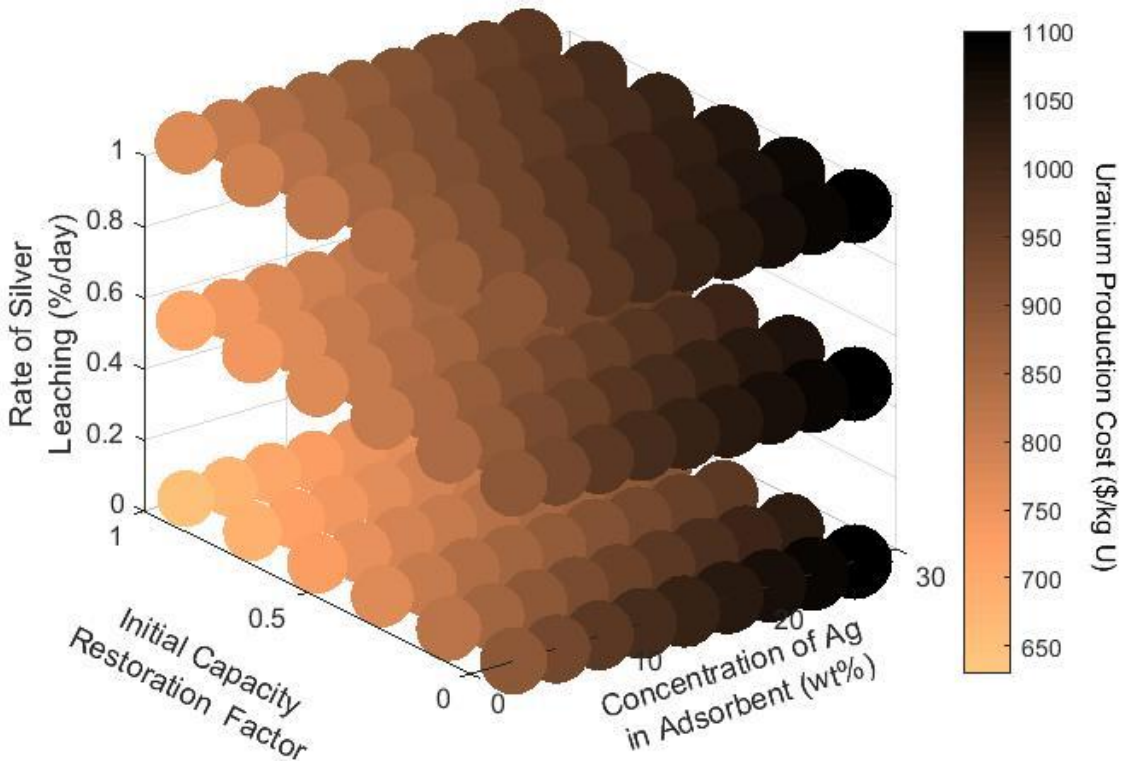

Figure 40: Hypothetical uranium production cost by modified ORNL adsorbents achieving a variety of uptake performances with smaller range of silver leaching rates

In both cases the cost was calculated by assuming the initial capacity restoration factor, indicated on the y-axis, was achieved during the first adsorbent exposure cycle with all subsequent deployments experiencing the leaching of silver nanoparticles over time. This was modeled by determining the average mass of silver contained in the adsorbent during the exposure campaign, as shown previously in Eqn. 25. Since the nanoparticle loss rate is tied to the ultimate uptake achieved by means of the remaining silver content, which

govern the capacity restoration factor, this relationship had to be altered for conduction of the break-even analysis. Therefore the coefficient predicting the rate of increase in capacity restoration factor as a function of adsorbent formulation was recalculated with each parameter set such that it would yield the desired capacity restoration factor for the given weight of silver nanoparticles.

Given the difficulty in accurately interpreting detailed conclusions from 3, and in this case 4, dimensional plots, a series of contour plots were used to display resulting break-even adsorbent formulation and performance parameters. This requires holding one of the predictor variables constant, selected to be there loss rate of silver nanoparticles. Figure 40 displays the uranium production cost of modified ORNL adsorbents could they achieve the initial capacity restoration factor indicated on the y-axis, while suffering the leaching of silver nanoparticles at the rate observed in UT surrogate adsorbents.

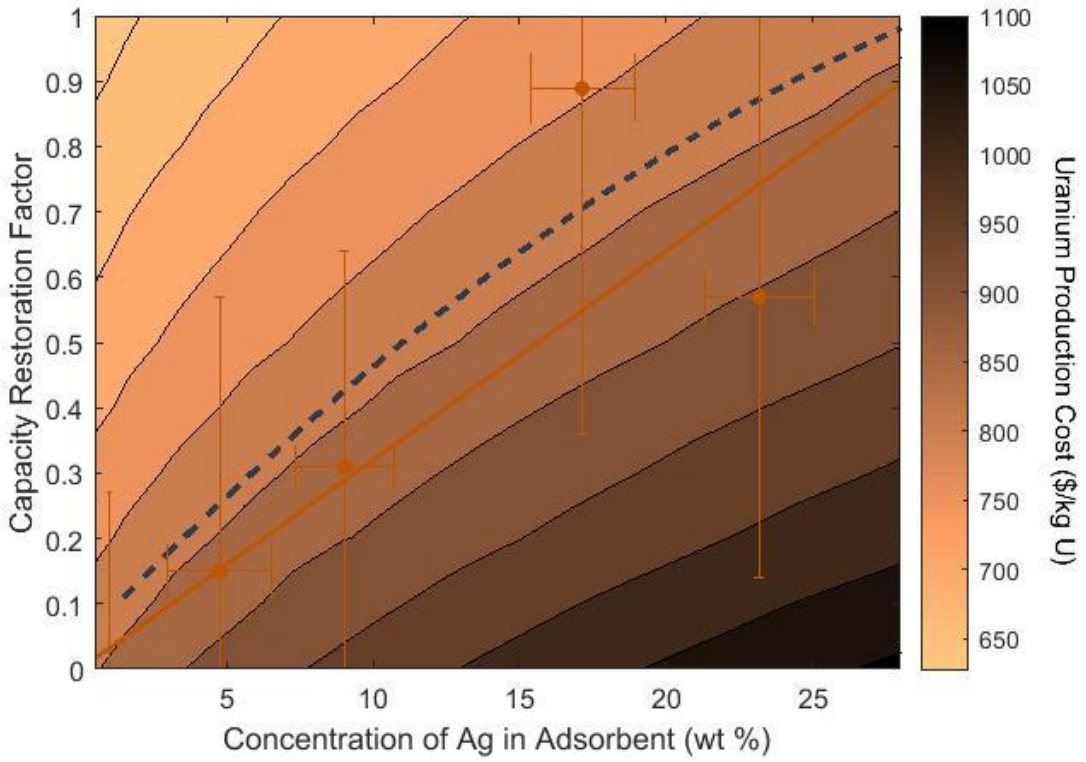

Figure 41: Break-even analysis of modified ORNL adsorbents subject to the observed loss rate of silver nanoparticles while achieving the capacity restoration factor indicated on the first use

The navy blue dotted line represents the break-even parameters. Therefore any adsorbent formulation achieving the indicated capacity restoration factor at the given silver concentration would result in a cost above the navy line and thus offer at least a marginal cost savings as compared to unmodified adsorbents suffering a 30% loss in uptake due to biofouling. The capacity restoration factor observed for the adsorbent formulations tested at UT are provided for reference. As discussed previously in Chapter 8.2, while the adsorbents doped with 17% silver nanoparticles by weight appeared to successfully lower the cost of seawater uranium as compared to the unmodified fouled fibers the large uncertainty bars and deviation from the linear trend require caution in drawing conclusions.

It is also worth pointing out that while the presumably non-physical negative restoration factor observed for adsorbents doped with 1wt% silver nanoparticles is not itself displayed, but the relevant range of its associated uncertainty can be seen in Figure 40. The linear model for capacity restoration factor as a function of adsorbent formulation derived in the previous section is also displayed, as the solid burnt orange line, for reference as this is believed to be the most accurate categorical characterization of silver doped adsorbents. The uranium production cost for silver doped adsorbents would approach the break-even point if the capacity restoration factor predicted by a given weight of silver nanoparticles were to increase by an average factor of 1.5, a modest improvement.

An additional break-even analysis is conducted by considering an enhancement in the reusability of the silver doped adsorbents. It is possible that industrially extruded adsorbents would better retain the silver nanoparticles in the polymer matrix. Additionally, it is possible that at silver concentrations lower than the value examined in the reusability section would be subject to less leaching; some of the silver nanoparticles in the laboratory synthesized adsorbent may have not been fully encased in the polymer and simply resting on the surface. Therefore an additional break-even analysis, pictured in Figure 41, considers no loss of silver nanoparticles over time and looks at the uranium production cost for a range of adsorbent formulations and hypothetical capacity restoration factors.

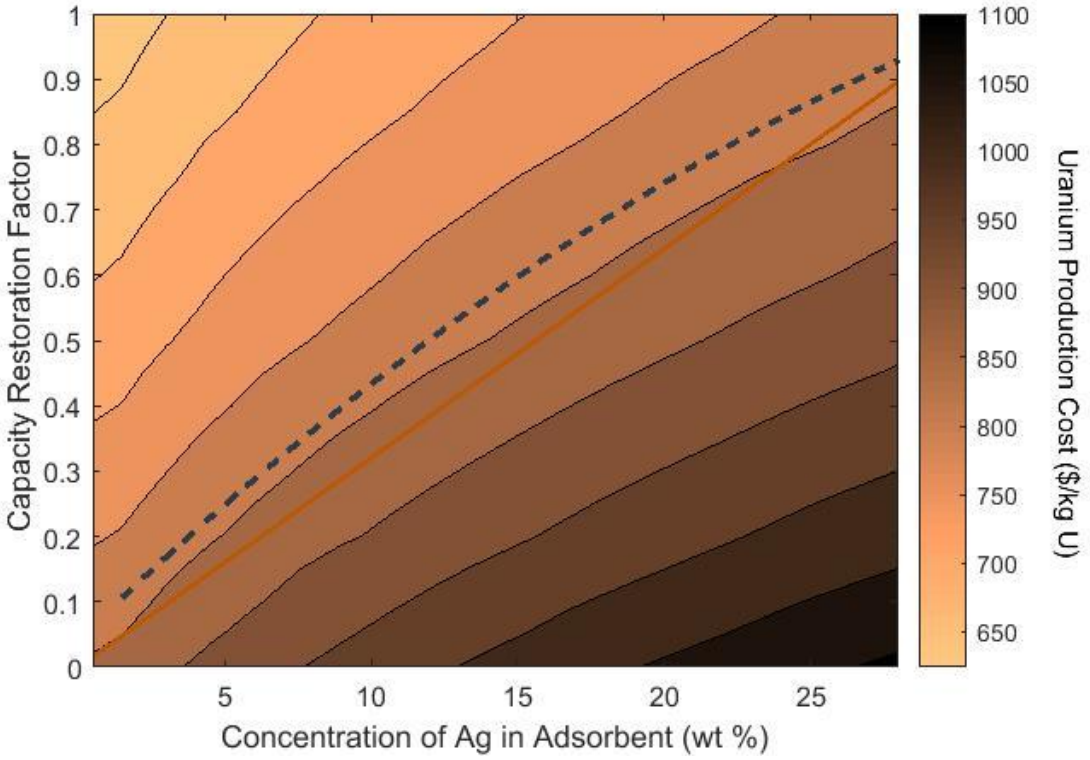

Figure 42: Break-even analysis of modified ORNL adsorbents achieving the capacity restoration factor indicated and leaching no silver nanoparticles over time

The break-even parameters resulting in a cost savings is again indicated by including all uranium production costs residing above the navy blue dotted line and the linear model predicting capacity restoration factor as a function of silver content in adsorbent is represented by the burnt orange line. As expected, a marginally larger number of adsorbent formulation and capacity restoration factor combinations are included in the range of parameters leading to a cost savings. This is particularly true for adsorbents with higher silver content by weight as the leaching of silver occurs at a faster rate in absolute mass of silver terms. Additionally, the empirical model for observed capacity restoration

factor lies closer to the break-even line with capacity restoration needing to increase by a factor of only 1.4 on average, for the model to approach the break-even cost.

It is also possible however that the ORNL adsorbents will experience leaching of silver nanoparticles at a faster rate. The hollow gear shaped fibers are specifically designed to have increased surface area [2], potentially allowing more silver nanoparticles to evacuate the adsorbent. Therefore, a loss rate an order of magnitude higer than the silver leaching rate observed, approximately 1% initial silver content per day was considered for a final break-even analysis. A loss rate this high may not necessarily be likely due to the non-soluble nature of elemental silver, but is nonetheless explored in an effort to be conservative. The results can be seen in Figure 42.

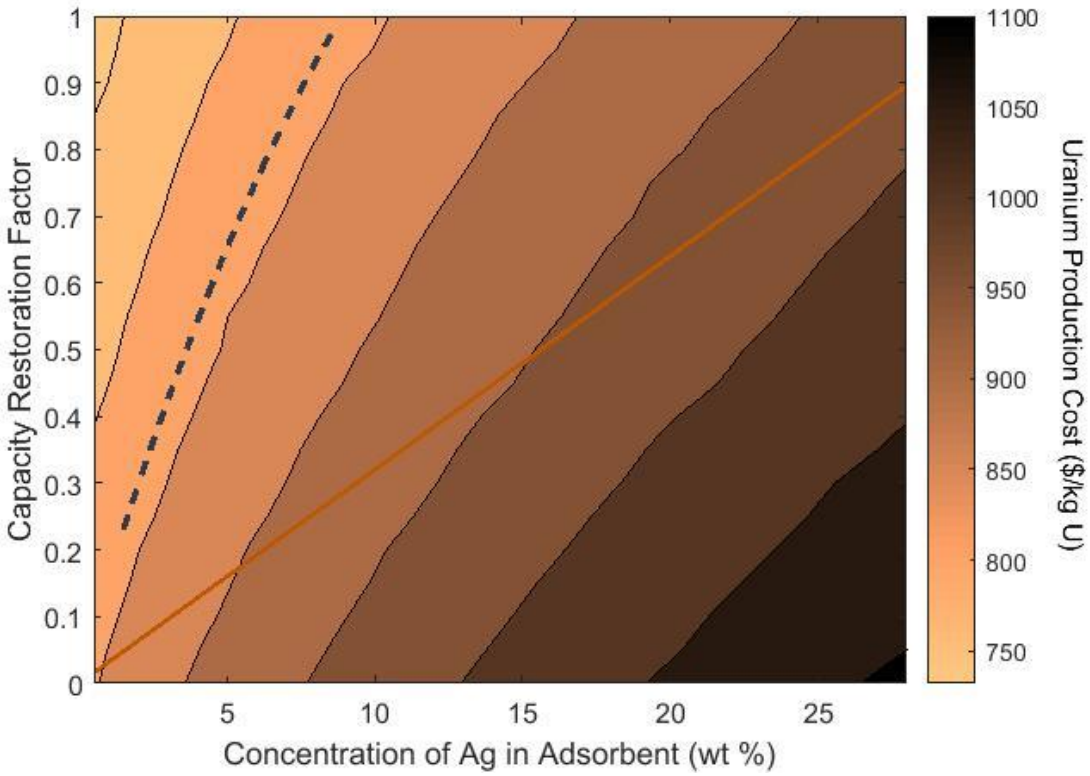

Figure 43: Break-even analysis of modified ORNL adsorbents achieving the capacity restoration factor indicated and leaching silver nanoparticles at a rate of 1% initial mass per day

As expected the capacity restoration performance parameters required for adsorbents experiencing an exaggereated silver nanoparticle leaching rate are much greater in order to offer a cost savings as compared to the unmodified fouled adsorbents. This is particularly evident for adsorbent formulations containing larger amounts of silver nanoparticles by mass as they have incurred a much higher production cost but reap a proportionally diminished reward, as compared to adsorbents with better reusability, given that the capacity restoration drops off as silver leaches out of the material. In order for silver doped adsorbents to be economically advantageous if the silver leaching rate were in

fact an order of magnitude higher than observed, then the capacity restoration abilities would need to increase by a factor of approximately 3.3.

Chapter 9: Uncertainty Quantification

Given the high degree of uncertainty surrounding the recovery of uranium from seawater and its associated cost, it is particularly important to identify and understand the uncertainties present in this method of capacity restoration factor determination. The quantification of uncertainty in the capacity restoration factor must then be propagated, along with all other sources of uncertainty, to the final seawater uranium production cost.

This section first describes the propagation of experimental uncertainties present in quantification of the capacity restoration factor using standard propagation of uncertainty procedures. The subsequent propagation of the calculated uncertainty in the capacity restoration factor to the cost of producing seawater uranium via silver doped adsorbents using a Monte Carlo method of uncertainty quantification is then described.

9.1: Capacity Restoration Uncertainty

At the onset of experimental design significant effort was made to identify all possible sources of uncertainty. In doing so it became apparent that there exists a bifurcation: uncertainty can either be eliminated or quantified and propagated through to the final uncertainty value. The general strategy was to first attempt to reduce the sources of uncertainty, and then those which could not be fully eliminated were quantified by the use of replicates. This sub-section details each of the identified sources contributing to the uncertainty in the capacity restoration factor and means taken to alleviate or quantify them.

In doing so, the distinction is first made between epistemic and aleatoric uncertainty, where the latter is the focus of this section. Epistemic uncertainty can be considered analogous to systematic uncertainty, while aleatoric uncertainties are those that differ each time an identical experiment is run and include statistical effects. Aleatoric uncertainties must be quantified so that they may be propagated through final calculations

of capacity restoration of uptake, and eventually seawater uranium production cost. In the case of both aleatoric and epistemic uncertainties there is a desire to mitigate them as much as possible.

The tables below attempt to identify all of the uncertainties present in the ultimate determination of the performance enhancement offered by the use of silver nanoparticles, as determined using uranium uptake by activated carbon, along with plans for alleviating them. In the case of the aleatoric uncertainties listed in Table 12 the quantification, which may be an analytical calculation applied to each sample or a value observed across populations, is also included. Further explanation of each uncertainty is discussed following the table. Table 13 enumerates epistemic uncertainties, which will not be quantified, and the efforts to reduce them.

Table 12: Aleatoric uncertainties identified in experimental procedures for the determination of capacity restoration factor

Source of Uncertainty	Symbol	Quantification	Mitigation
Statistical variation in count rate of samples	$\sigma_{c_{sample}}$	$\sqrt{c_{sample}}$	Count for long enough periods of time to achieve 10,000 net counts, resulting in 1% uncertainty.
Statistical variation in count rate of standard materials	$\sigma_{c_{std}}$	$\sqrt{c_{std}}$	Count for long enough periods of time to achieve 10,000 net counts, resulting in 1% uncertainty.
Uncertainty in concentration of standard material	$\sigma_{X_{std}}$	0.7% for U 0.8% for Ag	Selection of standard reference materials that are certified by NIST to have a high degree of precision.
Homogeneity of AC content in adsorbent	$\sigma_{AC_{ads}}$	2%	Replace filament polyethylene matrix based adsorbents with activated carbon suspensions.
Random variation in uptake across replicate adsorbent samples exposed to the same conditions	$\sigma_{U_{rep}}$	6-10%	Deployment of large sample sizes in the same condition to determine standard deviation across samples. For all batches and deployment experiments, include a control adsorbent that is always subjected to the same conditions to ensure uptake value is consistent.

Table 13: Epistemic uncertainties identified in experimental procedures for the determination of capacity restoration factor

Source	Mitigation
Flow/water contact difference amongst different adsorbents due to location in container	Will be theoretically similar issue across both conditions since speed of mixing was consistent across tanks so keeping track of adsorbent placement in tank will allow comparison between samples of the same placement in different conditions.
Drying technique of adsorbents post deployment (some U may be in the water on the surface but not truly adsorbed)	Dry adsorbent using vacuum filtration rather than pat-drying or rinsing with DI water, which may shift the equilibrium to removing U off the adsorbents.

An additional source of aleatoric uncertainty that exists is that of taking measurements of weight and time. This would be relevant regarding the uncertainty in the mass of any adsorbent sample along with the mass fraction of its constituents. The high precision of laboratory scales results in uncertainties on the order of ±.00009 g; even with adsorbent samples weighing as little as 0.1g this amounts to a less than 0.1% uncertainty. Similarly time measurements will contribute very litter uncertainty when incorporated into NAA calculations and deployment kinetics. The irradiation and counting facilities at the Nuclear Engineering Teaching Laboratory make use of automated timers that are quite precise such that even on short irradiations, uncertainty on the order of fractions of second would not make significant contributions. Exposure and deployment periods of adsorbent will however be timed manually. The introduction of uncertainty form this procedure is estimated to be on the order of a minute, which can be considered in the noise of

deployments on the order of days Therefore these uncertainties will be neglected on the basis that mass and time measurements will introduce very little uncertainty compared to the others listed in Table 12.

Given the use of a comparator method for calculating isotopic concentrations using NAA the resulting uncertainty is a function of: the precision of the standard as declared by NIST, $\sigma_{X_{std}}$, the uncertainty in the counts attributed to the photo-peak of interest for the standard, c_{std} , and the uncertainty in the number of counts in the photopeak of the sample, c_{sample}.

The uncertainty in the photo-peak associated with both the standard and samples is a function of the stochastic nature of radioactive decay. Since this process is characterized by a Gaussian distribution the uncertainty can be calculated from the number of counts, c (Eqn. 42Eqn.).

$$\sigma_{counts} = \sqrt{c}$$

Eqn. 42

The uncertainty in the calculated sample concentration, $\sigma_{X_{sample}}$, can be determined using the propagation of uncertainty on the comparator method, discussed in the background section on NAA, where

$$\sigma_{X_{sample}} = \sqrt{\left(\frac{\partial X_{sample}}{\partial X_{std}}\right)^2 \sigma_{X_{std}}^2 + \left(\frac{\partial X_{sample}}{\partial c_{sample}}\right)^2 \sigma_{c_{sample}}^2 + \left(\frac{\partial X_{sample}}{\partial c_{std}}\right)^2 \sigma_{c_{std}}^2}$$

Eqn. 43

which expands to Eqn. 44

$$\sigma_{X_{sample}} = \sqrt{\left(\frac{W_{std}}{W_{sample}}\frac{c_{sample}}{c_{std}}\right)^2 \sigma_{X_{std}}^2 + \left(X_{std}\frac{W_{std}}{W_{sample}}\frac{1}{c_{std}}\right)^2 \sigma_{c_{sample}}^2 + \left(-X_{std}\frac{W_{std}}{W_{sample}}\frac{c_{sample}}{c_{std}^2}\right)^2 \sigma_{c_{std}}^2}$$

Eqn. 44

This calculation of uncertainty in uptake of uranium by activated carbon must additionally account for the variation across identical adsorbent samples. This aleatoric uncertainty was quantified, and to an extent mitigated, through the use of control adsorbents. With each new batch of adsorbent and/or each new deployment experiment the uptake of a control adsorbent was tested to ensure the uptake performance maintains consistency or if it was not maintained then allowing for the appropriate correction of epistemic error.

The quantification of the random variation was determined from the deployment of replicate samples subjected to the same conditions. The uncertainty associated with the random variation in uptake ability across replicates, $\sigma_{U_{rep}}$, was calculated from the standard deviation of the set of replicates, having a mean uptake U_{rep}. The uncertainty for uptake per unit mass activated carbon initially derived above (Eqn. 44) must be amended by adding, in relative terms, this random variation. Therefore, $\sigma_{U_{AC}}$becomes what is shown in Eqn. 45.

$$\sigma_{U_{AC}} = \left(\frac{\sqrt{\sigma_{X_{AC}}^2 + \sigma_{X_{AC_0}}^2}}{U_{AC}} + \frac{\sigma_{U_{rep}}}{U_{rep}} \right) U_{AC}$$

Eqn. 45

The final value of interest is the degree to which the proposed mitigation technique inhibits biological growth in order to enhance uranium uptake. This was quantified using the capacity restoration factor, indicating how closely uptake could be restored to that of the unfouled adsorbents. The uptake and associated uncertainty was determined as described above for populations of silver doped adsorbents, the unmodified negative

control adsorbents, and the unmodified adsorbents that were not exposed to biofouling inducing conditions.

In the case of adsorbents exposed to uranium spiked DI water the uncertainty on the uptake of the unfouled adsorbents was calculated using the previously establish pseudo first order kinetics model. In that case the uncertainty on the uptake experienced by the unfouled adsorbents, $\sigma_{Unfouled}$ is a function of the kinetic parameters,K_1 and q_e, characterizing the adsorbents predicted performance as discussed previously in Eqn. 18 in Chapter 4.2.1.

$$\sigma_{Unfouled} = \sqrt{(1 - e^{-K_1 t})^2 \sigma_{q_e}^2 + (-q_e t e^{-K_1 t})^2 \sigma_{K_1}^2}$$

Eqn. 46

These were all combined to determine the capacity restoration factor,R, Eqn. 47 defined previously and shown again here:

$$R = \frac{U_{Ag} - \mathrm{U}_{control}}{\mathrm{U}_{unfouled} - U_{control}}$$

Eqn.47

Given the independence of the uncertainties, the standard propagation of uncertainty can again be used to determine the uncertainty of in the restoration factor where the uncertainty in the modified and unmodified adsorbents are denoted by σ_{U} for the respective adsorbents (Eqn. 48).

$$\sigma_R = \sqrt{\left(\frac{1}{(U_{unfouled} - U_{control})}\right)^2 \sigma_{U_{Ag}}^2 + \left(\frac{U_{Ag} - U_{unfouled}}{(U_{unfouled} - U_{control})^2}\right)^2 \sigma_{U_{control}}^2 + \left(\frac{U_{control} - U_{Ag}}{(U_{unfouled} - U_{control})^2}\right)^2 \sigma_{U_{unfouled}}^2}$$

Eqn. 48

The capacity restoration factor and associated uncertainty for each set of adsorbents consisting of varying levels of silver concentration was calculated as outlined above. Given that these values were then used to regress the predictive function for capacity restoration per unit of silver content, as shows in Figure 32 and Eqn. 30, it was necessary to determine the uncertainty on the regression coefficient in order to ultimately propagate uncertainty to the final objective function of interest, uranium production cost.

Given the use of an orthogonal least squares regression, the standard error, s_β can be determined according to Eqn. 49.

$$s_\beta = \frac{1+\beta^2}{\sqrt{s_w^2 + 2\beta 2cov(R,w) + \beta^2 s_y^2}}$$

Eqn. 49

where s_w and s_R are the variances in the silver content and corresponding restoration factor, respectively. The standard error of the regression coefficient was calculated using the scipy.odr package for orthogonal distance regression discussed previously. The regression coefficient and associated uncertainty were determined to be $0.032 \pm .006$.

Lastly the uncertainty is the reusability of silver doped adsorbents was considered. The standard method of uncertainty propagation was thus carried out on the determination of the leaching rate, L, of silver nanoparticles, shown in Eqn. 50.

$$L = \left(\frac{B-A}{B}\right)\left(\frac{100\%}{t_i}\right)$$

Eqn.50

where B and A represent the silver concentration in adsorbent before and after the exposure to uranium spiked seawater for an immersion period of t_i days. Given that the uncertainty

in the length of the exposure cycle was assumed to be negligible, the uncertainty in the leaching rate, σ_L is described by Eqn. 51.

$$\sigma_L = \sqrt{\left(\frac{100A}{B^2 t}\right)^2 \sigma_B^2 + \left(\frac{1}{At}\right)^2 \sigma_A^2}$$

Eqn.51

Given that the ultimate goal of this work was to mitigate the performance loss due to marine biofouling for the purpose of reducing the cost of seawater uranium, the uncertainty on the uranium production cost was quantified as will be discussed in the following section.

9.2: Seawater Uranium Production Cost Uncertainty

The uncertainty calculated for the capacity restoration factor must likewise be propagated to the resulting uranium production cost. The complex nature of the cost calculation however renders the possibility of obtaining closed form solutions for the derivative of the cost function not feasible. Instead the uncertainty in the uranium production cost was determined using a Monte Carlo method of uncertainty quantification.

Monte Carlo methods, broadly, rely on a large number of random iterations to obtain numerical results to deterministic problems [114]. When used for uncertainty quantification, the stochastic nature is leveraged by randomly generating an alternative value for each input parameter and calculating the new value of the objective function, in this case the final uranium production cost. Multiple iterations are then conducted such that the large number of point estimates can be used to construct a distribution of the production cost. Given that the resulting distribution describing the uranium production cost should approach normality, according to the central limit theorem, the upper and lower confidence intervals can be determined.

Key to the implementation of the Monte Carlo method of uncertainty propagation is the ability to determine an appropriate alternative random value for each input parameter. This requires that the probability density function be known, or at least approximated, such that a random number in the range (0, 1) can be correlated to a new input parameter value by means of the cumulative distribution function.

While the probability density function for any single input parameter may not be explicitly known, a normal distribution may be developed for all empirical input quantities based off the first and second moment, which are derived from the sample data. It is worth noting that decision variables and value parameters, which are selected by the modeler, are not treated as probabilistic and thus not incorporated into the uncertainty propagation; the impacts of inputs of this type, such as interest rates or selected deployment parameters, are better served by sensitivity analyses. Instead only the measurable inputs, such as performance parameters and material costs, are subjected to variation in the Monte Carlo uncertainty propagation.

For reference, the distribution of uranium production costs achieved from the use of unmodified adsorbents subjected to a 30% loss due to marine biofouling is displayed in Figure 43. This histogram, derived from 10,000 Monte Carlo iterations, indicates on the left axis the likelihood that a Monte Carlo evaluation of the cost will fall into the bin indicated on the x-axis. Additionally, the cumulative probability curve is depicted using the secondary (right) axis to display the probability that the uranium productions cost is less than or equal to the x-axis value.

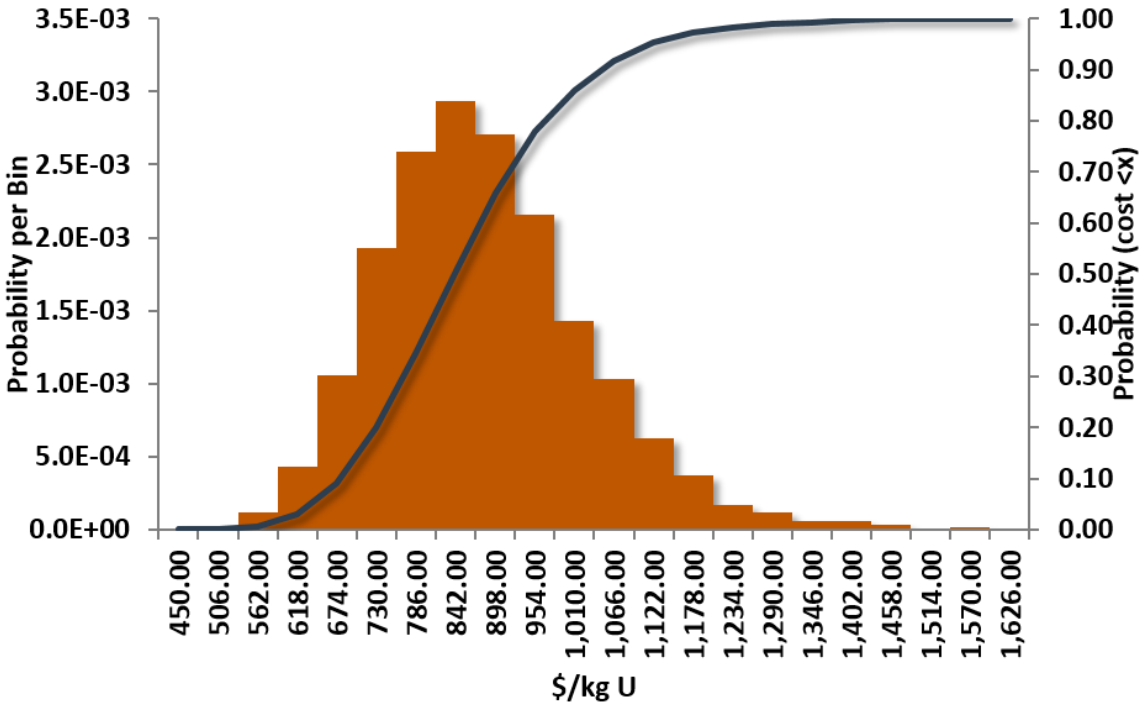

Figure 44: Distribution of uranium production costs achieved using Monte Carlo uncertainty propagation for the reference unmodified fouled ORNL adsorbents

In addition to providing the 95% confidence interval, [$610/kg U to $1,198/kg U] surrounding the project uranium production cost, $835/kg U, visual inspection of the histogram offers additional information. The apparent non-normality of the histogram indicates the existence of a dominant input. In the case of the seawater uranium recovery cost, the dominant variable is the collection of variables influencing the uptake realized given that the cost of seawater uranium is essentially calculated by dividing a complex sum of lifecycle costs encountered by the lifetime uranium recovery of a unit mass of adsorbent. Therefore a decrease in adsorbent uptake, resulting from the variation of: either of the kinetic parameters, the coefficients governing the degradation of adsorbent uptake upon

reuse, or any parameters affecting the capacity restoration factor, will have a proportionally larger effect on the final uranium production cost as compared to an equivalent relative increase of the uranium uptake. This phenomenon results in the observed skewed right distribution, highlighting the importance of uptake in not only the uranium production unit cost but also associated uncertainty, thus further supporting the motivation for this work.

The Monte Carlo method of uncertainty propagation was likewise applied to silver doped adsorbents. The projected uranium production cost via the passive collection scheme utilizing silver doped ORNL adsorbents, assuming they could achieve the same performance characteristic of the surrogate adsorbents can be seen with the associated uncertainty in Figure 44 as a function of silver content in adsorbent.

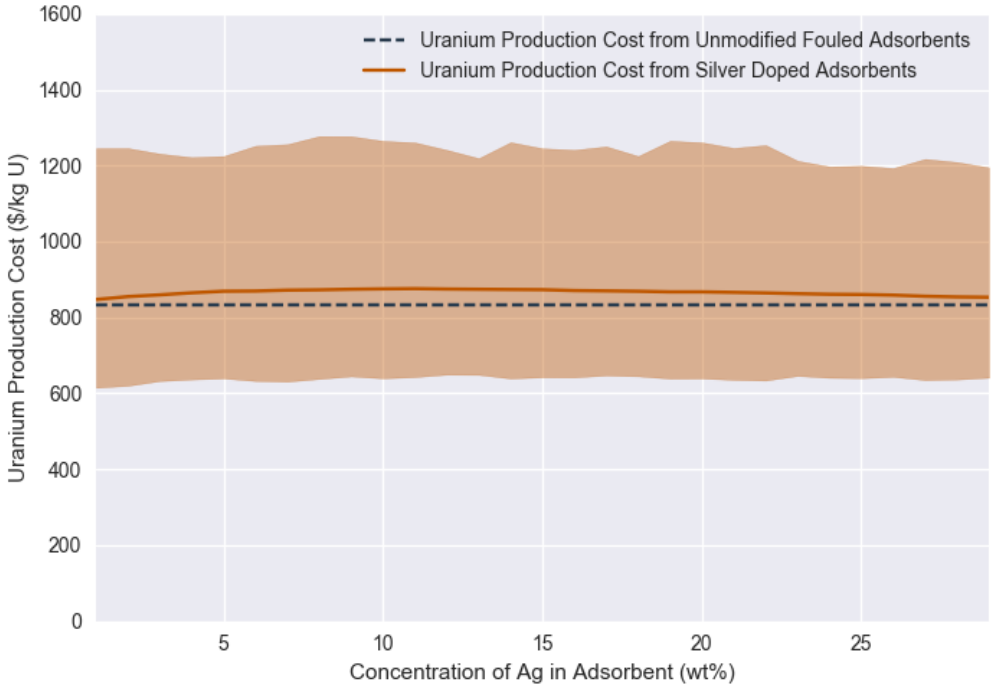

Figure 45: Projected uranium production cost and associated uncertainty as a function of silver concentration in adsorbent.

The solid line represents the projected uranium production cost while the transparent range represents the 95% confidence interval surrounding that cost. It is apparent that each individual production cost is, like the base case, characterized by a skewed right distribution. For reference the base case uranium production cost calculated for the unmodified adsorbents subjected to a 30% loss in uptake due to biofouling is represented by the dotted line.

It is clear that given the high uncertainty surrounding the capacity restoration factor and uranium production cost it is possible that silver doping could lead to a cost savings. This is further illustrated when the 95% confidence interval surrounding the base case uranium production cost is considered as seen in Figure 45.

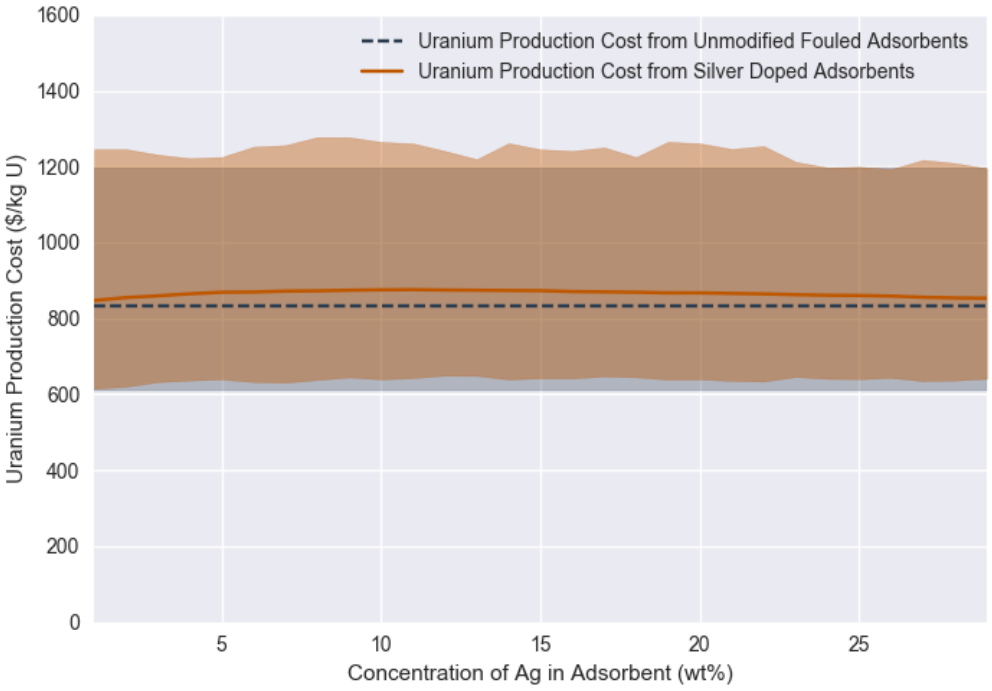

Figure 46: Confidence interval surrounding uranium production cost for silver doped and unmodified fouled adsorbents

Therefore, although none of the projected uranium production costs calculated for the silver doped adsorbents lie below that of the unmodified biofouled adsorbents, this should still be considered a worth-while investigation. A perturbation in one of the many costs or performance parameters characterizing the recovery of seawater uranium, even those unrelated to the capacity restoration abilities of silver nanoparticles, could result in the silver doped adsorbents becoming more economical than suffering the effects of marine biofouling. Additionally, the previously conducted break-even analyses showed that only a moderate improvement in capacity restoration performance, on the order of a 50% increase

in the capacity restoration factor for each adsorbent formulation would result in a cost savings.

Chapter 10: Conclusions and Recommendations

The economic recovery of uranium from seawater could have a transformative effect on decisions made regarding installation of carbon free electricity generation facilities. While the adsorption technology has been proven on a laboratory scale, continued improvement of the recovery process in order to decrease the cost of an industrial operation is a major focus area of ongoing research and development. Recent experiments have shown that marine biofouling of the adsorbent surface can reduce uranium uptake by approximately 30%, leading to an increase in the unit recovery cost. Therefore, this work has presented an approach for alleviating the loss in uptake caused by microorganism growth, i.e. biofouling, on the surface of adsorbents through the use of silver nanoparticles, a known toxin to biological growth. The capacity restoration offered by this mitigation method was considered in light of the associated implementation cost in order to quantify potential cost savings and the necessary break-even adsorbent formulation and performance parameters.

The literature was first studied to provide an understanding of the fundamentals of marine biofouling. This review was significant in revealing that the mechanism of biofouling remains consistent across various environments and surfaces, thus supporting the use of surrogate adsorbent materials for experimentation. Additionally, understanding of the evolution of biofilms led to the ability to focus mitigation efforts on the early stages of biofouling, specifically the colonization of bacteria, which support higher orders of fouling growth. Existing methods of mitigating marine biofouling were then explored for coupling with the passive collection of seawater uranium via the amidoxime-based polymeric adsorbents. Although many commercial and experimental techniques have been developed, none were found in the literature that could be suitable for the recovery of

uranium from seawater due to either blockage of adsorption abilities or economic and logistical barriers. Therefore non-marine fouling mitigation methods and the growing field of anti-microbial plastics were surveyed. Ultimately it was decided that the proven antimicrobial properties of silver nanoparticles used in a variety of fields would be applied to this novel application. Lastly, the literature was surveyed for a suitable means of quantifying the efficacy of this mitigation method, by means of the restoration of heavy metal uptake. After a down-selection of heavy metal quantification techniques neutron activation analysis was identified as the most appropriate.

It was immediately realized that the sophisticated and costly fabrication process of the ONRL uranium adsorbents made it impractical to conduct experiments at UT using the amidxoime-based polymeric adsorbents. Therefore, a method of producing surrogate adsorbents to allow for the completion of uptake and fouling trials at a much faster rate and more importantly, lower cost was established. The first task was to identify appropriate surrogate materials that could be used to accurately represent fouling of the organic substrate thus precluding the of adsorption heavy metals. After a survey of commercially available products, composites made of activated carbon in a high density polyethylene matrix were found to be the most appropriate choice. The HDPE functioned as the grafting surface to provide structural integrity as well as to exactly mirror the ORNL adsorbents, while the activated carbon adsorbed uranium, albeit with lower selectivity than amidoxime. Since the amidoxime ligands are grafted onto the ORNL adsorbents via an irradiation induced co-polymerization reaction, requiring equipment that is not available at UT, an alternative method of ligand grafting was designed. After a literature review of industrial and laboratory scale processing techniques for activated carbon it was determined that a physical synthesis method would be most easily replicated. A commercially available

Filastruder kit, designed for the manufacture of 3D printer filaments from thermoplastics, was repurposed to extrude polyethylene embedded with activated carbon.

Although significant experimentation was carried out in an effort to achieve homogenous extrusion products, significant variation in uptake performance persisted. Therefore, filament type adsorbents were eventually replaced with adsorbent suspensions to avoid aggregations of activated carbon resulting in non-uniform distributions of available surface area across adsorbents. A 9-day time series of adsorbent suspension exposures to spiked solution was carried out in order to establish the kinetic parameters governing uranium uptake by activated carbon according to a first order pseudo kinetic model.

Once appropriate surrogate adsorbent materials were selected, the conditions to be used for adsorbent deployments were determined. The established kinetic models were used to determine exposure times and uranium spiking levels to achieve suitable consistency of performance while minimizing experimental time to allow for a large number of trails. In most cases, adsorbents were exposed to solutions spiked to 500ppm uranium for a period on the order of two days.

Moving in the direction of appreciating complexity, the pre-fouling conditions required to induce biofouling that would be impactful enough to observe a statistically significant drop in uptake ability were identified. A biphasic deployment procedure was utilized following experiments conducted at PNNL with the ORNL adsorbents. Adsorbents were first exposed to a fouling solution of AB media cultured with the marine fouling microorganism *Vibrio fischeri* to ensure bacterial colonization of the adsorbent surface. Length of exposure to the fouling solution was determined to have negligible influence on the degree of uptake loss due to biofouling, therefore pre-fouling phases on the order of two days were implemented.

Surrogate adsorbents were doped with a range of silver nanoparticle concentrations between approximately 1 and 25% by weight, so the capacity restoration performance could be analyzed. Significant work went into determining the range of silver nanoparticle concentrations to be tested as to not result in exorbitant material cost upon scale-up but while maintaining adequate antimicrobial properties.

The literature was first reviewed to find the minimum concentration of silver nanoparticles capable of generating an antibacterial effect, with values as low as 1wt% and below leading to observable inhibition of bacterial growth. Subsequent experimentation was carried out collaboratively through UT and PNNL to test a range of silver concentrations on the specific marine fouling microorganism, *Vibrio fischeri that* would be used in adsorbent fouling experiments. Due to regulations imposed by PNNL regarding the use of silver nanoparticles silver micropowder was instead analyzed in the toxicity scoping experiments.

Microtox tests were used to examine the EC_{50} or the effective concentration of silver powder that reduces the bacterial populations' metabolism by a factor of 50%; given the bioluminescent ability of *Vibrio fischeri* and correlation between bioluminescence and bacterial metabolism a decrease in luminescence can be correlated to toxicity. These experiments showed that a concentration of silver micropowder as low as 5% by weight could successfully produce an antibacterial effect.

The upper bound of silver nanoparticle concentration was likewise identified to avoid testing adsorbent formulations that would never be economical to produce. The preliminary break-even analysis thus compared the uranium production cost of adsorbents retaining full capacity, but doped with varying levels of silver nanoparticles, to the cost of adsorbents suffering the 30% loss in uptake due to marine biofouling. It was determined that adsorbents containing quantities of silver any greater than approximately 25% by

weight would be better served by experiencing the 30% loss in uptake as opposed to encountering the exacerbated adsorbent production cost. Having determined the bounds of appropriate silver concentrations the surrogate adsorbents were then doped with varying levels within this range. In the case of adsorbent suspensions the activated carbon and silver nanoparticles were simply combined by manual means while in the case of the filament type adsorbents the activated carbon and silver nanoparticles were incorporated into the high density polyethylene matrix through repeated extrusion using the Filastruder.

The performance of the silver doped adsorbents was then tested and compared to that of the negative control adsorbents. The improvement in uptake offered by the silver nanoparticles was quantified by means of a quantity termed the capacity restoration factor, which normalizes the increase in uptake achieved by silver doped adsorbents to the loss in uptake suffered by the unmodified control adsorbents as compared to unfouled adsorbents.

A variety of uptake restoration trials were conducted using an array of fouling scenarios. In the initial experiments, adsorbents were exposed to extreme fouling conditions, which had been proved to induce significant reduction of uptake ability. Adsorbents were first exposed to a pre-fouling stage where nutrient rich AB media cultured with *Vibrio fischeri* was allowed to foul the adsorbent surface before removal and subsequent deployment in uranium spiked solution. These initial trials were successful in observing some degree of capacity restoration, but capacity restoration factors were determined to be on the order of 0.1 and lower. This was assumed to be primarily a result of the silver nanoparticles inability to prevent the formation of the abiotic conditioning film made up of macromolecules that were abundant in the media. Therefore, additional performance analysis trials were carried out utilizing fouling solutions containing depreciating volumes of the macromolecule rich media by diluting the fouling solution with sterile sodium chloride solution. Silver doped adsorbents subjected to these fouling

and deployment conditions were observed to have higher capacity restoration factors, but not high enough to achieve a significant cost reduction. Therefore, a final performance trial was conducted, absent any media, in an attempt to reduce the effects of the abiotic conditioning layer as well as to better mirror the experience of the national laboratory adsorbents should they to be deployed on an industrial scale in true marine conditions.

Adsorbents doped with varying degrees of silver, including a negative control, were fouled and exposed to real seawater in a single phase, with no pre-fouling treatment. While seawater was again spiked to achieve 500μg/g uranium, no pre-fouling was conducted and no growth media was added, thus closely approximating the experience of adsorbents placed in a true marine atmosphere. A batch of adsorbents was also deployed in uranium spiked seawater that had been sterilized via vacuum filtration to 0.22 microns and maintained without any light to represent the unfouled adsorbent performance in real seawater. The capacity restoration factors observed by adsorbents in this trial was used then assumed to be replicable by the ORNL AF1 adsorbents and used to calculate the effects on uranium production cost.

Subsequent experimentation was carried out post-deployment to verify that the observed increases in uranium uptake by the silver doped adsorbents was in fact a result of biofouling mitigation as opposed to some other mechanism. The bioaccumulation of organic growth on the adsorbent surface was quantified by analyzing the weight gain of all adsorbent formulations after deployment. Adsorbents doped with appreciating levels of silver nanoparticles experienced less relative weight gain, indicating that the silver nanoparticles were successful in preventing bacterial and/or algal colonization of the adsorbent surface.

Additionally, the viability of the bacterial population persisting on the adsorbent surface after deployment was analyzed. After deployment and analysis of uptake

adsorbents were placed in sterile AB media to allow growth of remaining bacteria. Visual inspection of the transparency of media quickly indicated that a much larger population of microorganisms existed on the negative control adsorbents as compared to the silver doped samples. This was quantified via a serial dilution which confirmed the orders of magnitude difference in bacterial colony forming units resulting from the different adsorbent formulations.

The uptake performance of the silver doped adsorbents was lastly tested with regards to reusability given that the currently proposed scheme for industrial scale seawater uranium recovery via the national laboratory adsorbents requires multiple recycles of adsorbent fibers. Absent an elution process to remove uranium from the surrogate adsorbents, the reusability was examined by quantifying the rate of silver nanoparticle leaching. Although not used in the uptake trials due to reproducibility issues, the filament type adsorbents were utilized in the reusability experiments as they were believed to better represent the currently available adsorbents.

A sample of adsorbent filaments was analyzed for silver concentration using NAA before and after deployment in uranium spiked real seawater. ANOVA was used to compare the content of the samples before and after deployment and found no statistically significant difference between the two means. Erring on the side of caution however, the moderate decrease in silver concentration observed was nonetheless incorporated into the uranium production cost model. It was assumed that the rate of silver leaching would remain constant over adsorbent exposure time and thus a loss of 0.1% of initial silver nanoparticle mass per day was likewise applied to the leading uranium adsorbents.

Next, the cost of incorporating this mitigation strategy into industrial seawater uranium production was determined. This is particularly important given that some previously analyzed alternative adsorbents had a production cost, often associated with

increased chemical consumption, that outweighed the benefits of moderate improvements in capacity, and the same could be true for mitigating biofouling. Therefore the uranium production cost was calculated for a variety of adsorbent formulations and corresponding capacity restoration performance to determine which combinations of parameters lead to a cost savings.

The cost to produce uranium recovered by silver doped adsorbents was determined using previously published methods for modeling seawater uranium production cost, and then incorporating the material cost of silver nanoparticles. The cost of silver nanoparticles was adjusted to reflect the economies of scale benefits they would gain from a growing market due to use in seawater uranium recovery as well as other fields seeking to take advantage of their biocidal effects and improvements in production technology. The capacity restoration factors observed and discussed in the proceeding results section were then used to derive an empirically based model for capacity restoration factor experienced and subsequent uranium production cost realized. Unfortunately, the performance observed in the UT surrogate adsorbents doped with silver nanoparticles was not sufficient enough to outweigh the increase in production cost were this technique to be implemented in the currently available ORNL adsorbents were they produced on an industrial scale. Therefore break-even analyses were conducted to examine potentially favorable adsorbent formulations, capacity restoration factors, and silver nanoparticle leaching rates.

Lastly, the uncertainty surrounding the calculation of the capacity restoration factor observed in the surrogate adsorbents as well as the calculated cost of recovering seawater uranium with silver doped ORNL adsorbents was detailed. The quantification of experimental uncertainties present in the determination of the capacity restoration factor was resolved using standard propagation of uncertainty procedures. This uncertainty was subsequently propagated to the cost of producing seawater uranium using a Monte Carlo

method of uncertainty propagation. It was determined that given the significant uncertainty surrounding the cost of producing seawater uranium, there do exist a number of scenarios where the silver doping of adsorbents would be economically favorable.

Therefore, while the doping of adsorbents with silver nanoparticles cannot be considered to categorically offer a cost savings by means of biofouling mitigation, this was still a worth-while investigation given the significant impact uptake has on seawater uranium production cost and uncertainty, and more broadly, the transformative effect seawater uranium could have on large scale implementation of nuclear power. While the silver doping and deployment conditions utilized in these laboratory experiments did not affect uranium uptake as strongly as was hoped to offer a cost savings, inhibitory effect on microbial and/or phytoplankton growth was observed and thus this approach still has promise. A variety of minor perturbations in one of the many costs or performance parameters characterizing the recovery of seawater uranium, even those unrelated to the capacity restoration abilities of silver nanoparticles, could result in the silver doped adsorbents becoming more economical than suffering the effects of marine biofouling. Additionally, the break-even analysis showed that only a moderate improvement in capacity restoration performance, approximately a 50% increase in the capacity restoration factor of any given adsorbent formulations would render the silver doped adsorbents competitive to their unmodified counterparts.

It is also possible that when deployed in the open ocean adsorbents could experience a loss in uptake even greater than the 30% observed in experiments by Park et al with real seawater. In this case the capacity restoration offered by silver nanoparticles would provide an even greater economic benefit, potentially outweighing the mitigation cost.

If this work were to be continued in the future, efforts could be made to achieve that 50% increase in capacity restoration factor by exploring methods of improving the capacity restoration abilities of the silver doped adsorbents. First and foremost, the performance should be tested in the ORNL adsorbents to examine the transferability of restoration. While assumed to be unlikely, it is possible that the silver nanoparticles offer diminished or improved capacity restoration abilities in the amidoxime-based polymeric adsorbents due to differences such as surface area or interaction with the other chemicals used in adsorbent synthesis and elution of uranium. Given that the currently available adsorbents are characterized by a greater surface area to volume ratio, it is entirely possible that the capacity restoration offered per mass of silver would be more impactful as a greater portion of non-particles would be present on the surface as opposed to the inner layers of the polymer matrix.

Additionally, literature observations correlating silver nanoparticle size to biocidal effects could be explored by testing adsorbents doped with a range of silver nanoparticle sizes [97]. A limitation of time and resources as well as commercially available nanoparticles made extensive testing of a range of particle sizes not feasible for this work. If uranium from seawater were to be considered for implementation on an industrial scale then further exploration of particle size would be warranted.

This work has also been important in concluding that the abiotic conditioning film makes a non-trivial contribution to the reduction of uranium uptake. While it is unfortunate that the silver nanoparticles did not appear to offer a means of preventing or reversing the settling of the macromolecules, the ability to identify that particular stage of biofouling as impactful in reducing uranium uptake by adsorbents is important in guiding future work. Given this new insight, future efforts can be made to mitigate this phenomenon specifically, perhaps by changing the chemistry of the adsorbent fibers themselves as to not

support the adsorption of organic material, or by targeting marine regions with low dissolved organic carbon content for deployment.

References

[1] T. Ku, K. G. Knauss, and G. G. Mathieu, "Uranium in open ocean: concentration and isotopic composition," *Deep Sea Res.*, vol. 24, no. 11, pp. 1005–1017, 1977.

[2] S. Das, Y. Oyola, R. T. Mayes, C. J. Janke, L.-J. Kuo, G. Gill, J. R. Wood, and S. Dai, "Extracting Uranium from Seawater: Promising AF Series Adsorbents," *Ind. Eng. Chem. Res.*, vol. 55, no. 15, pp. 4110–4117, 2015.

[3] J. Park, G. A. Gill, J. E. Strivens, L.-J. Kuo, R. T. Jeters, A. Avila, J. R. Wood, N. J. Schlafer, C. J. Janke, E. A. Miller, M. Thomas, R. S. Addleman, and G. T. Bonheyo, "Effect of Biofouling on the Performance of Amidoxime-Based Polymeric Uranium Adsorbents," *Ind. Eng. Chem. Res.*, 2016.

[4] J. Kim, C. Tsouris, R. T. Mayes, Y. Oyola, T. Saito, C. J. Janke, S. Dai, E. Schneider, and D. Sachde, "Recovery of Uranium from Seawater: A Review of Current Status and Future Research Needs," *Sep. Sci. Technol.*, vol. 48, no. 3, pp. 367–387, 2013.

[5] S. Mahendra, D. Li, A. Zhang, K. Zodrow, Q. Li, and P. J. J. Alvarez, "Polysulfone ultrafiltration membranes impregnated with silver nanoparticles show improved biofouling resistance and virus removal," vol. 43, pp. 715–723, 2009.

[6] J. Mansouri, S. Harrisson, and V. Chen, "Strategies for controlling biofouling in membrane filtration systems: challenges and opportunities," *J. Mater. Chem.*, vol. 20, no. 22, p. 4567, 2010.

[7] S. Brown, Y. Yue, L. Kuo, N. Mehio, M. Li, G. Gill, C. Tsouris, R. T. Mayes, T. Saito, and S. Dai, "Uranium Adsorbent Fibers Prepared by Atom-Transfer Radical Polymerization (ATRP) from Poly (vinyl chloride) - co -chlorinated Poly (vinyl chloride) (PVC- co -CPVC) Fiber," 2016.

[8] S. Das, Y. Oyola, R. T. Mayes, C. J. Janke, G. Gill, J. R. Wood, and S. Dai, "Extracting Uranium from Seawater : Promising AI Series Adsorbents," 2016.

[9] M. Wahl, "Marine epibiosis. I. Fouling and antifouling: Some Basic Aspects," *Mar. Ecol. Prog. Ser.*, vol. 58, pp. 175–189, 1989.

[10] M. Lejars, A. Margaillan, and C. Bressy, "Fouling Release Coatings : A Nontoxic Alternative to Biocidal Antifouling Coatings," *Chem. Rev.*, vol. 112, no. 8, pp. 4347–4390, 2012.

[11] M. E. Callow and R. L. Fletcher, "The influence of low surface energy materials on bioadhesion-a review," *Int. Biodeterior. Biodegradation*, vol. 34, no. 3–4, pp. 333–348, 1994.

[12] P. Y. Qian, S. C. K. Lau, H. U. Dahms, S. Dobretsov, and T. Harder, "Marine biofilms as mediators of colonization by marine macroorganisms: Implications for antifouling and aquaculture," *Mar. Biotechnol.*, vol. 9, no. 4, pp. 399–410, 2007.

[13] A. Rosenhahn, S. Soren, H. Jurgen Kreuzer, and M. Grunze, “The role of Inert Surfae Chemistry in Marine Biofouling Prevention,” *Phys. Chem. Chem. Phys.*, vol. 12, no. 17, pp. 4275–4286, 2010.

[14] S. Kang, E. M. V Hoek, H. Choi, and H. Shin, “Effect of membrane surface properties during the fast evaluation of cell attachment,” *Sep. Sci. Technol.*, vol. 41, no. 7, pp. 1475–1487, 2006.

[15] M. Pasmore, P. Todd, S. Smith, D. Baker, J. Silverstein, D. Coons, and C. N. Bowman, “Effects of ultrafiltration membrane surface properties on Pseudomonas aeruginosa biofilm initiation for the purpose of reducing biofouling,” *J. Memb. Sci.*, vol. 194, no. 1, pp. 15–32, 2001.

[16] S. T. Kang, A. Subramani, E. M. V Hoek, M. A. Deshusses, and M. R. Matsumoto, “Direct observation of biofouling in cross-flow microfiltration: Mechanisms of deposition and release,” *J. Memb. Sci.*, vol. 244, no. 1–2, pp. 151–165, 2004.

[17] S. B. Sadr Ghayeni, P. J. Beatson, R. P. Schneider, and A. G. Fane, “Adhesion of waste water bacteria to reverse osmosis membranes,” *J. Memb. Sci.*, vol. 138, no. 1, pp. 29–42, 1998.

[18] A. Terada, A. Yuasa, S. Tsuneda, A. Hirata, A. Katakai, and M. Tamada, “Elucidation of dominant effect on initial bacterial adhesion onto polymer surfaces prepared by radiation-induced graft polymerization,” *Colloids Surfaces B Biointerfaces*, vol. 43, no. 2, pp. 99–107, 2005.

[19] M. P. Schultz, J. a Bendick, E. R. Holm, and W. M. Hertel, “Economic impact of biofouling on a naval surface ship.,” *Biofouling*, vol. 27, no. 1, pp. 87–98, 2011.

[20] R. A. Braithwaite and L. A. McEvoy, *Marine biofouling on fish farms and its remediation*, vol. 47. 2004.

[21] L. D. Chambers, K. R. Stokes, F. C. Walsh, and R. J. K. Wood, “Modern approaches to marine antifouling coatings,” *Surf. Coatings Technol.*, vol. 201, no. 6, pp. 3642–3652, 2006.

[22] D. M. Yebra, S. Kiil, and K. Dam-Johansen, “Antifouling technology - Past, present and future steps towards efficient and environmentally friendly antifouling coatings,” *Prog. Org. Coatings*, vol. 50, no. 2, pp. 75–104, 2004.

[23] M. Candries, M. Atlar, and C. D. Anderson, “Considering the use of alternative antifoulings : the advantages of foul-release systems,” in *Conference on Marine Research for Environmental Sustainability*, 2000, pp. 88–95.

[24] P. Shivapooja, Q. Wang, B. Orihuela, D. Rittschof, G. P. L??pez, and X. Zhao, “Bioinspired surfaces with dynamic topography for active control of biofouling,” *Adv. Mater.*, vol. 25, no. 10, pp. 1430–1434, 2013.

[25] B. M. Forrest and K. A. Blakemore, “Evaluation of treatments to reduce the spread of a marine plant pest with aquaculture transfers,” *Aquaculutre*, vol. 257, no. 1–4,

pp. 333–345, 2006.

[26] I. Fitridge, T. Dempster, J. Guenther, and R. De Nys, “The impact and control of biofouling in marine aquaculture : a review,” *Biofouling J. Bioadhesion Biofilm Res.*, vol. 28, no. 7, pp. 649–669, 2016.

[27] J. W. Costerton, P. S. Stewart, and E. P. Greenberg, “Bacterial biofilms: a common cause of persistent infections.,” *Science (80-.).*, vol. 284, no. 5418, pp. 1318–1322, 1999.

[28] P. Appendini and J. H. Hotchkiss, “Review of antimicrobial food packaging.pdf,” *Innov. Food Sci. Emerg. Technol.*, vol. 3, pp. 113–126, 2002.

[29] T. Fadida, Y. Kroupitski, U. M. Peiper, T. Bendikov, S. Sela Saldinger, and E. Poverenov, “Air-ozonolysis to generate contact active antimicrobial surfaces: Activation of polyethylene and polystyrene followed by covalent graft of quaternary ammonium salts,” *Colloids Surfaces B Biointerfaces*, vol. 122, pp. 294–300, 2014.

[30] J. J. Wu, G. J. Lee, Y. S. Chen, and T. L. Hu, “The synthesis of nano-silver/polypropylene plastics for antibacterial application,” *Curr. Appl. Phys.*, vol. 12, no. SUPPL. 2, 2012.

[31] J. Deng, L. Wang, L. Liu, and W. Yang, “Developments and new applications of UV-induced surface graft polymerizations,” *Prog. Polym. Sci.*, vol. 34, no. 2, pp. 156–193, 2009.

[32] Z. Lu, M. Meng, Y. Jiang, and J. Xie, “UV-assisted in situ synthesis of silver nanoparticles on silk fibers for antibacterial applications,” *Colloids Surfaces A Physicochem. Eng. Asp.*, vol. 447, pp. 1–7, 2014.

[33] A. G. Shard and J. P. S. Badyal, “Surface oxidation of polyethylene, polystyrene, and PEEK: the synthon approach,” *Macromolecules*, vol. 25, no. 7, pp. 2053–2054, 1992.

[34] M. M. Bilek and D. R. McKenzie, “Plasma modified surfaces for covalent immobilization of functional biomolecules in the absence of chemical linkers: Towards better biosensors and a new generation of medical implants,” *Biophys. Rev.*, vol. 2, no. 2, pp. 55–65, 2010.

[35] Q. Shi, N. Vitchuli, J. Nowak, J. M. Caldwell, F. Breidt, M. Bourham, X. Zhang, and M. McCord, “Durable antibacterial Ag/polyacrylonitrile (Ag/PAN) hybrid nanofibers prepared by atmospheric plasma treatment and electrospinning,” *Eur. Polym. J.*, vol. 47, no. 7, pp. 1402–1409, 2011.

[36] G. Ren, D. Hu, E. W. C. Cheng, M. A. Vargas-Reus, P. Reip, and R. P. Allaker, “Characterisation of copper oxide nanoparticles for antimicrobial applications,” *Int. J. Antimicrob. Agents*, vol. 33, no. 6, pp. 587–590, 2009.

[37] J. P. Ruparelia, A. K. Chatterjee, S. P. Duttagupta, and S. Mukherji, “Strain specificity in antimicrobial activity of silver and copper nanoparticles,” *Acta*

Biomater., vol. 4, no. 3, pp. 707–716, 2008.

[38] I. Perelshtein, G. Applerot, N. Perkas, E. Wehrschuetz-Sigl, A. Hasmann, G. Guebitz, and A. Gedanken, "CuO-cotton nanocomposite: Formation, morphology, and antibacterial activity," *Surf. Coatings Technol.*, vol. 204, no. 1–2, pp. 54–57, 2009.

[39] V. Aruoja, H. C. Dubourguier, K. Kasemets, and A. Kahru, "Toxicity of nanoparticles of CuO, ZnO and TiO2 to microalgae Pseudokirchneriella subcapitata," *Sci. Total Environ.*, vol. 407, no. 4, pp. 1461–1468, 2009.

[40] K. Y. Yoon, J. Hoon Byeon, J. H. Park, and J. Hwang, "Susceptibility constants of Escherichia coli and Bacillus subtilis to silver and copper nanoparticles," *Sci. Total Environ.*, vol. 373, no. 2–3, pp. 572–575, 2007.

[41] M. Heinlaan, A. Ivask, I. Blinova, H. C. Dubourguier, and A. Kahru, "Toxicity of nanosized and bulk ZnO, CuO and TiO2 to bacteria Vibrio fischeri and crustaceans Daphnia magna and Thamnocephalus platyurus," *Chemosphere*, vol. 71, no. 7, pp. 1308–1316, 2008.

[42] J. S. Kim, E. Kuk, K. N. Yu, J. H. Kim, S. J. Park, H. J. Lee, S. H. Kim, Y. K. Park, Y. H. Park, C. Y. Hwang, Y. K. Kim, Y. S. Lee, D. H. Jeong, and M. H. Cho, "Antimicrobial effects of silver nanoparticles," *Nanomedicine Nanotechnology, Biol. Med.*, vol. 3, no. 1, pp. 95–101, 2007.

[43] Y. Lv, H. Liu, Z. Wang, S. Liu, L. Hao, Y. Sang, D. Liu, J. Wang, and R. I. Boughton, "Silver nanoparticle-decorated porous ceramic composite for water treatment," *J. Memb. Sci.*, vol. 331, no. 1–2, pp. 50–56, 2009.

[44] M. Rai, A. Yadav, and A. Gade, "Silver nanoparticles as a new generation of antimicrobials," *Biotechnol. Adv.*, vol. 27, no. 1, pp. 76–83, 2009.

[45] I. Sondi and B. Salopek-Sondi, "Silver nanoparticles as antimicrobial agent: A case study on E. coli as a model for Gram-negative bacteria," *J. Colloid Interface Sci.*, vol. 275, no. 1, pp. 177–182, 2004.

[46] V. K. Sharma, R. A. Yngard, and Y. Lin, "Silver nanoparticles: Green synthesis and their antimicrobial activities," *Adv. Colloid Interface Sci.*, vol. 145, no. 1–2, pp. 83–96, 2009.

[47] U. Samuel and J. P. Guggenbichler, "Prevention of catheter-related infections: The potential of a new nano-silver impregnated catheter," *Int. J. Antimicrob. Agents*, vol. 23, no. SUPPL. 1, pp. 75–78, 2004.

[48] S. Shrivastava, T. Bera, A. Roy, G. Singh, P. Ramachandrarao, and D. Dash, "Characterization of enhanced antibacterial effects of novel silver nanoparticles," *Nanotechnology*, vol. 18, no. 22, pp. 1–9, 2010.

[49] Q. L. Feng, J. Wu, G. Q. Chen, F. Z. Cui, T. N. Kim, and K. J. O., "A mechanistic study of the antibacterial effect of silver ions on Escherichia coli and Staphylococcus

aureus," *J. Biomed. Mater. Res.*, vol. 52, pp. 662–668, 2000.

[50] H. J. Jeon, S. C. Yi, and S. G. Oh, "Preparation and antibacterial effects of Ag-SiO2 thin films by sol-gel method," *Biomaterials*, vol. 24, no. 27, pp. 4921–4928, 2003.

[51] J. Morones, J. Elechiguerra, A. Camacho, K. Holt, J. Kouri, J. Ramirez, and M. Yacaman, "The bactericidal effect of silver nanoparticles," *Nanotechnology*, vol. 16, pp. 2346–53, 2005.

[52] S. Cai, X. Xia, and C. Xie, "Corrosion behavior of copper/LDPE nanocomposites in simulated uterine solution," *Biomaterials*, vol. 26, no. 15, pp. 2671–2676, 2005.

[53] S. H. Jeong, S. Y. Yeo, and S. C. Yi, "The effect of filler particle size on the antibacterial properties of compounded polymer/silver fibers," *J. Mater. Sci.*, vol. 40, no. 20, pp. 5407–5411, 2005.

[54] Y. Dirix, C. Bastiaansen, W. Caseri, and P. Smith, "Preparation, structure and properties of uniaxially oriented polyethylene-silver nanocomposites," *J. Mater. Sci.*, vol. 34, no. 16, pp. 3859–3866, 1999.

[55] O. D. Sparkman, *Mass Spectrometry Desk Reference*, 1st ed. Pittsburgh, PA: Global View Publishing, 2000.

[56] S. Nelms, *Inductively Coupled Plasma Mass Spectrometry Handbook*. Taylor and Francis, 2005.

[57] E. Heftmann, *Chromatography: Fundamentals and applications of chromatography and related differential migration methods - Part A: Fundamentals and techniques*. Amsterdam, The netherlands, 2004.

[58] S. Landsberger, W. D. Cizek, and P. Domagala, "NADA: A versatile PC based program for neutron activation data analysis," *J. Radioanal. Nucl. Chem. Artic.*, vol. 160, no. 1, pp. 277–287, 1992.

[59] S. Landsberger, W. D. Cizek, and R. H. Campbell, "NADA92: An Automated, User-Friendly Program For Neutron Activation Data Analysis," *J. Radioanal. Nucl. Chem. Artic.*, vol. 180, no. 1, pp. 55–63, 1994.

[60] K. Kadirvelu and C. Thamaraiselvi, K. Namasivayam, "Removal of heavy metals from industrial wastewaters by adsorption onto activated carbon prepared from an agricultural solid waste," *Bioresour. Technol.*, vol. 76, pp. 63–65, 2001.

[61] K. Kadirvelu, M. Kavipriya, C. Karthika, M. Radhika, N. Vennilamani, and S. Pattabhi, "Utilization of various agricultural wastes for activated carbon preparation and application for the removal of dyes and metal ions from aqueous solutions," *Bioresour. Technol.*, vol. 87, no. 1, pp. 129–132, 2003.

[62] K. Kadirvelu and C. Namasivayam, "Activated carbon from coconut coirpith as metal adsorbent : adsorption of Cd (II) from aqueous solution," *Adv. Environ. Res.*, vol. 7, no. November 2015, pp. 471–478, 2003.

[63] M. Kobya, E. Demirbas, E. Senturk, and M. Ince, "Adsorption of heavy metal ions from aqueous solutions by activated carbon prepared from apricot stone," *Bioresour. Technol.*, vol. 96, no. 13, pp. 1518–1521, 2005.

[64] J. M. Dias, M. C. M. Alvim-Ferraz, M. F. Almeida, J. Rivera-Utrilla, and M. Sanchez-Polo, "Waste materials for activated carbon preparation and its use in aqueous-phase treatment: A review," *J. Environ. Manage.*, vol. 85, no. 4, pp. 833–846, 2007.

[65] A. Demirbas, "Agricultural based activated carbons for the removal of dyes from aqueous solutions: A review," *J. Hazard. Mater.*, vol. 167, no. 1–3, pp. 1–9, 2009.

[66] J. W. Lim, Y. Choi, H. S. Yoon, Y. K. Park, J. H. Yim, and J. K. Jeon, "Extrusion of honeycomb monoliths employed with activated carbon-LDPE hybrid materials," *J. Ind. Eng. Chem.*, vol. 16, no. 1, pp. 51–56, 2010.

[67] S. Eder, M. Byers, and E. Schneider, "Use of NAA to Detect Uptake of Uranium and other Elements in Adsorbents," *Proc. Am. Nucl. Soc. 2017 Annu. Meet.*, vol. 116, no. 1, 2017.

[68] L. Currie, "Limits for Qualitative Detection and Quantitative Determination. Application to Radiochemistry," *Ann. Chem.*, vol. 40, no. 3, pp. 586–593, 1968.

[69] J. C. Barlow, "Large Surface Area Activated Charcoal and the Inhibition of Aspirin Absorption," *Ann. Emerg. Med.*, vol. 5, no. 18, pp. 547–552, 1989.

[70] L. Zikovsky, "Determination of Uranium in Food in Quebec by Neutron Activation Analysis," *J. Radioanal. Nucl. Chem. Artic.*, vol. 267, no. 3, pp. 695–697, 2006.

[71] L. Kuo, C. J. Janke, J. R. Wood, J. E. Strivens, S. Das, Y. Oyola, R. T. Mayes, and G. A. Gill, "Characterization and Testing of Amidoxime-Based Adsorbent Materials to Extract Uranium from Natural Seawater," *Ind. Eng. Chem. Res.*, vol. 55, no. 15, pp. 4285–4293, 2016.

[72] T. S. Breusch and A. R. Pagan, "A Simple Test for Heteroscedasticity and Random Coefficient Variation," *Econom. J. Econom. Soc.*, vol. 47, no. 5, pp. 1287–1294, 1979.

[73] A. Mellah, S. Chegrouche, and M. Barkat, "The removal of uranium (VI) from aqueous solutions onto activated carbon : Kinetic and thermodynamic investigations," *J. Colloid Interface Sci.*, vol. 296, pp. 434–441, 2006.

[74] M. Caccin, F. Giacobbo, M. Da, R. Luigi, and B. Mario, "Adsorption of uranium , cesium and strontium onto coconut shell activated carbon," *J. Radioanal. Nucl. Chem. Artic.*, vol. 297, pp. 9–18, 2013.

[75] M. Flicker Byers and E. Schneider, "Sensitivity of Seawater Uranium Cost to System and Design Parameters," in *GLOBAL 2015 21st International Conference & Exhibition: " Nuclear Fuel Cycle for a Low-Carbon Future,"* 2015.

[76] M. Byers, M. N. Haji, E. Schneider, and A. H. Slocum, “A Higher Fidelity Cost Analysis of Wind and Uranium from Seawater Acquisition SymBiotic Infrastructure,” *Trans. Am. Nucl. Soc. 2016 Annu. Meet.*, vol. 115, pp. 271–274, 2016.

[77] S. Das, W. P. Liao, M. Flicker Byers, C. Tsouris, C. J. Janke, R. T. Mayes, E. Schneider, L. J. Kuo, J. R. Wood, G. A. Gill, and S. Dai, “Alternative Alkaline Conditioning of Amidoxime Based Adsorbent for Uranium Extraction from Seawater,” *Ind. Eng. Chem. Res.*, 2015.

[78] M. Flicker Byers and E. Schneider, “Uranium from Seawater Cost Analysis: Recent Updates,” *Proc. Am. Nucl. Soc. 2017 Annu. Meet.*, vol. 116, no. 1, pp. 85–88, 2017.

[79] M. Flicker Byers and E. Schneider, “Uranium from Seawater Cost Analysis: Recent Updates,” in *Transactions of the American Nuclear Society 2016 Annual Meeting*, 2016.

[80] M. F. Byers and E. a. Schneider, “Optimization of the Passive Recovery of Uranium from Seawater,” *Ind. Eng. Chem. Res.*, no. November, 2015.

[81] K. E. Parker, E. C. Golovich, and D. M. Wellman, “Uranium Adsorption on Granular Activated Carbon-Batch Testing,” *PNNL Tech. Rep.*, vol. PNNL-22805, no. RPT-DVZ-AFRI-016.

[82] M. M. Aji, B. Gutti, and B. K. Highina, “Application Of Activated Carbon In Removal Of Iron And Manganese From Alau Dam Water In Maiduguri,” *Columban J. Life Sci.*, vol. 17, no. 1, pp. 35–39, 2015.

[83] A. bin Jusoh, W. H. Cheng, W. M. Low, A. Nora’aini, and M. J. Megat Mohd Noor, “Study on the removal of iron and manganese in groundwater by granular activated carbon,” *Desalination*, vol. 182, no. 1–3, pp. 347–353, 2005.

[84] R. Yuan, B. Zhou, C. Shi, L. Yu, C. Zhang, and J. Gu, “Biodegradation of 2-methylisoborneol by bacteria enriched from biological activated carbon,” *Front. Environ. Sci. Eng.*, vol. 6, no. 5, pp. 701–710, 2012.

[85] M. K. Sang and K. D. Kim, “The volatile-producing Flavobacterium johnsoniae strain GSE09 shows biocontrol activity against Phytophthora capsici in pepper,” *J. Appl. Microbiol.*, vol. 113, no. 2, pp. 383–398, 2012.

[86] “Flavobacterium johnsoniae UW101,” *JGI Genome Portal*. [Online]. Available: http://genome.jgi.doe.gov/flajo/flajo.home.html.

[87] A. Nakhamchik, C. Wilde, and D. A. Rowe-magnus, “Cyclic-di-GMP Regulates Extracellular Polysaccharide Production , Biofilm Formation , and Rugose Colony Development by,” *Appl. Environ. Microbiol.*, vol. 74, no. 13, pp. 4199–4209, 2008.

[88] E. C. Irving, Æ. D. J. Baird, and J. M. Culp, “Cadmium Toxicity and Uptake by Mats of the Freshwater ´ b) Hilse Diatom : Navicula pelliculosa (Bre,” *Arch Env. Contam Toxicol*, vol. 57, no. 3, pp. 524–530, 2009.

[89] H. W. Shin, “Rapid attachment of spores of the fouling alga Ulva fasciata on biofilms,” *J. Environ. Biol.*, vol. 29, no. 4, pp. 613–619, 2008.

[90] S. Karthikeyan and R. Balasubramanian, “Evaluation of the marine algae Ulva fasciata and Sargassum sp . for the biosorption of Cu (II) from aqueous solutions,” *Bioresour. Technol.*, vol. 98, no. 2, pp. 452–455, 2007.

[91] M. Simoes, M. Pereira, S. Sillankorva, J. Azeredo, and M. Vieira, “The effect of hydrodynamic conditions on the phenotype of Pseudomonas fluorescens biofilms,” *Biofouling*, vol. 23, no. 4, pp. 249–258, 2007.

[92] I. Poirier, P. Hammann, L. Kuhn, and M. Bertrand, “Strategies developed by the marine bacterium Pseudomonas fluorescens BA3SM1 to resist metals : A proteome analysis,” *Aquat. Toxicol.*, vol. 128–129, pp. 215–232, 2013.

[93] A. Carbon and L. Jakob, “Short-Term Effect of the Soil Amendments Activated Carbon, Biochar, and Ferric Oxyhydroxide on Bacteria and Invertebrates,” *Environ. Sci. Technol.*, vol. 47, no. August 2016, p. 8674−8683, 2013.

[94] A. Chavez-dozal, C. Gorman, M. Erken, P. D. Steinberg, D. Mcdougald, and M. K. Nishiguchi, “Predation Response of Vibrio fischeri Biofilms to Bacterivorus Protists,” *Appl. Environ. Microbiol.*, vol. 79, no. November 2012, pp. 553–558, 2016.

[95] S. Girotti, L. Bolelli, A. Roda, G. Gentilomi, and M. Musiani, “Improved detection of toxic chemicals using bioluminescent bacteria,” *Anal. Chim. Acta*, vol. 471, pp. 113–120, 2002.

[96] E. Schneider and D. Sachde, “The Cost of Recovering Uranium from Seawater by a Braided Polymer Adsorbent System,” *Sci. Glob. Secur.*, vol. 21, no. 2, pp. 134–163, 2013.

[97] G. A. Martinez-Castanon, N. Nino-Martinez, F. Martinez-Gutierrez, J. R. Martinez-Mendoza, and F. Ruiz, “Synthesis and antibacterial activity of silver nanoparticles with different sizes,” *J. Nanoparticle Res.*, vol. 10, no. 8, pp. 1343–1348, 2008.

[98] S. Pal, Y. K. Tak, and M. Song, “Does the Antibacterial Activity of Silver Nanoparticles Depend on the Shape of the Nanoparticle? A Study of the Gram-Negative Bacterium Escherichia coli▽,” *Appl. Environ. Microbiol.*, vol. 73, no. 6, pp. 1717–1720, 2007.

[99] S. Parvez, C. Venkataraman, and S. Mukherji, “A review on advantages of implementing luminescence inhibition test (Vibrio fischeri) for acute toxicity prediction of chemicals,” *Environ. Int.*, vol. 32, no. 2, pp. 265–268, 2006.

[100] D. Bhandari, S. M. Wells, S. T. Retterer, and M. J. Sepaniak, “Characterization and Detection of Uranyl Ion Sorption on Silver Surfaces Using Surface Enhanced Raman Spectroscopy,” *Anal. Chem.*, vol. 81, no. 19, pp. 8061–8067, 2009.

[101] J. Jiang, L. Ma, J. Chen, P. Zhang, H. Wu, Z. Zhang, S. Wang, W. Yun, L. Yingru, J.

Jia, and J. Liao, “SERS detection and characterization of uranyl ion sorption on silver nanorods wrapped with Al 2 O 3 layers,” *Microchim Acta*, pp. 1–23, 2017.

[102] C. A. Charitidis, P. Georgiou, M. A. Koklioti, A.-F. Trompeta, and V. Markakis, “Manufacturing nanomaterials : from research to industry,” *Manuf. Rev.*, vol. 11, no. 1, pp. 1–23, 2014.

[103] Interdisciplinary Centre for Nanostructured Materials and Interfaces, “Silver Nanoparticles : Situation and Perspective for Industrial Application in the Lombardia Region,” *Ital. Assoc. Ind. Res.*, 2013.

[104] Grand View Research, “Silver Nanoparticles Market By Application (Electronics & Electrical , Healthcare , Food & Beverages , Textiles) And Segment Forecasts To 2022,” 2015.

[105] M. Peters and K. Timmerhaus, *Plant Design and Economics for Chemical Engineers*, 4th ed. 1991.

[106] P. T. Boggs and J. E. Rogers, ““Orthogonal Distance Regression,” *“Statistical Anal. Meas. error Model. Appl. Proc. AMS-IMS-SIAM Jt. summer Res. Conf.*, vol. 112, p. 186, 1989.

[107] K. Levenberg, “A Method for the Solution of Certain Non-Linear Problems in Least Squares,” *Q. Appl. Math.*, vol. 2, pp. 164–168, 1944.

[108] D. Marquardt, “An Algorithm for Least-Squares Estimation of Nonlinear Parameters,” *SIAM J. Appl. Math.*, vol. 11, no. 12, pp. 431–441, 1963.

[109] T. Malthus, “An Essay on the Principle of Population,” *J. Johnson*.

[110] K. Pruitt and D. N. Kamau, “Mathematical models of bacterial growth , inhibition and death under combined stress conditions,” *J. Ind. Microbiol.*, vol. 12, pp. 221–231, 1993.

[111] H. Akaike, “A New Look at the Statistical Model Identification,” *IEEE Trans. o Autom. Control*, vol. 19, no. 6, pp. 716–723, 1974.

[112] N. Sugiura, “Further analysts of the data by akaike ’ s information criterion and the finite corrections,” *Communivations Stat. Methods*, vol. 7, no. 1, pp. 13–26, 1978.

[113] C. Hurvich and C.-L. Tsai, “Regression and time series model selection in small samples,” *Biometrika*, vol. 76, no. 2, pp. 297–307, 1989.

[114] N. Metropolis and S. Ulman, “The Monte Carlo Method,” *J. Am. Stat. Assoc.*, vol. 44, no. 247, pp. 335–341, 1949.

Vita

Maggie Byers is a whole hearted supporter of nuclear energy and hopes that the prospect of seawater uranium recovery will be impactful in seeing a growth in the world's reliance on clean nuclear power.

She enjoys drinking Prosecco as well as taking the time to appreciate the aesthetics of a nicely set table.

Permanent address (or email): MargaretEliseByers@gmail.com

This dissertation was typed by Margaret Elise Byers